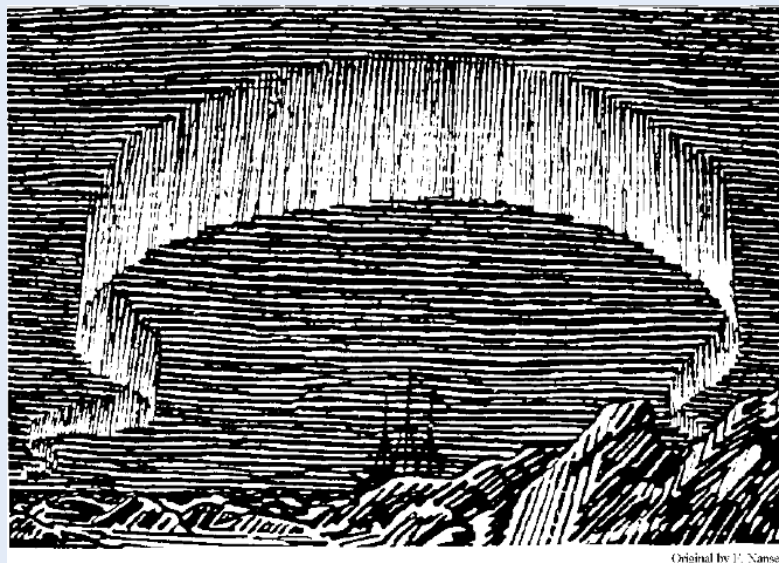




Time-Frequency Characterization of Harmonizable Random Processes

Heidi Hindberg



Original by J. Nansen

A dissertation for the degree of Philosophiae Doctor

UNIVERSITY OF TROMSØ
Faculty of Science
Department of Physics and Technology

June 2009

Abstract

In this thesis we study how to characterize nonstationary harmonizable random processes simultaneously in time and frequency. Unlike stationary random processes, harmonizable processes can have a frequency content that changes with time. Rather than working directly with the process itself, we analyze the second-order moment functions of the process and characterize the process from these moments. The second-order moments of a harmonizable process can be represented in the dual-time domain, the dual-frequency domain, the ambiguity domain and the time-frequency domain, where all domains are connected through Fourier transforms. The time-frequency domain often offers the most intuitive descriptions of the process, thus it will be the main focus of this thesis. We propose estimators of the time-frequency spectra, and we analyze the statistical properties of the estimators. The proposed estimators enjoy a great freedom in that they have many parameters that can be adjusted, and different choices of these parameters will be discussed. We demonstrate the estimator on both simulated complex-valued data and real-world real-valued data.

The ambiguity domain is connected to the time-frequency domain through a 2-D Fourier transform. We can relate the support of the second-order moments in the ambiguity domain, which again is related to the concept of an underspread processes, to the smoothness of the time-frequency spectra. We propose an estimation procedure for the second-order moments in the ambiguity domain based on thresholding of empirical moments, as this will enable us to determine the support in this domain. The estimator is tested on simulated data, and we compare the estimated mean square error of our proposed estimator to a standard estimation approach.

In order to provide objective and dimensionless representations of the time-frequency behavior of a harmonizable process, we define spectral coherence measures. The spectral coherences measure the correlation between the time behavior and frequency behavior of the process (time-frequency coherence) or the correlation across frequencies (dual-frequency coherence). We show how previously defined coherences may be obtained through a linear estimation scheme, and we propose alternative spectral coherence measures based on a widely linear estimation scheme.

The time-frequency representations are applied to a specific stochastic problem, namely that of stochastic differential equations. By transforming the stochastic differential equation to the time-frequency domain and thus considering the second-order moments of the processes involved, we avoid the problems related to stochastic integration. We consider both random processes in time and random fields in spatial variables. We develop a general theory, and we consider both theoretical and simulated examples that corroborate the theory.

Acknowledgments

This is where I get to give thanks to all the people who have helped me throughout these four years. The Norwegian Research Council supported my PhD financially under project 162831/V00, for which I am grateful. This thesis would not have been made had it not been for my supervisor Prof. Alfred Hanssen, who is a brilliant researcher, and I feel privileged to have worked with him. Thank you for inspiring and challenging me over these four years, it has been a priceless experience.

During my PhD, I got to stay for a year in London, UK, visiting the excellent young researcher Prof. Sofia Olhede. My year abroad has taught me a lot, and I am grateful to her for making it a fabulous year. Thank you for taking the time to work with me, and for being genuinely interested in the work we did together. You are an inspiration for all women trying to make it in a research field traditionally dominated by men.

These four years would have been lonely had it not been for my office room mates. I thank Anthony and Øystein for the company. A special thanks goes to Dr. Tor-Arne Øigård, who made every day at the office a giggling competition. I also thank Dr. Yngve Birkelund, Dr. Robert Jenssen and Dr. Yngvar Larsen for help, advice and technical support.

Last, but definitely not least, I thank my family and friends. You all mean the world to me. My biggest thanks goes to my fiancée Tor, to whom I owe everything. Thank you for listening to me and for always trying to understand what I was talking about, and for helping me relax once in a while. This is for you.

Heidi Hindberg, Tromsø, April 2009

Contents

1	Introduction	1
2	Harmonizable Processes	4
2.1	Continuous Time	4
2.1.1	Cross-moments	7
2.1.2	Stationary processes	7
2.1.3	Analytic processes	8
2.2	Discrete Time	9
2.2.1	Estimators of the second-order moments	10
2.2.2	Simulation of improper processes	12
2.3	Random Fields	13
3	The Kirkwood-Rihaczek Time-Frequency Spectra	15
3.1	Estimation	16
3.1.1	Estimation based on the inner product formulation	17
3.2	Statistical Properties	18
3.2.1	Marginals	19
3.2.2	Choice of parameters	20
3.3	Numerical Examples	22
3.3.1	Improper piecewise stationary process	22
3.3.2	Improper process with time-varying variance	25
3.3.3	Bat recording	26
3.3.4	Guitar recording I	29
3.3.5	Guitar recording II	30
3.4	Discussion	33
4	Estimation of the Ambiguity Function	35
4.1	Properties of the Empirical Ambiguity Function	36
4.1.1	Distribution for underspread processes	37
4.1.2	Moments for some special cases	39
4.2	Thresholding Procedure	41
4.2.1	Estimating the variance	41
4.2.2	Spread	42

4.3	Numerical Examples	43
4.3.1	Moving average process	44
4.3.2	Uniformly modulated process	45
4.3.3	Time-varying moving average	46
4.3.4	Deterministic chirp in additive Gaussian white noise	46
4.4	Discussion	47
5	Generalized Spectral Coherence	49
5.1	Time-Frequency Coherence	49
5.2	Dual-Frequency Coherence	51
5.3	Geometry	52
5.4	Properties	54
5.4.1	Proper processes	54
5.4.2	Analytic processes	54
5.4.3	Real-valued processes	54
5.4.4	Generalized Cross-Coherences	55
5.5	Discussion	55
6	Stochastic Differential Equations	57
6.1	Differential Equation Basics	57
6.1.1	System interpretation	58
6.1.2	The HKR-spectrum of differential equations	61
6.1.3	Time-varying coefficients	61
6.1.4	Homogeneous solution	62
6.2	Particular Solutions in the Dual-Frequency Domain	62
6.2.1	Random coefficients	63
6.3	Differential Equations in Time and Space	64
6.4	Examples	66
6.4.1	Langevin equation for Brownian motion	66
6.4.2	System with random coefficients	67
6.4.3	Pulse response	69
6.4.4	Spatial differential equations	71
6.5	Remarks	75
7	Summary	77

Chapter 1

Introduction

This thesis deals with random processes and their second-order moment functions, with representations simultaneously in time and frequency as the main theme. We focus on how to represent the second-order moments in time-frequency, how to estimate time-frequency quantities and we will show how time-frequency representations can provide insight into the field of stochastic differential equations. A random process is a function of time, where for each time instant t the process is a random variable. The random process is governed by the probability densities of these random variables, both the marginal distributions at each time instant, and the joint distributions between different time instants. The analysis of random processes has traditionally been dominated by the assumption that the random process is stationary, for which the probability densities governing the process do not change with time. In recent years there has been an increasing interest in nonstationary processes. Harmonizable processes, introduced in [Loève, 1945; Loève, 1946], is a very large class of nonstationary processes that has been widely studied, see e.g., [Rao, 1985; Yaglom, 1987; Lii and Rosenblatt, 2002; Hanssen and Scharf, 2003; Scharf et al., 2005]. A harmonizable process is representable as a superposition of random, correlated, infinitesimal complex harmonic oscillators. The associated infinitesimal complex random amplitude is often called the increment process [Yaglom, 1987] or the generalized Fourier transform [Thomson, 2000]. We limit ourselves to work within the harmonizable class throughout this thesis.

Although we live in a real-valued world, complex-valued signals and processes find applications in many different fields. A standard example is communications, where complex-valued signals are used to improve the efficiency of communications systems, see e.g., [Proakis and Salehi, 2002]. Complex-valued processes are also encountered when analyzing blood flow [Olhede and Walden, 2003] or oceanic currents [Lilly and Gascard, 2006], to name a few specific examples. Traditionally, complex-valued processes have been treated in a manner similar to that of real-valued processes, modified to include a single complex conjugation applied in the moment definition [Picinbono, 1993]. However, the conventional conjugation pattern may not exhaust all the statistical information available from the second-order moments of the complex-valued process, the alternative conjugation pattern may need to be considered as well. We call quantities resulting from the conventional conjugation pattern Hermitian quantities, while quantities obtained from the alternative

conjugation pattern are denoted complementary quantities. Important results concerning the second-order statistics of complex-valued processes can be found in [Picinbono and Bondon, 1997; Schreier and Scharf, 2003b; Schreier and Scharf, 2003a; Scharf et al., 2005].

Both the Hermitian and the complementary second-order moments of a harmonizable process can be described in four domains, namely the dual-time domain, the dual-frequency domain, the ambiguity domain and the time-frequency domain. All four domains are related through Fourier Transforms (FT) and thus contain the same statistical information, but they focus on different features of the process. Since nonstationary processes may have a time-varying frequency content, much effort has been devoted to representing processes simultaneously in global time and global frequency. The time-frequency domain is the one of the four which has the most intuitive interpretation. We can compare a time-frequency representation to a musical score sheet, which tells the musician what tones (frequencies) to play at which time instants. The time-frequency domain is also the easiest to interpret results in. This is not to say that some processes may not have a more natural expression in one of the other domains. Harmonizable cyclostationary processes [Yaglom, 1987], e.g., are most naturally described in the dual-frequency domain.

A multitude of different time-frequency representations have been proposed [Cohen, 1995; Hlawatsch, 1998; Flandrin, 1999], and the most popular representations are the members of Cohen's class of bilinear representations [Cohen, 1995]. The Kirkwood-Rihaczek time-frequency spectrum was introduced in a quantum mechanic context by Kirkwood [Kirkwood, 1933], and later by Rihaczek [Rihaczek, 1968] in a deterministic signal theory context. We prefer to represent the process in the time-frequency domain through the Kirkwood-Rihaczek spectrum, because it is the only member of Cohen's class that is a Hilbert space inner product. Another possible time-frequency descriptor related to the Kirkwood-Rihaczek spectrum is the time-frequency spectral coherence. Spectral coherences are objective and normalized dimensionless measures of the second-order statistic of a random processes. The second-order moments may also be expressed by a spectral coherence in the dual-frequency domain. The spectral coherences, in addition to being objective and normalized, have the advantage that the Hermitian and the complementary information may be merged together in one measure.

The ambiguity domain is also a time-frequency domain, but it describes the second-order moments in local time (time shifts) and local frequency (frequency offsets). The ambiguity domain has historically been given little attention in connection with random processes. However, lately there has been some interest in this domain connected to the concept of underspread processes [Kozek, 1997]. A random process is (strictly) underspread if its ambiguity function is nonzero only for some small area around the origin in the ambiguity plane. The ambiguity function relates the degree of smoothness in the other three domains, because assuming smoothness in global time is equivalent to assuming a decay in local frequency in the ambiguity domain, and assuming smoothness in the global frequency is equivalent to assuming a decay in the local time in the ambiguity domain. The field of global time-frequency analysis have been troubled by the fact that there are infinitely many possible time-frequency representations. There are no definite rules as to what properties a time-frequency spectrum must fulfill, even if systematic approaches

have been attempted [Loynes, 1968]. Thus, many different time-frequency spectra are defined and all satisfy different sets of conditions, and all spectra are claimed to be the best in some way. The problem becomes choosing a suitable time-frequency representation, which may even be process dependent. In [Matz and Hlawatsch, 2006], it was shown that many different classes of global time-frequency spectra yield approximately equal results for underspread processes. The behavior in the ambiguity domain is related to the behavior in time-frequency in this manner, and this behavior is thus interesting from a time-frequency viewpoint.

The thesis is organized as follows. In Chapter 2 we introduce the concept of harmonizable processes and the Hermitian and complementary second-order moments. We also introduce different concepts used later in the thesis, and give a quick summary of how the quantities in the dual-time domain and the dual-frequency-spectra may be estimated. The four following Chapters contain original work, where parts have been published and parts are under consideration for publishing. The Kirkwood-Rihaczek spectra are discussed in more detail in Chapter 3. We propose estimators for the spectra, and these estimators are tested on simulated and real-world data. This work has partially been published in [Hindberg et al., 2006]. Chapter 4 deals with the Hermitian ambiguity function, more specifically how to estimate it when the underlying process is underspread. Our estimation procedure allows us to estimate how underspread the process is as well, which is interesting in connection to the global time-frequency description. This work was partly presented at a conference [Hindberg et al., 2008] and is currently under review [Hindberg and Olhede, 2009]. We propose spectral coherence measures in both time-frequency and dual-frequency in Chapter 5, these measures simultaneously utilize both the Hermitian and the complementary quantities of complex-valued harmonizable processes. This work was published in [Hindberg and Hanssen, 2007]. We consider stochastic differential equations in Chapter 6, and provide additional insight into these type of stochastic equations through representations in the time-frequency domain. Finally, we provide a summary of the thesis in Chapter 7.

Chapter 2

Harmonizable Processes

This Chapter will serve as an introduction to harmonizable processes and related concepts. We consider both continuous and discrete time, and all eight Hermitian and complementary second-order moments are introduced for each case. In practice, all second-order moment functions must be estimated from available data. We will focus on estimation in two of the possible domains in Chapter 3 and 4. For completeness, this Chapter contains a sketch on how the moments in the other two domains can be estimated. In testing estimators one needs to be able to simulate data. We propose a method to simulate data from a nonstationary complex-valued process. Finally, we briefly introduce the concepts of harmonizable random fields.

2.1 Continuous Time

In this thesis, $X(t)$ will denote a zero-mean, continuous-time, and harmonizable complex-valued random process. The process has a Cramér-Loève, or spectral representation [Cramér, 1940; Loève, 1978]

$$X(t) = \int e^{j2\pi ft} d\tilde{X}(f), \quad (2.1)$$

where $d\tilde{X}(f)$ is the complex-valued increment process of $X(t)$ [Yaglom, 1987]. All integrals are over the entire real axis unless otherwise specified. From (2.1), we can interpret the random process $X(t)$ as a superposition of correlated, random, infinitesimal harmonic oscillators, since the complex-valued weight function $d\tilde{X}(f)$ is random, and contributes by an infinitesimal amount for each frequency f . We are, however, not interested in the actual values of the increment process $d\tilde{X}(f)$, but rather its moments, or correlation properties. If the process in question is Gaussian, the first and second-order moments of the process describe the moments of the process to all orders. The first-order moment of $X(t)$ is assumed to be zero, thus we concentrate on the second-order moments. We note that many real-world processes are not Gaussian, and for these processes one must also consider higher-order moment functions.

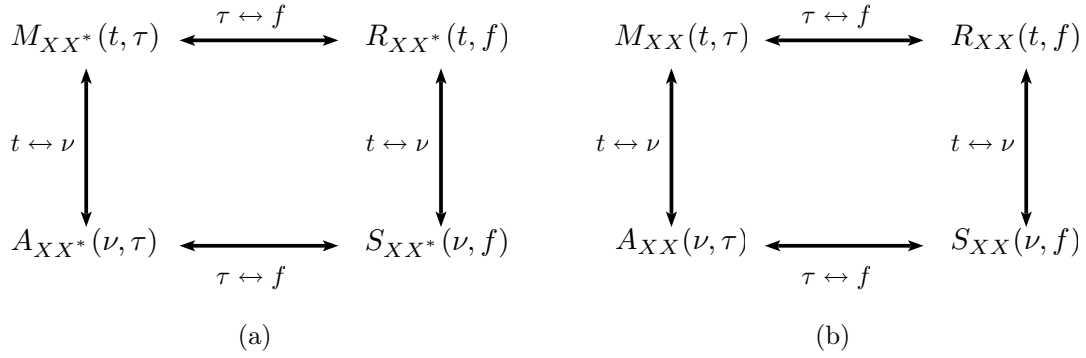


Figure 2.1: (a) Relations between the Hermitian second-order moments. (b) Relations between the complementary second-order moments.

The Hermitian second-order moments of $X(t)$ can be expressed by the Hermitian dual-time correlation

$$M_{XX^*}(t, \tau) = \text{E} \{ X(t) X^*(t - \tau) \}, \quad (2.2)$$

the Hermitian dual-frequency spectrum

$$S_{XX^*}(\nu, f) d\nu df = \text{E} \left\{ d\tilde{X}(f + \nu) d\tilde{X}^*(f) \right\}, \quad (2.3)$$

the Hermitian Kirkwood-Rihaczek time-frequency spectrum (or HKR-spectrum)

$$R_{XX^*}(t, f) df = \text{E} \left\{ X(t) \left[d\tilde{X}(f) e^{j2\pi ft} \right]^* \right\}, \quad (2.4)$$

or the Hermitian ambiguity function

$$A_{XX^*}(\nu, \tau) = \int S_{XX^*}(\nu, f) e^{j2\pi f \tau} df = \int M_{XX^*}(t, \tau) e^{j2\pi \nu t} dt. \quad (2.5)$$

Here, $\text{E} \{ \cdot \}$ is the expectation operator and $*$ denotes complex conjugation. The variables t and f are global variables of time and frequency, respectively. Likewise, τ is a local time variable, or time shift, and ν is a local frequency variable, or frequency offset. If we define the Hilbert space inner product between two random variables Q and Z as $\langle Q, Z \rangle = \text{E} \{ Q Z^* \}$, we see that $S_{XX^*}(\nu, f)$, $M_{XX^*}(t, \tau)$ and $R_{XX^*}(t, f)$ are Hilbert space inner products, while the Hermitian ambiguity function is not.

The four quantities are linked through FTs as shown in Figure 2.1(a), and thus contain the same statistical information. However, each quantity has a different focus. The Hermitian dual-time correlation tells us how the process at the global time t is correlated to the process at a time instant shifted τ from this time. Similarly, the Hermitian dual-frequency spectrum relates the increment process at different frequencies. The HKR-spectrum measures the correlation between the process itself at time t and the modulated

increment process at frequency f , the latter being the integrand of the spectral representation in (2.1). The Hermitian ambiguity function has no simple interpretation as a correlation. However, we may note that a relatively large value of $|A_{XX^*}(\nu, \tau)|$ at a point (ν_0, τ_0) in the ambiguity plane tells us that for some time(s) t , the process at time t is strongly correlated with the process shifted by τ_0 from t . Likewise, the increment process is, for some frequency (or frequencies) f , correlated to the increment process shifted from f by ν_0 . It is a function of local variables that describes the correlation lengths of the process in time and frequency.

A complex-valued process will, in addition to the Hermitian second-order moments, have complementary second-order moments [Picinbono and Bondon, 1997; Schreier and Scharf, 2003b]. These are the complementary dual-time correlation

$$M_{XX}(t, \tau) = \text{E} \{X(t)X(t - \tau)\}, \quad (2.6)$$

the complementary dual-frequency spectrum

$$S_{XX}(\nu, f)d\nu df = \text{E} \left\{ d\tilde{X}(f + \nu)d\tilde{X}(-f) \right\}, \quad (2.7)$$

the complementary Kirkwood-Rihaczek time-frequency spectrum (or the CKR-spectrum)

$$R_{XX}(t, f)df = \text{E} \left\{ X(t)d\tilde{X}(-f)e^{-j2\pi ft} \right\}, \quad (2.8)$$

and the complementary ambiguity function

$$A_{XX}(\nu, \tau) = \int S_{XX}(\nu, f)e^{j2\pi f\tau} df = \int M_{XX}(t, \tau)e^{j2\pi\nu t} dt. \quad (2.9)$$

These complementary quantities are also related through FTs, as shown in Figure 2.1(b).

As the Hermitian quantities, the complementary correlations all contain the same statistical information, but with different focus. The difference between $M_{XX^*}(t, \tau)$ and $M_{XX}(t, \tau)$ is the complex conjugation of $X(t - \tau)$ in the former. Thus, for real-valued processes, these two quantities are identical, and it follows that all complementary quantities are equal to their corresponding Hermitian quantities for real-valued processes. We note that a real-valued process will have an increment process with the Hermitian symmetry $d\tilde{X}(-f) = d\tilde{X}^*(f)$. The complementary quantities can be interpreted through correlations similarly as the Hermitian quantities (except for the ambiguity function). The complementary dual-time correlation is the correlation between the process itself at t and the complex conjugated of the process at time $t - \tau$, and so on. However, it is not intuitively clear what we can infer from a correlation between the process itself and its complex conjugate. A process that has no complementary correlations, i.e., $M_{XX^*}(t, \tau) = 0, \forall t, \tau$, is denoted a proper process [Neuser and Massey, 1993], and a proper process has to be complex-valued. For an improper complex-valued harmonizable process we require one of the four Hermitian quantities and one of the four complementary quantities to completely describe the second-order moments of the process. Finally, we note that $X(t)$ is a harmonizable process if and only if the dual-frequency spectra are 2-dimensional FTs of the dual-time correlations, and both $S_{XX^*}(\nu, f)$ and $S_{XX}(\nu, f)$ are absolute integrable over the entire dual-frequency plane [Yaglom, 1987].

2.1.1 Cross-moments

It may be of interest to study how two different mutually harmonizable processes $X(t)$ and $Y(t)$ are correlated. The Hermitian second-order cross-moments of the two mutually harmonizable processes are defined as

$$M_{XY^*}(t, \tau) = \mathbb{E} \{ X(t)Y^*(t - \tau) \} \quad (2.10)$$

$$S_{XY^*}(\nu, f)d\nu df = \mathbb{E} \left\{ d\tilde{X}(f + \nu)d\tilde{Y}^*(f) \right\} \quad (2.11)$$

$$R_{XY^*}(t, f)df = \mathbb{E} \left\{ X(t) \left[d\tilde{Y}(f)e^{j2\pi ft} \right]^* \right\} \quad (2.12)$$

$$A_{XY^*}(\nu, \tau) = \int S_{XY^*}(\nu, f)e^{j2\pi f\tau} df, \quad (2.13)$$

and the complementary cross-moments are defined similarly. Here, $d\tilde{X}(f)$ and $d\tilde{Y}(f)$ are the increment processes of $X(t)$ and $Y(t)$, respectively. The cross-moments have a similar interpretation as correlation between different time instants and frequencies, but here as a correlation between two different processes. Note that for general complex-valued processes, we have $M_{XY^*}(t, \tau) \neq M_{YX^*}(t, \tau)$, and the same applies to the seven other second-order moments. The moments in (2.2)–(2.9) are sometimes referred to as autocorrelations, since they only involve a single process $X(t)$.

2.1.2 Stationary processes

Stationary processes constitute an important subclass of harmonizable processes, for which the probability densities governing the process do not change with time. In order to check for stationarity in the strictest sense, one must consider the joint probability distribution for the process at different time instants. This is quite complicated, and it is common to consider weaker types of stationarity instead. A process is said to be wide sense stationary [Priestley, 1988; Picinbono and Bondon, 1997] if its second-order moments are of the form

$$M_{XX^*}(t, \tau) = M_{XX^*}(\tau) \quad M_{XX}(t, \tau) = M_{XX}(\tau) \quad (2.14)$$

$$S_{XX^*}(\nu, f) = S_{XX^*}(f)\delta(\nu) \quad S_{XX}(\nu, f) = S_{XX}(f)\delta(\nu) \quad (2.15)$$

$$R_{XX^*}(t, f) = S_{XX^*}(f) \quad R_{XX}(t, f) = S_{XX}(f) \quad (2.16)$$

$$A_{XX^*}(\nu, \tau) = M_{XX^*}(\tau)\delta(\nu) \quad A_{XX}(\nu, \tau) = M_{XX}(\tau)\delta(\nu). \quad (2.17)$$

Here, $S_{XX^*}(f)df = \mathbb{E} \left\{ d\tilde{X}(f)d\tilde{X}^*(f) \right\}$ is the so-called power spectral density of the process, $M_{XX^*}(\tau) = \mathbb{E} \{ X(t)X^*(t - \tau) \}$ is the conventional autocorrelation function, and $S_{XX}(f)$ and $M_{XX}(\tau)$ are the complementary equivalents. Also, $\delta(\cdot)$ is Dirac's delta function. We note that for stationary processes, both dual-frequency spectra and both ambiguity functions are nonzero only for $\nu = 0$. This line $\nu = 0$ is called the stationary manifold. The time-frequency spectra do not change with time, and the dual-time correlation is independent of the global time, it only depends on the difference between the two

time instants. In the following we understand that a stationary process is stationary in the wide sense. Note that strict sense stationary implies the wide sense, but not vice versa.

Motivating example for complementary correlations

To illustrate the importance of the information contained in the complementary quantities, we consider a simple example. Let $Y(t)$ denote a real-valued, stationary process with power spectral density $S_{YY^*}(f)$. We define a complex-valued process $X(t)$ as

$$X(t) = e^{j2\pi f_0 t} Y(t), \quad (2.18)$$

where f_0 is a constant frequency. In other words, we let the process $Y(t)$ amplitude modulate the complex carrier $\exp(j2\pi f_0 t)$. We obtain the Hermitian dual-frequency spectrum of $X(t)$ as

$$S_{XX^*}(\nu, f) = S_{YY^*}(f - f_0)\delta(\nu). \quad (2.19)$$

Since $S_{XX^*}(\nu, f)$ is nonzero only on the stationary manifold $\nu = 0$, the process $X(t)$ appears to be a stationary process with power spectral density $S_{YY^*}(f - f_0)$. However, the complementary dual-frequency spectrum of $X(t)$ is

$$S_{XX}(\nu, f) = S_{YY^*}(f + f_0)\delta(\nu - 2f_0), \quad (2.20)$$

i.e., it is nonzero only on the line $\nu = 2f_0$ parallel to the stationary manifold. The process $X(t)$ is in fact a harmonizable cyclostationary process. We see that if we only consider the Hermitian quantities, we would erroneously conclude that the process is stationary.

2.1.3 Analytic processes

Analytic signals have been used in a wide variety of fields, and especially in time-frequency analysis, because it can reduce the bandwidth of real-valued signals, see e.g., [Flandrin, 1999]). The concept of instantaneous frequency also requires that the signal under consideration is analytic. Simply put, an analytic signal is a signal whose FT is zero for negative frequencies. Thus, an analytic harmonizable process has the spectral representation (2.1), but with integration limits from 0 to ∞ . Most analytic processes can be thought of as corresponding to a real-valued process, i.e., we remove the frequency content for $f < 0$ from the real-valued process to obtain the analytic process (see e.g., [Picinbono, 1993] for a more detailed treatment of analytic processes). Thus, if $X(t)$ is the analytic process corresponding to the real-valued harmonizable process $Y(t)$, we have

$$X(t) = \int_0^{\infty} e^{j2\pi ft} d\tilde{X}(f) = 2 \int_0^{\infty} e^{j2\pi ft} u(f) d\tilde{Y}(f), \quad (2.21)$$

where

$$u(f) = \begin{cases} 1 & f \geq 0 \\ 0 & f < 0 \end{cases} \quad (2.22)$$

is the unit step function. The factor 2 is included such that $\text{Re}\{X(t)\} = Y(t)$, where $\text{Re}\{\cdot\}$ denotes the real value operator (correspondingly, $\text{Im}\{\cdot\}$ is the imaginary value operator). Analytic processes are necessarily complex-valued, since they have a one-sided spectral representation. An analytic process corresponding to a real-valued stationary process is proper [Picinbono and Bondon, 1997], whereas an analytic process corresponding to a real-valued harmonizable process is in general improper [Schreier and Scharf, 2003b].

Since $d\tilde{X}(f)$ has its support on non-negative frequencies only, the second-order moments of an analytic process will have limited support. The Hermitian dual-frequency spectrum is supported on $\{f \geq 0, \nu \geq -f\}$, and the complementary dual-frequency spectrum is supported on $\{f \leq 0, \nu \geq -f\}$. The HKR-spectrum is nonzero for $f \geq 0$ and the CKR-spectrum is nonzero for $f \leq 0$. In the case where $X(t)$ corresponds to a real-valued process $Y(t)$, the second-order moments of $X(t)$ can be expressed as functions of the second-order moments of $Y(t)$, see [Hindberg, 2005] for details.

2.2 Discrete Time

Even though random processes are easy to handle mathematically in continuous time, real-world data will have to be considered in discrete time. A zero-mean, discrete-time, and harmonizable complex-valued random process has a spectral representation [Cramér, 1940; Loève, 1978]

$$X[n] = \int_{-1/2}^{1/2} e^{j2\pi fn} d\tilde{X}(f). \quad (2.23)$$

In this thesis, we use $[\cdot]$ to denote a discrete variable and (\cdot) to denote a continuous variable, while (\cdot, \cdot) and $[\cdot, \cdot)$ denotes a mixed pair of variables. If $X[n]$ is sampled from a continuous-time process $X(t)$ with sampling frequency f_s , then $X[n]$ has the spectral representation (2.23) with integration limits going from $-f_s/2$ to $f_s/2$. We assume that $f_s = 1$ unless otherwise specified. Likewise, $X[n]$ is always assumed to be alias-free, i.e., $X(t)$ is bandlimited and the sampling rate satisfies the Nyquist criterion [Shannon, 1949].

The Hermitian moments of a discrete-time harmonizable process are given by

$$M_{XX^*}[n, \eta] = \text{E} \{X[n]X^*[n - \eta]\} \quad (2.24)$$

$$S_{XX^*}(\nu, f) d\nu df = \text{E} \left\{ d\tilde{X}(f + \nu) d\tilde{X}^*(f) \right\} \quad (2.25)$$

$$R_{XX^*}[n, f] df = \text{E} \left\{ X[n] \left[d\tilde{X}(f) e^{j2\pi fn} \right]^* \right\} \quad (2.26)$$

$$A_{XX^*}(\nu, \eta) = \sum_{n=-\infty}^{\infty} M_{XX^*}[n, \eta] e^{j2\pi\nu n}, \quad (2.27)$$

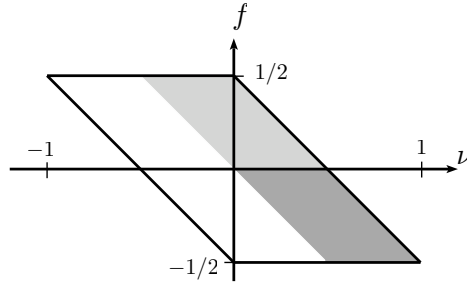


Figure 2.2: The dual-frequency spectra for a discrete-time processes are nonzero only within the parallelogram. The lighter shaded area and darker shaded area are the support of the Hermitian and complementary dual-frequency spectrum, respectively, for analytic discrete-time processes.

and the complementary moments are given by

$$M_{XX}[n, \eta] = \text{E} \{ X[n]X[n - \eta] \} \quad (2.28)$$

$$S_{XX}(\nu, f) d\nu df = \text{E} \left\{ d\tilde{X}(f + \nu) d\tilde{X}(-f) \right\} \quad (2.29)$$

$$R_{XX}[n, f] df = \text{E} \left\{ X[n] d\tilde{X}(f) e^{-j2\pi fn} \right\} \quad (2.30)$$

$$A_{XX}(\nu, \eta) = \sum_{n=-\infty}^{\infty} M_{XX}[n, \eta] e^{j2\pi\nu n}. \quad (2.31)$$

The ambiguity functions may also be expressed as inverse FTs of the dual-frequency spectra. Note that the form of the dual-frequency spectra are the same as for continuous-time. However, for a discrete-time process, $S_{XX^*}(\nu, f)$ is nonzero only for $-1/2 \leq f \leq 1/2$ and $-1/2 \leq f + \nu \leq 1/2$, which gives us values of ν between -1 and 1. Figure 2.2 shows the support of the dual-frequency spectra in this case. Extending the concepts of cross-moments and stationary processes to discrete-time processes is straightforward. A discrete-time analytic harmonizable process is defined by (2.23) with integration limits from 0 to 1/2. The support of the dual-frequency spectra for analytic processes is also shown in Figure 2.2.

2.2.1 Estimators of the second-order moments

As we in practice will deal with processes in discrete time, we will have available finite length realizations of the process, and we aim to learn about the process itself from these realizations. Thus, we need to be able to *estimate* the second-order quantities of the process based on one realization $x[n]$ of the process $X[n]$ (that may be sampled from a continuous-time process). If more than one realization is available, we estimate the quantity separately from each realization and average the different estimates. We deal with estimation of the KR-spectra and the Hermitian ambiguity function in Chapter 3 and Chapter 4, respectively.

For completeness, we will here briefly sketch how the other second-order quantities can be estimated.

A general estimator of the Hermitian dual-time correlation is [Martin and Flandrin, 1985]

$$\widehat{M}_{XX^*}[n, \eta] = \sum_{m=-\infty}^{\infty} x[n+m]\Phi[m, \eta]x^*[n-\eta+m]. \quad (2.32)$$

The complementary dual-time correlation can likewise be estimated by [Hindberg, 2005]

$$\widehat{M}_{XX}[n, \eta] = \sum_{m=-\infty}^{\infty} x[n+m]\Phi[m, \eta]x[n-\eta+m]. \quad (2.33)$$

Here, $\Phi[u, \kappa]$ is a data window that corresponds to a smoothing in the global time direction. [Larsen, 2003] states that for white processes, the dual-time correlation is restricted to the line $\eta = 0$. For broadband processes, the dual-time correlation is expected to decay rapidly as a function of η . We therefore seek to avoid smoothing in the local time direction. A white process is characterized by that it is completely uncorrelated in time, i.e., $M_{XX^*}[n, \eta] = \text{E}\{|X[n]|^2\} \delta[\eta]$ and, if the process is improper, $M_{XX}[n, \eta] = \text{E}\{X^2[n]\} \delta[\eta]$, where $\delta[\eta]$ is the Kronecker delta.

The multitaper approach to spectral estimation was introduced in [Thomson, 1982]. Using the multitaper formalism, the Hermitian and complementary dual-frequency spectrum can be estimated by [Larsen, 2003; Hindberg, 2005]

$$\widehat{S}_{XX^*}(\nu, f) = \frac{1}{M} \sum_{m=0}^{M-1} \frac{Z_m(f+\nu)Z_m^*(f)}{\lambda_m}, \quad (2.34)$$

and

$$\widehat{S}_{XX}(\nu, f) = \frac{1}{M} \sum_{m=0}^{M-1} \frac{Z_m(f+\nu)Z_m(-f)}{\lambda_m}, \quad (2.35)$$

where

$$Z_m(f) = \sum_{n=0}^{N-1} x[n]v_m[n]e^{-j2\pi fn}. \quad (2.36)$$

Here, $\{v_m[n]\}_{m=1}^M$ is a set of M orthogonal data tapers, and $\{\lambda_m\}$ is a set of associated eigenvalues. We produce M estimates of the increment process through M tapered Discrete-Time FTs (DTFT) of the data with the M orthogonal tapers. For each taper v_m , the estimate $Z_m(f)$ replaces $d\widetilde{X}(f)$ in the definitions of the dual-frequency spectra and the expectation operator is ignored. The M obtained estimates of the spectra are then averaged to produce the final estimates.

The Discrete Prolate Spheroidal Sequences (DPSSs) [Slepian, 1978] are a preferred choice for the data tapers in this procedure, but other choices are possible. The DPSSs are optimal data tapers in the following sense. Out of all data tapers of length N , the zero

order DPSS with time-bandwidth product NW is the taper that has most of its energy in the frequency domain concentrated in the frequency band $[-W, W]$. We next consider the set of all data tapers of length N that are orthogonal to the zero order DPSS. The first order DPSS is the data taper in this set that has most of its energy concentrated in the frequency band $[-W, W]$. The second-order DPSS is likewise determined by considering the set of all tapers that are orthogonal to both the zero order and the first order DPSS, and so on. Because the DPSSs are designed to have most of their energy inside their main lobe $[-W, W]$, they have low sidelobe levels that will reduce spectral leakage. Averaging over multiple orthogonal windows reduces the variance of the estimator as well. When we work with DPSS, we must specify the length of the taper N and the time-bandwidth product NW , which corresponds to specifying the bandwidth for the chosen length. See [Larsen, 2003] and [Hindberg, 2005] for further details on these estimators.

2.2.2 Simulation of improper processes

In order to test estimators, we often want to employ the estimators to simulated data sets for which we know the true form of the second-order moments. A method for simulating from a specified improper stationary process $Y[n]$ was proposed in [Rubin-Delanchy and Walden, 2007]. One specifies the wanted $S_{YY^*}(f)$ and $S_{YY}(f)$ of the process $Y[n]$, and simulate realizations of the process by a manipulation of white noise. The improper stationary process is given by

$$Y[n] = \sum_{m=-\infty}^{\infty} g[m]\epsilon[n-m] + \sum_{m=-\infty}^{\infty} h[m]\epsilon^*[n-m]. \quad (2.37)$$

Here, $g[n]$ and $h[n]$ are filters derived from $S_{YY^*}(f)$ and $S_{YY}(f)$, and $\epsilon[n]$ is proper white noise. To simulate from this process, we limit the summation to some interval $m = -M, \dots, M$ that include the significant filter coefficients of the filters and generate a realization of $\epsilon[n]$, see [Rubin-Delanchy and Walden, 2007] for further details.

Inspired by this, we propose to specify a nonstationary improper process from $Y[n]$ by applying a time-varying variance, $\sigma^2[n]$, to the proper white noise in (2.37),

$$X[n] = \sum_{m=-\infty}^{\infty} g[m]\sigma[n-m]\epsilon[n-m] + \sum_{m=-\infty}^{\infty} h[m]\sigma[n-m]\epsilon^*[n-m]. \quad (2.38)$$

The process $X[n]$ is ensured to be harmonizable if the DTFT of $\sigma^2[n]$,

$$\Sigma(f) = \sum_{n=-\infty}^{\infty} \sigma^2[n]e^{-j2\pi n f}, \quad (2.39)$$

is absolutely integrable. We find the second-order moments of this harmonizable process

as

$$M_{XX^*}[n, \eta] = \sum_{m=-\infty}^{\infty} \sigma^2[n-m] (M_{gg^*}[m, \eta] + M_{hh^*}[m, \eta]) \quad (2.40)$$

$$S_{XX^*}(\nu, f) = \Sigma(\nu) (S_{gg^*}(\nu, f) + S_{hh^*}(\nu, f)) \quad (2.41)$$

$$R_{XX^*}[n, f] = \sum_{m=-\infty}^{\infty} \sigma^2[n-m] (R_{gg^*}[m, f] + R_{hh^*}[m, f]) \quad (2.42)$$

$$A_{XX^*}(\nu, \eta) = \Sigma(\nu) \sum_{m=-\infty}^{\infty} (M_{gg^*}[m, \eta] + M_{hh^*}[m, \eta]) e^{-j2\pi\nu m} \quad (2.43)$$

and

$$M_{XX}[n, \eta] = \sum_{m=-\infty}^{\infty} \sigma^2[n-m] (M_{gh}[m, \eta] + M_{hg}[m, \eta]) \quad (2.44)$$

$$S_{XX}(\nu, f) = \Sigma(\nu) (S_{gh}(\nu, f) + S_{hg}(\nu, f)) \quad (2.45)$$

$$R_{XX}[n, f] = \sum_{m=-\infty}^{\infty} \sigma^2[n-m] (R_{gh}[m, f] + R_{hg}[m, f]) \quad (2.46)$$

$$A_{XX}(\nu, \eta) = \Sigma(\nu) \sum_{m=-\infty}^{\infty} (M_{gh}[m, \eta] + M_{hg}[m, \eta]) e^{-j2\pi\nu m}. \quad (2.47)$$

Here, we have implicitly defined second-order auto and cross-functions for the deterministic filters $g[n]$ and $h[n]$ corresponding to the second-order moments of harmonizable processes. Thus, the Hermitian quantities of $X[n]$ depend on the corresponding Hermitian quantities of the deterministic filters. The complementary quantities of $X[n]$, however, depends on the corresponding complementary cross-moments of $g[n]$ and $h[n]$. This is caused by the fact that the noise is proper, thus eliminating all terms where two noise terms have equal conjugation. We note that this is only one of many possible ways of extending the simulation process to include nonstationary processes.

2.3 Random Fields

We consider random functions of time and space, so-called random fields [Yaglom, 1987]. Let $X(r, t)$ be an inhomogeneous, harmonizable random field at time t and at a scalar spatial variable r . We will only consider one-dimensional space, but the extension to higher-dimensional space is straightforward. The spectral representation of $X(r, t)$ is [Larsen, 2003; Hanssen, 2009]

$$X(r, t) = \iint e^{j2\pi(qr+ft)} d\tilde{X}(q, f), \quad (2.48)$$

where q is related to the wavenumber k by $k = 2\pi q$, and the increment field $d\tilde{X}(q, f)$ is now two-dimensional. The Hermitian second-order moments of a random field are given

by the Hermitian spatio-temporal correlation

$$M_{XX^*}(r, \rho, t, \tau) = \mathbb{E} \{X(r, t)X^*(r - \rho, t - \tau)\}, \quad (2.49)$$

the Hermitian dual-frequency dual-wavenumber spectrum

$$S_{XX^*}(\kappa, q, \nu, f)d\kappa dq d\nu df = \mathbb{E} \left\{ d\tilde{X}(q + \kappa, f + \nu)d\tilde{X}^*(q, f) \right\}, \quad (2.50)$$

the HKR time-frequency space-wavenumber spectrum

$$R_{XX^*}(r, q, t, f)df dq = \mathbb{E} \left\{ X(r, t) \left(d\tilde{X}(q, f)e^{j2\pi(tf+qr)} \right)^* \right\} \quad (2.51)$$

and the Hermitian spatio-temporal ambiguity function

$$A_{XX^*}(\kappa, \rho, \nu, \tau) = \iint S_{XX^*}(\kappa, q, \nu, f)e^{j2\pi(f\tau+q\rho)}dqdf. \quad (2.52)$$

We define the complementary second-order moments of random fields in a straightforward similar manner. Cross-moments of random fields are also easily defined from these expressions.

If a random field is homogeneous, the increment field is orthogonal in wavenumber q , and the probability densities governing the field does not depend on the spatial coordinate. This is similar to the stationary case, for which the increment process is orthogonal in frequency. A homogeneous and stationary random field has a Hermitian dual-frequency dual-wavenumber spectrum of the form

$$S_{XX^*}(\kappa, q, \nu, f) = S_{XX^*}(q, f)\delta(\nu)\delta(\kappa), \quad (2.53)$$

and a HKR time-frequency space-wavenumber spectrum

$$R_{XX^*}(r, q, t, f) = S_{XX^*}(q, f). \quad (2.54)$$

Thus, $S_{XX^*}(\kappa, q, \nu, f)$ is restricted to $\{(\kappa, q, \nu, f) | \kappa = 0, q \in \mathbb{R}, \nu = 0, f \in \mathbb{R}\}$, which is denoted the stationary and homogeneous manifold for random fields. We note that $R_{XX^*}(r, q, t, f)$ for homogeneous and stationary fields does not change with time t or with the spatial coordinate r .

The formalism for random fields is very similar to that of random processes, with what appears as only a simple expansion to a bivariate random function instead of a univariate random function. Mathematically, the extension is simple, but physically a random field will have inherent constraints related to the physical medium that the field exists in. One of the main challenges is that a spatial medium can be dispersive, such that different frequencies propagate through the medium at different speeds [Cohen, 1995]. See [Hanssen, 2009] for a detailed treatment of random fields in dispersive media.

Chapter 3

The Kirkwood-Rihaczek Time-Frequency Spectra

Time-frequency analysis is an important tool for analyzing nonstationary random processes. Cohen's class [Cohen, 1966] consists of the time-frequency spectra that are bilinear (or quadratic) functions of the signal, and that are covariant to shifts in time and frequency. The spectrogram and the Wigner-Ville spectrum [Wigner, 1932; Ville, 1948] are perhaps the most popular members of this class. A common misconception is that these are distributions of *power* or *energy* over time and frequency. This is not correct, and we quote Wigner's theorem [Wigner, 1971] from [Flandrin, 1999] "There exists no time-frequency representation that is bilinear, has correct marginal distributions, and is nonnegative everywhere." Energy/power is a nonnegative quadratic quantity of the process, such that any distribution of energy/power has to be a bilinear function of the process. Also, a joint distribution of energy/power in time-frequency should, analogous to joint distributions of random variables, have marginal distributions equal to the energy/power marginal distributions in time and frequency separately. Wigner's theorem states that there are no distributions that fulfill all three demands. Thus, no time-frequency spectrum is a joint distribution of energy/power over time and frequency.

However, the HKR-spectrum can unambiguously be interpreted as a distribution of correlation, or a complex Hilbert space inner product between the process and its infinitesimal stochastic Fourier generator, as discussed in [Scharf et al., 2005]. It is related to the Wigner-Ville distribution and the spectrogram through a general time-frequency distribution [Claasen and Mecklenbräuker, 1980]. Unlike the Wigner-Ville and the spectrogram, the Hermitian Kirkwood-Rihaczek distribution is a complex-valued quantity. It is very important to understand the uniqueness of the fact that the HKR time-frequency spectrum is a Hilbert space inner product. In fact, no other members of the time-frequency spectra contained in Cohen's class are inner products. This is a very significant result, which renders the interpretation of HKR-spectrum attractive from a fundamental and practical point of view.

Among its other attractive properties, we mention that the time marginal and the

frequency marginal of the HKR-spectrum are the instantaneous power of the process

$$\int R_{XX^*}(t, f)df = M_{XX^*}(t, 0) = E \{|X(t)|^2\} \quad (3.1)$$

and the power spectral density

$$df \int R_{XX^*}(t, f)dt = S_{XX^*}(0, f)df, \quad (3.2)$$

respectively (see [Hanssen and Scharf, 2003; Scharf et al., 2005] for further details). We also note that the CKR-spectrum has a time marginal

$$\int R_{XX}(t, f)df = M_{XX}(t, 0) = E \{X^2(t)\}, \quad (3.3)$$

and a frequency marginal

$$df \int R_{XX}(t, f)dt = S_{XX}(0, f)df \quad (3.4)$$

which corresponds to the complementary spectral density of a stationary processes. Correct marginals is one of the most sought after properties of time-frequency representations, one needs correct marginals for the time-frequency spectrum to be a distribution of energy/power. As we have argued, from Wigner's theorem we know that it is impossible to define such a distribution. Also, the KR-spectra are obviously not distributions of energy/power, since they are complex-valued quantities. However, the KR-spectra have an interpretation as a joint distribution of correlations in time and frequency, and the marginals are the marginal distribution of correlations in time and the marginal distribution of correlations in frequency.

3.1 Estimation

We will now propose useful estimators for the various KR-spectra. Any member of Cohen's class can be estimated by [Martin and Flandrin, 1985]

$$\widehat{R}_{XX^*}[n, f] = \sum_{m, \mu=-\infty}^{\infty} x[n+m]\phi[m, \mu]x^*[n+m-\mu]e^{-j2\pi\mu f}, \quad (3.5)$$

where the kernel $\phi[m, \mu]$ determines which time-frequency spectrum is estimated. Estimation of the KR-spectra was discussed in [Scharf et al., 2005], and the kernel $\phi'[m, \mu] = w_1[m]w_2[\mu]w_3[m-\mu]$ was proposed, where $w_1[m]$, $w_2[\mu]$, and $w_3[m]$ are three window functions chosen by the user (all windows are assumed to be real-valued and symmetric). The CKR-spectrum is *not* a member of Cohen's class as it is not covariant under frequency shifts. If $X(t)$ has the CKR-spectrum $R_{XX}(t, f)$, then $X(t)e^{j2\pi f_0 t}$ will have a

CKR-spectrum $e^{j4\pi f_0 t} R_{XX}(t, f + f_0)$. The significance of this is not clear, and we still propose an estimator for the CKR-spectrum which is theoretically equivalent with the class of estimators in (3.5). Even if this class of estimators was specified in order to estimate time-frequency spectra in Cohen's class, there is no obvious reason why it cannot be extended to estimate the CKR-spectrum. This estimator is easily implemented, but a direct implementation will be computationally intensive. It is also not obvious how the windows in this estimator should be chosen. Instead, we will use the inner product formulation of the KR-spectra directly, which will result in an alternative, direct, and intuitive estimator which provides additional insight into the geometry of the KR-spectra.

3.1.1 Estimation based on the inner product formulation

We have N samples of a realization $x[n]$, $n = 0, 1, \dots, N - 1$, of the random process $X[n]$. In order to estimate $d\tilde{X}(f)$, we calculate a tapered DTFT of a local segment of the realization centered at sample n ,

$$\hat{z}[n, \mu; f] = \sum_{m=-N_F}^{N_F} x[n+m]v_F[m]v_B[\mu-m]e^{-j2\pi mf}, \quad (3.6)$$

for the time instants $\mu = -N_T, \dots, N_T$. This is a standard short-time FT, but where one of the data tapers depends on the time variable μ . We approximate the expectation operator in (2.4) and (2.8) with a weighted time-average and use $\hat{z}[n, \mu; f]df$ as a local estimate of $d\tilde{X}(f)$. This gives us an estimator of the HKR-spectrum as

$$\hat{R}_{XX^*}[n, f] = \sum_{\mu=-N_T}^{N_T} x[n+\mu]v_T[\mu] (\hat{z}[n, \mu; f]e^{j2\pi\mu f})^* \quad (3.7)$$

and the CKR-spectrum as

$$\hat{R}_{XX}[n, f] = \sum_{\mu=-N_T}^{N_T} x[n+\mu]v_T[\mu] \hat{z}[n, \mu; -f]e^{-j2\pi\mu f}. \quad (3.8)$$

Here, N_T and N_F determines the length of the segment used in the time average and the DTFT, respectively. The estimators proposed in (3.7) and (3.8) will be less computationally intensive than a direct implementation of (3.5). Roughly, for each time-frequency pair, the estimator in (3.5) requires two sums of length, say, L which results in L^2 operations, while (3.7) can be implemented with one sum and a Fast FT, i.e., in $L \log(L)$ operations. By inserting (3.6) in (3.7) and (3.8) and letting $N_T, N_F \rightarrow \infty$, we see that our estimators are theoretically equivalent to the estimators proposed in [Scharf et al., 2005], with $v_T[n] = w_1[n]$, $v_B[n] = w_2[n]$ and $v_F[n] = w_3[n]$.

The use of three different data windows leads to a very general estimator, and some considerations about which window types to be applied was presented in [Scharf and Friedlander, 2001]. The weighting window $v_T[\mu]$ can be chosen with the desired time resolution

for our estimate, normally with a typical bell shaped or Gaussian shaped amplitude. Likewise, since $v_B[m]$ and $v_F[m]$ will determine the frequency resolution, they should be chosen to have a narrow bandwidth and low sidelobe levels. We will see how the windows affect the marginals, resolution and cross-terms in the following. Note that the segment lengths N_T and N_F do not need to be chosen equally, in fact a choice of $N_F > N_T$ may improve the time-frequency resolution of the estimator.

3.2 Statistical Properties

Our direct estimator is theoretically equivalent to the kernel based estimator proposed in [Scharf et al., 2005], and will thus have the same asymptotic mean and variance. For a finite sample size, the expected value of the estimator for the HKR-spectrum is

$$\mathbb{E} \left\{ \widehat{R}_{XX^*}[n, f] \right\} = \sum_{\mu=-N_T-1/2}^{N_T} \int_{-1/2}^{1/2} R_{XX^*}[n + \mu, \xi] \Phi[\mu, f - \xi] d\xi. \quad (3.9)$$

The expected value of the CKR-spectrum is obtained by replacing $R_{XX^*}[n + \mu, \xi]$ with $R_{XX}[n + \mu, \xi]$ in (3.9). We define $\Phi[\mu, f]$ as the DTFT of the modulated kernel

$$\widetilde{\phi}[\mu, m] = e^{-j2\pi\mu f} v_T[\mu] v_F[m] v_B[\mu - m] \quad (3.10)$$

with respect to m ,

$$\Phi[\mu, f] = \sum_{m=-\infty}^{\infty} \widetilde{\phi}[\mu, m] e^{-j2\pi m f} = v_T[\mu] \int_{-1/2}^{1/2} V_B(\lambda) V_F^*(f - \lambda) e^{-j2\pi\mu(f-\lambda)} d\lambda. \quad (3.11)$$

Likewise, $V_F(f)$, $V_B(f)$ and $V_T(f)$ are the DTFTs of $v_F[m]$, $v_B[m]$ and $v_T[\eta]$, respectively. Thus, the expected value of the estimator is the true spectrum smoothed in time and frequency by the function $\Phi[\mu, f]$, and this function controls the time and frequency resolution of the estimate.

Because the KR-spectra are quadratic functions of the process, the variance of the estimators will depend on the fourth order moments of the process. If we assume that the process is Gaussian, we can use Isserlis' theorem [Isserlis, 1918] which relates the fourth-order moments of the process to the second-order moments. The variance of the estimators is given by

$$\begin{aligned} \text{Var} \left\{ \widehat{R}_{XX^{(*)}}[n, f] \right\} &= \iint_{-1/2}^{1/2} \sum_{\substack{m=-N_T \\ \mu=-N_T}}^{N_T} e^{j2\pi[\mu(f_1-f)+m(f-f_2)]} \\ &\left[R_{XX^*}[n + \mu, f_1] \Psi(f_1 + f_2 - 2f, f - f_2) \phi[\mu, m] R_{XX^*}^{(*)}[n + m, (-)f_2] \right. \\ &\left. + R_{XX^{(*)}}[n + \mu, f_1] \Phi^*[\mu, f + f_2] \Phi[m, f + f_1] R_{XX^{(*)}}^*[n + m, f_2] e^{j2\pi[m(f+f_1)-\mu(f+f_2)]} \right] df_1 df_2 \end{aligned}$$

where

$$\Psi(f', f) = \int_{-1/2}^{1/2} V_B(\lambda) V_F^*(f - \lambda) V_T(f' + f - \lambda) d\lambda \quad (3.12)$$

is the DTFT of $\Phi[\mu, f]$ with respect to μ . We have assumed that $N_T = N_F$ for convenience. Here, replacing $(-) = 1$ and $(*) = 1$ yields the variance of the Hermitian estimator and $(-) = -1$ and $(*) = *$ yields the variance of the complementary estimator. The form of the variance of the estimators is not very informative, but we note that the variance of the Hermitian estimator depends on the true Hermitian spectrum and the true complementary spectrum. However, the variance of the complementary estimator depends only on the true Hermitian spectrum. Thus, if a process is proper, the expected value of the complementary estimator will be zero, while the variance will be determined by the HKR-spectrum. In this case, the complementary estimator can have larger variance than the Hermitian estimator.

3.2.1 Marginals

The time marginal and frequency marginal of the HKR-spectrum are the instantaneous power of the process and the power spectral density of the process, respectively. We can thus obtain estimates of these two quantities by a simple integration (approximated with a Riemann sum) of the estimated HKR-spectrum over all frequencies (time marginal) and over all time instants (frequency marginal). In practice, the integration across frequencies are estimated with Monte Carlo integration (see e.g. [Robert and Casella, 2004]). For further insight into how the estimator and its windows work, we consider the expected value of these estimated marginals. The expected time marginal of the estimator is

$$P_{XX^*}[n] = \mathbb{E} \left\{ \int_{-1/2}^{1/2} \widehat{R}_{XX^*}[n, f] df \right\} = v_B[0] \sum_{\mu=-N_T}^{N_T} M_{XX^*}[n + \mu, 0] v_T[\mu] v_F^*[\mu]. \quad (3.13)$$

Note that the window $v_B[m]$ only contributes to a constant bias in the estimated marginal, it does not affect the smoothing in time. The smoothing is controlled by the product of the two windows $v_F[\mu]$ and $v_T[\mu]$. If $v_T[\mu]$ is supposed to control the resolution in time, we would typically chose it to be narrow in time. Also, $v_F[\mu]$ is related to the frequency resolution, which means it should be broad in time (narrow in frequency). If this is the case, we can approximate the time marginal with

$$P_{XX^*}[n] \approx v_B[0] v_F[0] \sum_{\mu=-N_T}^{N_T} M_{XX^*}[n + \mu, 0] v_T[\mu]. \quad (3.14)$$

Thus, the resolution in time will be determined mainly by the width of $v_T[\mu]$.

We find the expected frequency marginal to be

$$S_{XX^*}^M(f) = \mathbb{E} \left\{ \sum_{n=0}^{N-1} \widehat{R}_{XX^*}[n, f] \right\} = S_{XX^*}(0, f) \star V_B(f) \star [V_T(f) V_F^*(f)], \quad (3.15)$$

where \star denotes convolution. In the frequency domain, $V_F(f)$ will be narrow and $V_T(f)$ broad, such that we can approximate

$$S_{XX^*}^M(f) \approx S_{XX^*}(0, f) \star V_B(f) \star V_F^*(f). \quad (3.16)$$

The collective bandwidth of the two windows $v_B[m]$ and $v_F[m]$ approximately controls the degree of smoothing experienced by the frequency marginal. The estimator of the CKR-spectrum will have marginals with similar form, only depending on the complementary dual-time correlation and dual-frequency spectrum. The form of the expected marginals thus further support our understanding of how the three windows should be chosen.

3.2.2 Choice of parameters

The estimators of the KR-spectra have five main parameters that need to be chosen, the three windows and the two segment lengths. One can argue that the segment lengths are actually parameters of the windows themselves, but we chose to consider these as separate choices. We will consider how to choose the parameters in order to address the resolution, cross-terms and normalization properties of the estimator.

Resolution and cross-terms

When we talk about resolution (or localization) in connection to time-frequency analysis, we mean the ability of the estimators to separate different components in time and frequency, and how the estimator smears out impulses in time and frequency. For our estimator, an impulse at time $n = n_0$ will be smoothed out over the $2N_T + 1$ nearby samples, $n = n_0 - N_T, \dots, n_0 + N_T$. Likewise, a pure tone at frequency $f = f_0$ will be smoothed out over the band $f_0 - (W_F + W_B) \leq f \leq f_0 + W_F + W_B$, where W_F and W_B are the bandwidths of $v_F[n]$ and $v_B[n]$, respectively.

All members of Cohen's class suffer from what is called cross-terms or interference terms [Flandrin, 1999], which relates to the fact that the time-frequency spectra are bilinear functions of the process. For a multicomponent process, say $X[n] = X_1[n] + X_2[n]$, the HKR-spectrum will be $R_{XX^*}[n, f] = R_{X_1X_1^*}[n, f] + R_{X_2X_2^*}[n, f] + R_{X_1X_2^*}[n, f] + R_{X_2X_1^*}[n, f]$. This depends on the HKR-spectrum of each of the components, and the two cross-spectra between them. It is the cross-spectra that are denoted cross-terms. Cross-terms are generally unwanted in time-frequency estimates, even if they theoretically are bound to be present. If $X_1[n] = \delta[n_1]$ and $X_2[n] = \delta[n_2]$, we are guaranteed no cross-terms if $n_2 - n_1 > N_T + N_F$. Likewise, if we have two frequency components, one at $f = f_1$ and the other at $f = f_2$, the cross-terms are completely eliminated if $f_2 - f_1 > W_T + W_F$. We know that if a signal has limited support in time, it is not bandlimited in frequency. However, if the FT of a time limited signal is mainly concentrated in a frequency band, the correct choice of W_F and W_T will suppress the cross-terms such that they are negligible even if they are not completely removed. Note the inherent trade-off between resolution and cross-term suppression, as increasing N_F will improve the resolution in frequency, but at the same time it will increase the cross-terms between components separated in time.

Likewise, decreasing N_T will improve the time resolution, while W_T will increase and thus impair the cross-term suppression ability (see [Flandrin et al., 2003] for a discussion on this trade-off).

The estimator enjoys a great degree of freedom, as we chose three windows and two segment lengths whenever using it. However, this freedom can turn into a very time-consuming search for good choices of the parameters. Of course, the “best” choices will be different for different signals. We often found that sacrificing some time resolution by choosing v_T to be broader in time in order to facilitate cross-term reduction in frequency was a sensible approach. We also prefer the DPSSs because they reduce spectral leakage. In our experience, choosing all windows as zero-order DPSSs with small time-bandwidth products (around 3-6) and varying the segment lengths N_T and N_F provides an effective manner of using the estimators. This is reflected in the numerical examples throughout this thesis, where the window shapes themselves does not differ much, but the segment lengths vary. We denote NW_T , NW_F and NW_B as the time-bandwidth product of v_T , v_F and v_B , respectively, when the windows are specified to be zero-order DPSSs.

We note that some work has been performed on constructing windows that are optimally concentrated in the time-frequency domain, see e.g., [Daubechies, 1988], and it has been shown that the Hermite windows are optimal for the Wigner-Ville distribution [Bayram and Baraniuk, 2000]. The Hermite windows are a set of orthogonal windows, which may be employed in time-frequency multitaper estimation. [Thomson, 2000] has defined time-frequency multitaper estimation using the DPSSs, while [Aviyente and Williams, 2006] proposed multitaper estimates that are designed to optimize the frequency marginal of the estimate, and [Lilly and Park, 1995] employed multitwavelets in the estimation. The first step in our estimator in (3.6) may potentially be expanded to include a multitaper step to further decrease the variance of the estimate, but care must be taken to ensure that the orthogonality of the windows is utilized. This will of course also decrease the resolution of the estimate. [Wahlberg and Hansson, 2007] shows how a kernel estimator of the Wigner-Ville spectrum may be done numerically as a multitaper estimation. In [Wahlberg and Hansson, 2007], the kernel was chosen based on the ambiguity domain behavior of the process, and for a special class of locally stationary processes the optimal tapers were shown to be (approximately) equal to dilated Hermite functions.

Window normalization

We have seen how the windows can be chosen with different lengths and shapes to obtain the desired resolution in the estimate of the KR-spectra. There has been a lot of interest in finding windows that obey certain optimality criteria when it comes to resolution either in time or frequency, such as the already mentioned DPSSs and the Hermite windows. However, window normalization has not been given much attention. A correct normalization of the windows gives estimates of the KR-spectra whose magnitude values will be in the correct range. If one needs to compare the KR-spectra of two different processes, where different windows have been used in the estimation procedure, a correct normalization will allow us to compare the magnitudes of the estimated KR-spectra. We also

need correct normalization to be able to estimate the instantaneous power and the power spectral density of the process from the estimated HKR-spectrum.

We consider the expected values of the time marginal in (3.13) to define a usable normalization. To reduce the bias in the marginal, we have to choose $v_B[0] = 1$ and $\sum_{\mu} v_T[\mu]v_F^*[\mu] = 1$. If $\tilde{v}_T[\mu]$, $\tilde{v}_B[m]$, and $\tilde{v}_F[m]$ are the non-normalized windows, we define the normalized windows by

$$v_T[\mu] = \frac{\tilde{v}_T[\mu]}{\sum_{\mu} \tilde{v}_T[\mu]}, \quad v_F[m] = \tilde{v}_F[m] \frac{\sum_{\mu} \tilde{v}_T[\mu]}{\sum_{\mu} \tilde{v}_T[\mu] \tilde{v}_F[\mu]}, \quad v_B[m] = \frac{\tilde{v}_B[m]}{\tilde{v}_B[0]}. \quad (3.17)$$

The normalization of v_T and v_F can be chosen differently, as long as the sum over the product of these two windows is unity. In the frequency domain, this normalization leads to

$$\int_{-1/2}^{1/2} V_T(f)V_F^*(f) df = \int_{-1/2}^{1/2} V_B(f) df = 1. \quad (3.18)$$

Thus, the proposed normalization reduces the bias in the frequency marginal as well. Scaling the windows does not affect the estimators resolution or cross-term suppression, but it ensures that the KR-spectra have magnitudes in the correct range. Windows are commonly normalized such that they have unity energy, but this does not make sense for our estimator. We base our normalization on reducing the bias in the time marginal of the estimated KR-spectra. The fact that this normalization scheme also reduces the bias in the frequency marginal speaks in favor of this approach. Finally, the proposed normalization also leads to the sum over μ and integral over f of the kernel in (3.11) equaling one, further supporting our chosen normalization.

3.3 Numerical Examples

We consider numerical examples in order to test our proposed estimators. The estimators are tested on improper simulated data to show the importance of the CKR-spectrum for complex-valued data and to demonstrate how the estimators work for both the spectra and the marginals. We next apply the estimators to three real-valued real-world data sets, a bat localization recording and two guitar recordings.

3.3.1 Improper piecewise stationary process

In order to illustrate how the complementary quantities can yield important information about random processes and simultaneously check our estimator, we will now consider a piecewise stationary process. Let

$$X[n] = \begin{cases} X_1[n] & 0 \leq n < N/2 \\ X_2[n] & N/2 \leq n < N, \end{cases} \quad (3.19)$$

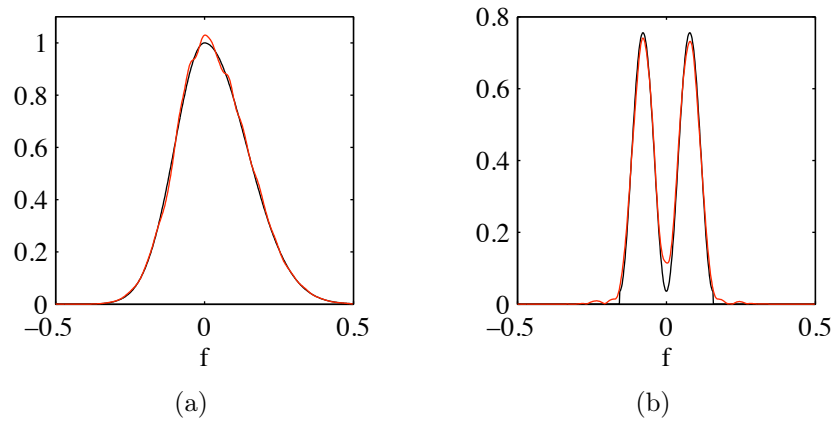


Figure 3.1: For the improper piecewise stationary process. (a) $S_{XX^*}(f)$ (black) and $|\hat{R}_{XX^*}[400, f]|$ (red). (b) $|S_{XX}(f)|$ (black) and $|\hat{R}_{XX}[400, f]|$ (red).

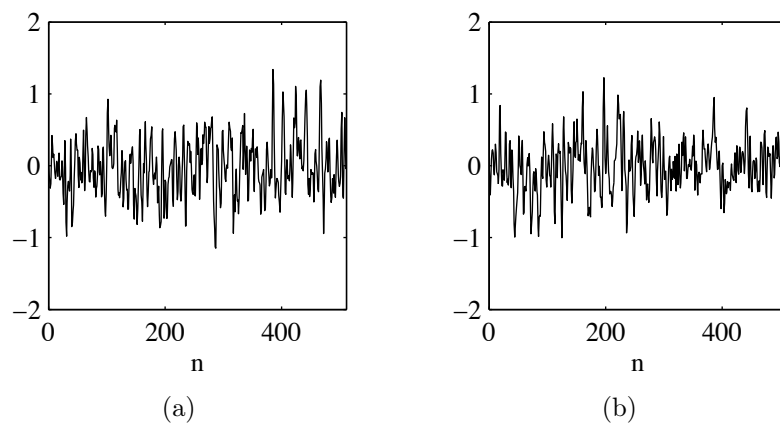


Figure 3.2: (a) Real part and (b) imaginary part of one realization of the improper piecewise stationary process.

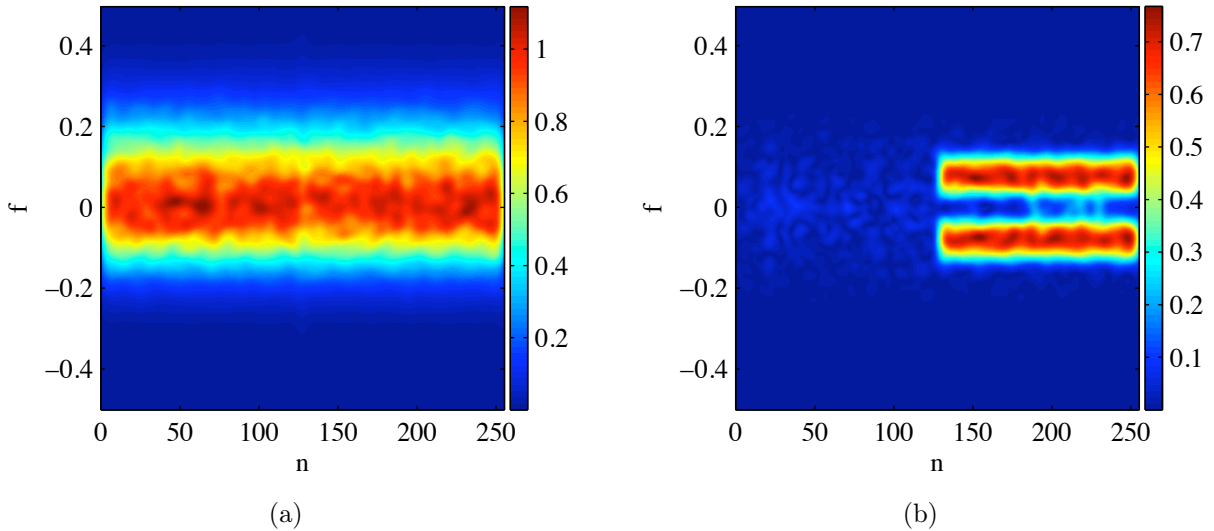


Figure 3.3: Estimated (a) HKR-spectrum and (b) CKR-spectrum of the improper piecewise stationary process.

where $X_1[n]$ is a proper stationary process and $X_2[n]$ is an improper stationary process. We let both processes have the same $S_{XX^*}(f)$ specified in Figure 3.1(a), and $X_2[n]$ will have the $S_{XX}(f)$ with an absolute value given in Figure 3.1(b), and a phase $\pi/6$. We choose $N = 512$ and simulate 500 realizations of the process using the method from Section 2.2.2, ignoring the filter coefficients for $|m| > 15$. For the KR-estimators, we use $N_F = 40$, $N_T = 30$, and the windows are all zero-order DPSSs with $NW_T = 6$ and $NW_F = NW_B = 3$. Figure 3.2 shows one realization of the process. One cannot tell from a visual inspection that the underlying process changed at $n = N/2$.

We estimate the KR-spectra from each realization, and averaged over the 500 realizations, an approach known as Monte Carlo simulation (see e.g., [Robert and Casella, 2004] for an introduction). The resulting spectra are shown in Figure 3.3. The estimated HKR-spectrum is approximately equal to $S_{XX^*}(f)$ for all time instants, as we expected. Likewise, the CKR-spectrum is approximately zero for $n = 0, \dots, N/2 - 1$ and then equal to $S_{XX}(f)$ for the remaining time instants. The fact that the estimated KR-spectra are approximately equal to $S_{XX^*}(f)$ and $S_{XX}(f)$ is also reflected in Figure 3.1, where the estimated KR-spectra for a fixed time instant $n = 400$ is shown with the theoretical spectra. Thus, the estimated KR-spectra are approximately equal to the theoretical KR-spectra, the estimators work well for this case. We also note that, as for the realization itself, the HRK-spectrum does not show any change occurring at $n = N/2$. The CKR-spectrum, however, changes drastically at this time. This simple example serves to show how ignoring the complementary correlations may lead to erroneous conclusions.

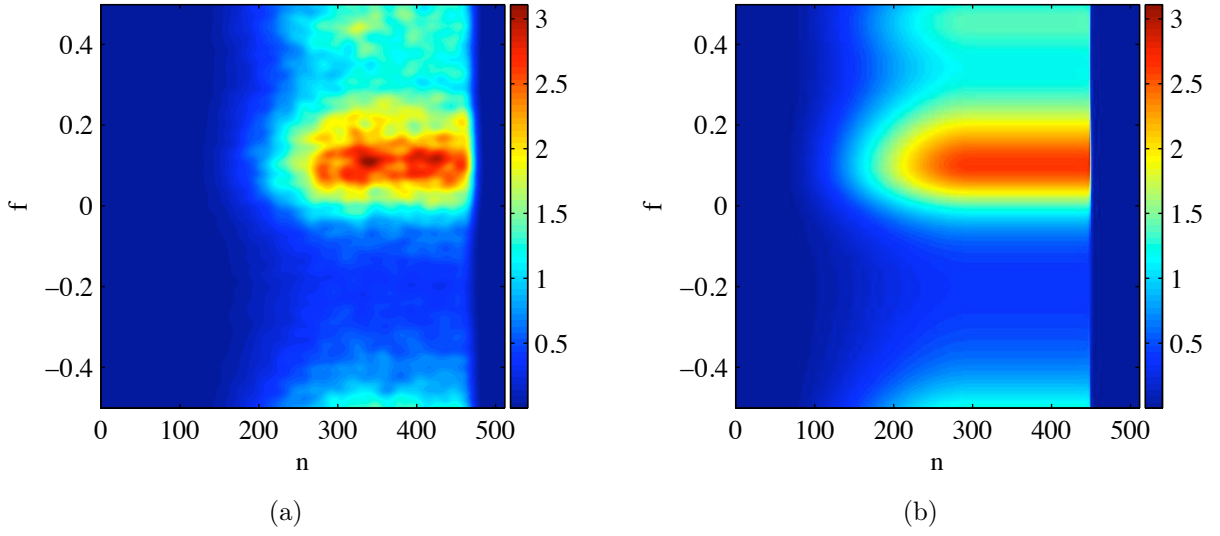


Figure 3.4: The absolute value of (a) the HKR-spectrum estimated from 200 realizations and (b) the theoretical HKR-spectrum of the improper process with time-varying variance.

3.3.2 Improper process with time-varying variance

We illustrate that both estimators give correctly shaped and normalized KR-spectra and marginals by considering a nonstationary improper random process. Realizations of the process was created using the method proposed in Section 2.2.2, and we kept the filter coefficients for $|m| \leq 20$. The stationary process $Y[n]$ is a complex-valued autoregressive process

$$Y[n] = \sum_{m=1}^L a_m Y[n-m] + \epsilon[n], \quad (3.20)$$

where $\epsilon[n]$ is improper white noise with $M_{\epsilon\epsilon^*}[n, \eta] = \delta[\eta]$ and $M_{\epsilon\epsilon}[n, \eta] = 0.6e^{j\pi/6}\delta[\eta]$. From $Y[n]$, we create the harmonizable process given in (2.38). Let $n = 0, \dots, N-1$ with $N = 512$, and we chose the coefficients $\{a_m\}$ such that the polynomial $A(z) = 1 - a_1z - \dots - a_Lz^L$ has the roots

$$\mathbf{p} = \begin{bmatrix} p_1 \\ p_2 \\ p_3 \\ p_4 \end{bmatrix} = \begin{bmatrix} 1 \\ -2 \\ -1.2 \\ 1.8 \end{bmatrix} - \begin{bmatrix} 2.3 \\ 0.4 \\ -3.1 \\ 0.7 \end{bmatrix} j. \quad (3.21)$$

The time varying standard deviation is given by

$$\sigma[n] = \begin{cases} 0 & n \in [0, 49] \text{ and } n \in [450, 511] \\ v[n-50] & n \in [50, 299] \\ 1 & n \in [300, 449] \end{cases} \quad (3.22)$$

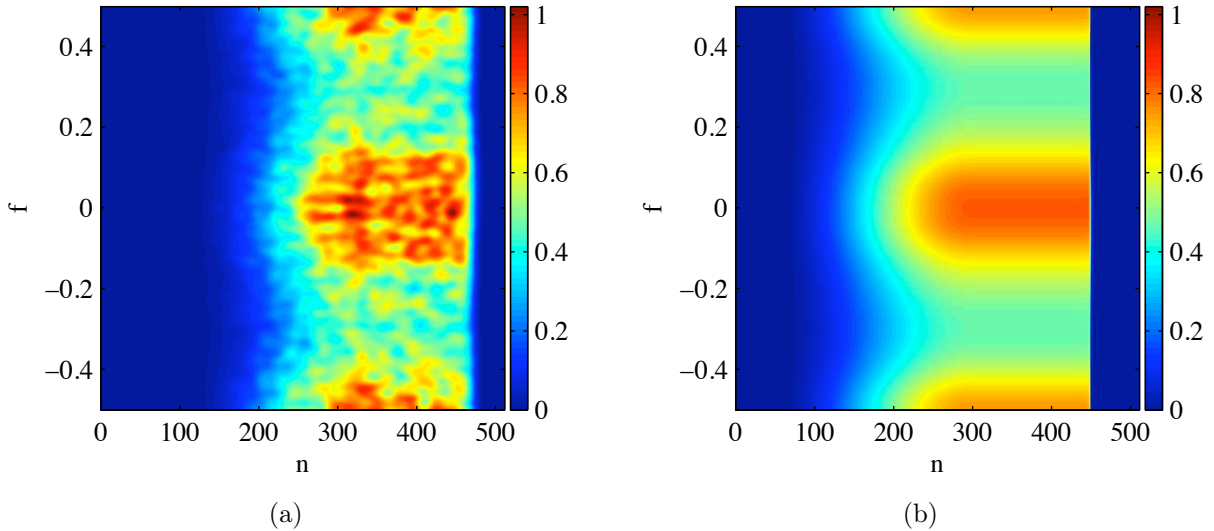


Figure 3.5: The absolute value of (a) the CKR-spectrum estimated from 200 realizations and (b) the theoretical CKR-spectrum of the improper process with time-varying variance.

where $v[n]$, $n = 0, \dots, 499$, is a Hanning window. For the estimator, we use $N_T = 30$ samples, $N_F = 60$ samples, and the windows are zero-order DPSSs with $NW_T = 6$ and $NW_F = NW_B = 3$. The theoretical KR-spectra for this process was given in (2.42) and (2.46). We generate $K = 200$ realizations of the process $X[n]$, and estimate the KR-spectra from these. The averaged spectra are shown in Figure 3.4 and Figure 3.5 together with the theoretical spectra. We see that the estimated spectra resemble the theoretical ones, and if we were to increase the number of realizations the likeness will increase. Note that the two pairs of spectra have the same range of magnitude, which supports our normalization scheme.

We estimate the time and frequency marginals by summing along each dimension of the averaged spectra. The theoretical marginals are easily obtained from (2.42) and (2.46). Figure 3.6 and Figure 3.7 shows the estimated and theoretical marginals of the HKR-spectrum and CKR-spectrum, respectively. The estimators give both the correct shape and the correct magnitude to the marginals, and the estimated and theoretical quantities are quite similar. These results support that the proposed window normalization correctly scales the estimates of the KR-spectra. This also shows that the marginals obtained from the estimated KR-spectra can be used as estimates for the instantaneous power, the power spectral density and the complementary equivalents.

3.3.3 Bat recording

We consider a real-valued data set consisting of a recorded digitized signal of the echolocation of large brown bats containing $N = 400$ samples, with sampling period $\Delta t = 7\mu\text{s}$,

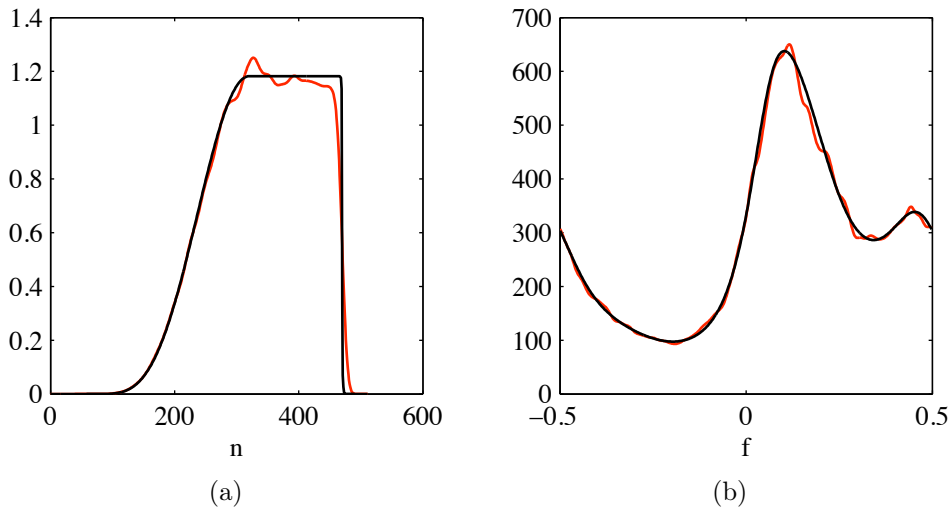


Figure 3.6: For the improper process with time-varying variance. (a) The time marginal and (b) frequency marginal of the HKR-spectrum. The estimated marginals are shown in red and the theoretical marginals are shown in black.

the data is courtesy of C. Condon, K. White, and A. Feng (Beckman Center, University of Illinois). This data set was also considered in [Hlawatsch and Boudreaux-Bartels, 1992; Cohen, 1995; Bayram and Baraniuk, 2000], where it was used to compare different members of Cohen's class. [Hlawatsch and Boudreaux-Bartels, 1992] found that the data consist of three nonlinear frequency modulation components (nonlinear chirps). We estimate the HKR-spectrum of the signal using $N_F = 50$ samples, $N_T = 30$ samples, and the windows are all zero-order DPSSs with $NW_T = 6$ and $NW_F = NW_B = 3$.

Figure 3.8 shows the result of the estimation for positive frequencies (the HKR-spectrum has a Hermitian symmetry in f for real-valued signals). We clearly see the three main components in both plots, and there are almost no cross-terms, even on a logarithmic scale. The nonlinear chirps have been smoothed out, which is not ideal, but unavoidable. If better localization is needed, methods such as reassignment can be employed [Auger and Flandrin, 1995; Xiao and Flandrin, 2007]. Our estimate seems to indicate the presence of a fourth chirp component in the signal. The logarithmic plot suggests that the data was not sampled fast enough, since the third and fourth chirp component seem to be cut off at the maximum frequency. We get a contribution at zero frequency for the time instants that are dominated by these two components, these low frequency contributions may be due to aliasing. These considerations were also made in [Bayram and Baraniuk, 2000], using a different time-frequency analysis tool.

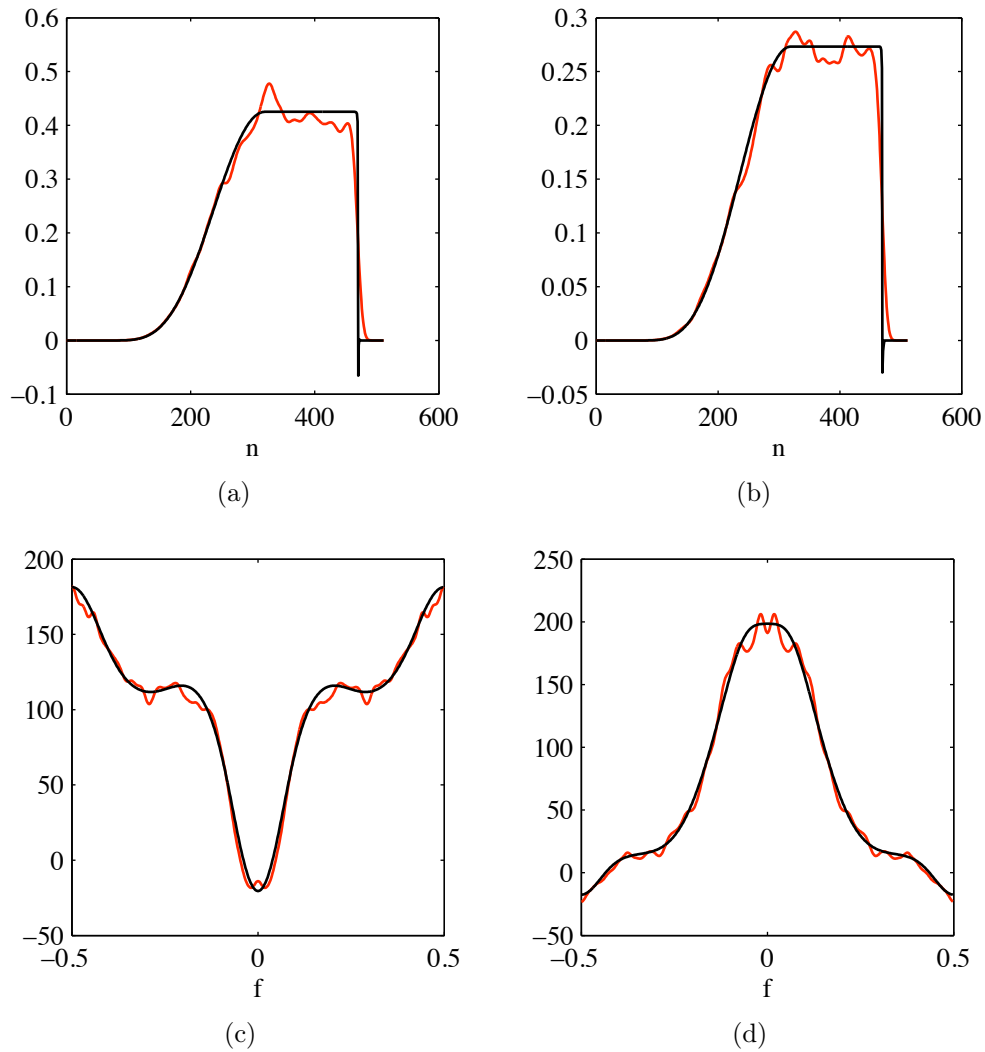


Figure 3.7: For the improper process with time-varying variance. (a) The real part and (b) imaginary part of the time marginal and (c) the real part and (d) imaginary part of the frequency marginal of the CKR-spectrum. The estimated marginals are shown in red and the theoretical marginals are shown in black.

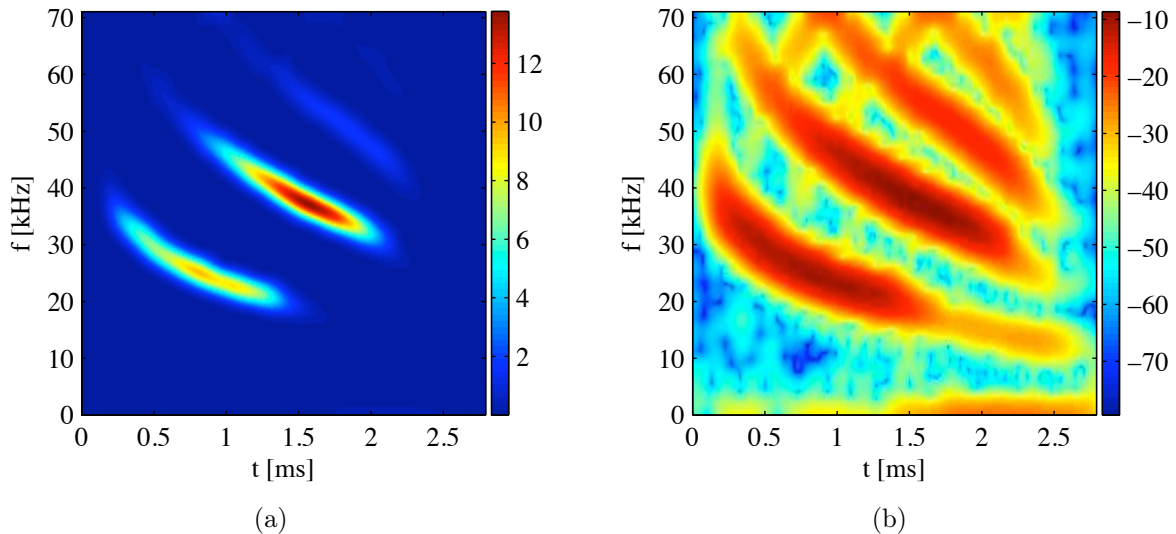


Figure 3.8: (a) $10^2 \cdot \left| \widehat{R}_{XX^*}[t, f] \right|$ and (b) $10 \log_{10} \left| \widehat{R}_{XX^*}[t, f] \right|$ of the bat recording.

3.3.4 Guitar recording I

To further assess the performance of our estimator for a nonstationary real-world data set, we carefully prepared an experiment as follows. We recorded the electrical output signal from the bridge Suhr SSV humbucker pickup on a Suhr Pro S2 electric guitar equipped with a spring loaded Gotoh variable (vibrato) tailpiece. By continuously varying the tailpiece with its vibrato bar, we produced a continuously pitch-varying signal with very interesting harmonic structure. The analog signal was sampled at 44.1 kHz/16 bits, and it was recorded straight to a MacBook Pro without any equalization or filtering. The analog-to-digital converter was an Apogee Duet audio interface.

First, the open low E-string (fundamental frequency of $f_E = 82.5$ Hz) was plucked with a stiff plectrum and the variable tailpiece was used to produce a deep and rather fast downbend to about 60 Hz (close to the tone B_1), followed by a fast release to the original tone in one single continuous controlled movement. Second, the open E and the open A-string (fundamental frequency of $f_A = 110$ Hz) were plucked simultaneously. This two-string chord, consisting of the musical interval called a perfect fourth or a *diatessaron*, also underwent a similar downbend followed by a release to the original equilibrium position. We thus understand that the harmonic structure of the single E-string pluck should be simpler than the multi-pitch harmonic structure of the dual-string perfect fourth.

The original data were downsampled by a factor of 10 prior to the analysis, giving us an effective Nyquist frequency of 2.2 kHz. The KR-spectrum was estimated using segment lengths of $N_T = 200$ and $N_F = 500$, and the three data windows were all chosen to be a zero-order DPSS with time-bandwidth product 3. In Figure 3.9 we show the magnitude of the estimated KR-spectrum for the guitar signal. The left panel shows the

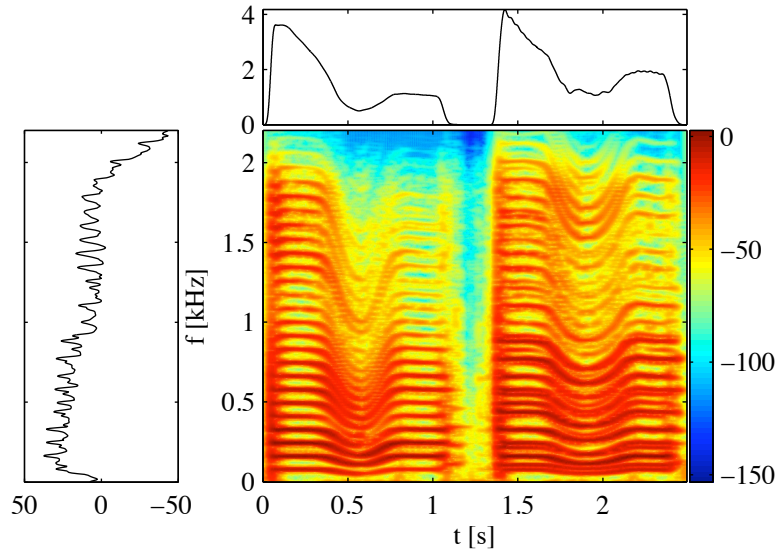


Figure 3.9: $10 \log_{10} \left| \widehat{R}_{XX^*}[t, f] \right|$ of guitar recording I, shown with the estimated time marginal $10^3 \widehat{P}_{XX^*}[t]$ (upper panel) and the estimated frequency marginal $10 \log_{10} \widehat{S}^M_{XX^*}(f)$ (left panel).

corresponding estimated frequency marginal, and the top panel shows the estimated time marginal. We see that while the frequency marginal has a spiky structure, it cannot reveal the real time-frequency variation of the signal, even when paired with the time marginal. The full KR-spectrum shows that for the single-string pluck, a harmonic structure with frequency components at $f_n(t) = n f_E(t)$ for integers n , with $f_E(t)$ being the time-varying fundamental frequency induced by the tailpiece motion. For the two-string part of the signal, the KR-spectrum no longer exhibits equidistant harmonic components, since two separate source oscillators exist. Some harmonics will overlap for the two strings, which shows up as an enhancement of these particular frequency components. In equilibrium, the perfect fourth interval is such that $k f_A \simeq n f_E$ for $(k, n) = (3, 4), (6, 8), (9, 12), \dots$, which is also readily identified from Figure 3.9. As demonstrated by this example, the estimated KR-spectrum has good resolution properties in both time and frequency, and we can discern the time-varying spectral components with great accuracy.

3.3.5 Guitar recording II

We conducted a two-channel experiment where one channel was the directly recorded output from an electric guitar, and the second channel was the same signal passed simultaneously through an analog envelope controlled lowpass filter (Moog Moogerfooger MF-101). The rest of the equipment used and the recording procedure are identical to those described in Section 3.3.4. The open low E-string was plucked with a stiff plectrum, and it was left

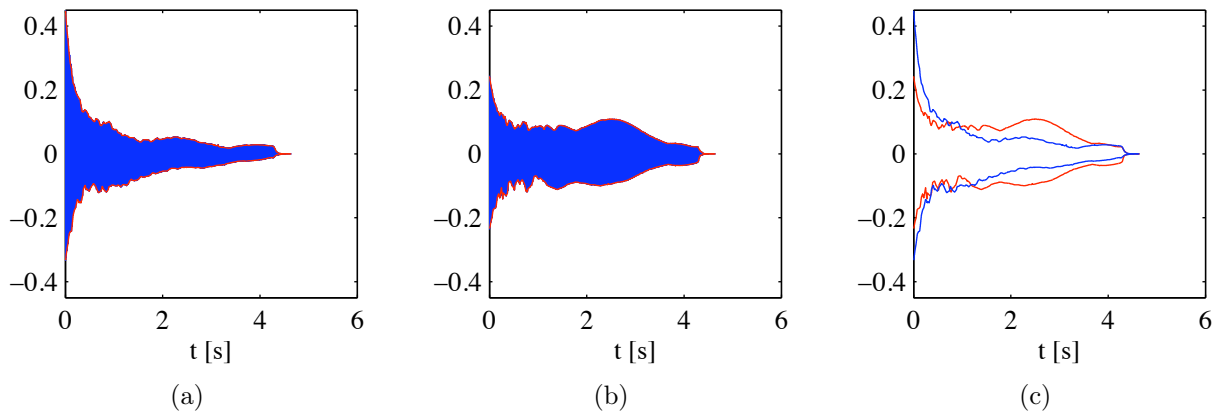


Figure 3.10: Guitar recording II. (a) Unfiltered guitar signal with estimated envelope (red line). (b) Filtered guitar signal with estimated envelope (red line). (c) Estimated envelope of unfiltered signal (blue line) and filtered signal (red line).

to develop for a while until it was mechanically damped with the plucking hand. The filter was used with a cutoff frequency of 250 Hz, a resonance parameter of 7, an amount of 10, and the filter was set to use smoothing. The manual for the filter is available for free download at <http://www.moogmusic.com/manuals/mf-101.pdf>.

Figure 3.10 shows the unfiltered and the filtered signal. The data was downsampled by a factor of 10 prior to the analysis, giving us an effective Nyquist frequency of 2.2 kHz. The HKR-spectrum of both the unfiltered and the filtered signal was estimated using the same parameters as for the first guitar recording, and the estimated spectra are shown in Figure 3.11. From the estimated HKR-spectrum of the unfiltered signal, we see how the estimator can express both the periodic components (pure tones) and impulses in time clearly. Three impulses occur towards the end of the time interval, we see this as lines in the time-frequency spectra for fixed t where all frequencies are present. The two first impulses are probably do to the guitarist touching other strings on the guitar, while the last impulse is the mechanically dampening of the E-string.

The filter is a lowpass filter, it will attenuate frequencies in the signal that are above the cutoff frequency. This particular filter employs an envelope follower, where the cutoff frequency of the filter increases with the envelope of the signal. The envelope is related to the magnitude of the signal, and we show the estimated envelope of both signals in Figure 3.10. The input to the filter consists of a pluck of a guitar string, which will have high magnitude when the string is plucked and the magnitude will decrease with time. Thus, we expect the cutoff frequency to be high for t close to 0, and then take smaller values as t increases. The filter is a time-varying lowpass filter where the bandwidth of the filter decreases with time, but this time variability is due to the change in envelope of the input signal. Indeed, we see from comparing the KR-spectra of the unfiltered and the filtered signal that the filter only attenuates very high frequencies at the start, and that lower and lower frequencies are attenuated as t increases. This would have been impossible

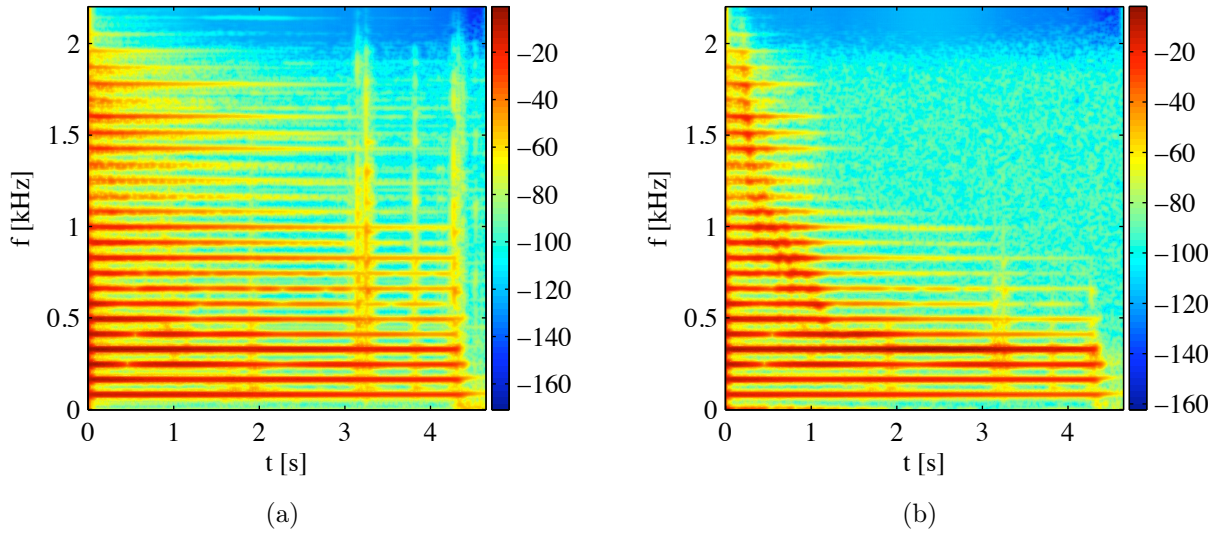


Figure 3.11: (a) $10 \log_{10} \left| \widehat{R}_{XX^*}[t, f] \right|$ of the unfiltered guitar signal for guitar recording II and (b) $10 \log_{10} \left| \widehat{R}_{YY^*}[t, f] \right|$ of the filtered guitar signal in guitar recording II.

to see from the power spectral density or the instantaneous power of the process.

The resonance setting used here leads to a lowpass filter with a non-constant gain. The gain will be approximately constant for low frequencies, but will have a higher gain for frequencies just below the cutoff frequency, thus boosting frequencies just below the cutoff frequency. We see that in time instants right before a frequency is removed by the filter, the corresponding line in the time-frequency spectrum is smeared out (has a ripple), this might be due to the resonance effect. From the envelope plot in Figure 3.10, we see that the magnitude of the filtered signal is lower than the magnitude of the unfiltered signal for $t = 0$, but after about 1 second the filtered signal is larger than the unfiltered signal. This might be due to the fact that the lowpass filter used here has a preamplifier. It could also be due to the boost of frequencies near the cutoff frequency that the filter provides. At values close to $t = 0$, the cutoff frequency is high such that high frequencies are boosted. However, these high harmonics does not contribute much to the total signal, even if they are boosted it may not be noticeable in the filtered signal. As the cutoff frequency decreases, lower harmonics with more influence on the filtered signal are boosted, which could potentially be noticeable in the filtered signal. This data set also demonstrate how useful time-frequency analysis can be.

3.4 Discussion

We have proposed estimators of the KR-spectra that while theoretically equivalent to the estimators proposed in [Scharf et al., 2005], require less computational effort and provides us with an intuitive understanding of the windows used in the estimators. The three windows and two segment lengths that can be adjusted lend the estimators great flexibility, and we have discussed how to choose these parameters in order to improve resolution, suppress cross-terms and provide correct normalization of the estimate. We have discussed the statistical properties of both the spectra themselves and the marginals of the spectra. Simulated improper data was used to illustrate that the estimators give results that are similar to the true KR-spectra. Three real-world data sets were considered, and we found that the KR-spectra is a good tool for displaying the time-varying frequency content of transient signals. The guitar recordings especially illustrated the advantage of being able to represent a signal in time and frequency simultaneously. [Hanssen et al., 2006b] showed how conventional spectral analysis may be used to extract information about guitar signals. We have here showed how valuable time-frequency analysis can be. We could not have understood how the frequencies of the two guitar signals considered here changed with time by just considering the marginals. The KR-spectrum estimator has also been applied to sound recordings of a transversal flute made from *Heracleum laciniatum* [Hanssen et al., 2006a], where it was shown that this type of flute has very interesting subharmonics caused by nonlinear effects.

Chapter 4

Estimation of the Ambiguity Function

The Hermitian ambiguity function of deterministic signals have been used in a wide variety of fields, such as radar, sonar, communications and optics. In radar, the Hermitian ambiguity function is used to measure the distance and velocity of a moving target [Skolnik, 2001], and to select radar waveforms and for performance evaluation of radar systems (see e.g., [Rihaczek, 1969]). The Hermitian ambiguity function of a random process determines if the process is underspread or not. We have already noted that the concept of underspread processes connects the behavior in the ambiguity domain to the HKR-spectrum. If the Hermitian ambiguity function is supported only around the origin of the ambiguity plane, it implies that the HKR-spectrum of the process is smooth. We actually make the assumption of smoothness of the HKR-spectrum implicitly in the estimator presented in the previous Chapter. In order to determine whether a process is underspread or not based on realizations of the process, we need an estimator for the Hermitian ambiguity function.

There has been little work on how to estimate the Hermitian ambiguity function based on one discrete-time realization of a random process. One common approach is to estimate the Hermitian ambiguity function by means of a tapered Fourier transform of the estimator for the Hermitian dual-time correlation in (2.32) [Larsen, 2003], and the complementary ambiguity function can be estimated along the same lines. However, since our goal is to classify $X[n]$ as underspread or overspread, we are interested in the support in the ambiguity domain. The tapered Fourier transform approach will produce an estimate that is a smoothed version of the true Hermitian ambiguity function, thus increasing the support in the ambiguity domain. This estimate is also in general nonzero for the entire ambiguity plane, making it difficult to determine the essential support of the estimate.

The most popular estimator of the Hermitian ambiguity function is a direct implementation of the definition of the discrete-time Hermitian ambiguity function while ignoring the expectation operator, i.e., use the DTFT of (2.32) without a kernel. This is equivalent to considering $x[n]$ as a deterministic signal, not as a realization from a random process. It gives us the Empirical Ambiguity Function (EAF)

$$\hat{A}_{XX^*}(\nu, \eta) = \sum_{n=\max(0, \eta)}^{N-1+\min(0, \eta)} x[n]x^*[n - \eta]e^{-j2\pi\nu n}, \quad (4.1)$$

where $n = 0, \dots, N-1$ and $\eta = -(N-1), \dots, (N-1)$. We have assumed unity sampling frequency, and thus $-1/2 \leq \nu \leq 1/2$. The edges are dealt with using zero-padding, edge-effects of the Hermitian ambiguity function are discussed more carefully in [Hedges and Suter, 2002]. This estimator will not have an estimator-induced increased support in the ambiguity domain. However, the variance of the estimator is large, the expectation and standard deviation are of the same order of magnitude. And since $\widehat{A}_{XX^*}(\nu, \eta) \neq 0$ for all (ν, η) , it is not trivial to determine the support of the estimated function.

Estimation procedures for time-frequency spectra based on the underspread nature of the process have been proposed in [Jachan et al., 2007; Borgnat and Flandrin, 2008], however these methods utilize a user-tuned parameter to determine the support in the ambiguity domain. If the assumed support in the ambiguity domain is larger than the true support, estimators in global time or global frequency are not smoothed sufficiently. If the support is assumed to be too small, we accrue bias and smooth out details in the time-frequency spectrum. Optimally the decision on whether a contribution in the ambiguity domain is important or not should be based on whether the magnitude of the Hermitian ambiguity function is sufficiently large for us to suspect it is not noise generated but rather signal generated. Such ideas have also been used for processes observed in continuous time in [Sayeed and Jones, 1995] and [Wahlberg and Hansson, 2007], but where the theoretical properties of the process were assumed *known* to obtain the optimal kernel for smoothing the time-frequency spectrum.

We propose an estimator of the Hermitian ambiguity function that does not increase the support in the ambiguity domain, that has a lower variance than the EAF and which enables us to easily estimate the support of the Hermitian ambiguity function. The estimation method consists of a thresholding of the EAF, where the threshold is chosen based on statistical considerations of the EAF. In this Chapter, we assume that the process $X[n]$ is a Gaussian, analytic and proper harmonizable process. We consider analytic processes in order to avoid the well-known problem of aliasing and interference from negative frequencies when estimating the Hermitian ambiguity function of real-valued signals [Jeong and Williams, 1992], and we assume the process is proper in order to simplify variance expressions. We work with the discrete-time Hermitian ambiguity function, and will not consider problems related to whether this definition makes sense compared to the continuous-time definition (see e.g., [Sandberg and Hansson-Sandsten, 2009]).

4.1 Properties of the Empirical Ambiguity Function

In order to choose the correct threshold, we need to know the distribution of the EAF. The EAF is a complex-valued quantity, such that $\widehat{A}_{XX^*}(\nu, \eta)$ is a complex-valued random variable for fixed (ν, η) . We define the probability density function of a complex-valued Gaussian random variable $Z \sim \mathcal{N}^C(\mu, \sigma^2)$ as

$$p_Z(z) = \frac{1}{\pi\sigma^2} \exp\left[-\frac{|z - \mu|^2}{\sigma^2}\right], \quad (4.2)$$

where μ is the mean and σ^2 is the variance of Z [Neuser and Massey, 1993]. We show that under certain conditions, the centered and normalized EAF is distributed as a zero-mean, unity variance complex-valued Gaussian random variable outside the support of the Hermitian ambiguity function. We also present a result on the distribution of the magnitude squared of the EAF, which we need in order to choose the correct threshold. In the following, $\mu_A(\nu, \eta]$ and $\sigma_A^2(\nu, \eta]$ denotes the expected value and variance of the EAF, respectively.

4.1.1 Distribution for underspread processes

We assume that $X[n]$ is an analytic process corresponding to a strictly underspread real-valued process. A strictly underspread process has a Hermitian ambiguity function that is zero for $(\nu, \eta] \notin \mathcal{D}$, where there exists some finite non-negative T and Ω such that $\mathcal{D} \subset [-\Omega, \Omega] \times [-T, T]$. We assume that the energy of the signal is distributed over the entire length of signal. Then the EAF evaluated at $(\nu, \eta]$ has an expected value

$$\mu_A(\nu, \eta] = \int_0^{1/2} \int_{-f}^{1/2-f} e^{j2\pi f\eta} S_{XX^*}(\lambda, f) e^{j\pi(N+\eta-1)(\lambda-\nu)} D_{N-|\eta]}(\lambda-\nu) d\lambda df. \quad (4.3)$$

Here, $D_N(f) = \sin(\pi Nf)/\sin(\pi f)$. Likewise, the EAF has a variance

$$\sigma_A^2(\nu, \eta] = \sum_{n=\max(0,\eta)}^{N-1+\min(0,\eta)} \sum_{\zeta=-(T-1)}^{T-1} e^{-j2\pi\nu\zeta} M_{XX^*}[n, \zeta] M_{XX^*}^*[n-\eta, \zeta] + O\left(\log\left[\frac{N}{T}\right]\right). \quad (4.4)$$

The function $O(\cdot)$ describes the limiting behavior of a function as follows. If, for two functions $z[n]$ and $q[n]$, we have $z[n] = O(q[n])$ as $n \rightarrow \infty$, then eventually $z[n] \leq cq[n]$, where c is a constant. A closely related order term is $z[n] = o(q[n])$, where eventually $z[n] < cq[n]$. The $O(\cdot)$ term in (4.4) is due to the discrete Hilbert transform [Marple, 1999] that is used to create the analytic extension of the real-valued realization. The expected value is a convolution between $D_N(\nu)$ and the Hermitian dual-frequency spectrum in the local frequency variable, and an inverse FT with respect to the global frequency. We express the variance of the EAF as functions of the Hermitian dual-time correlations, this form does not provide any intuitive insight.

Since $X[n]$ is Gaussian, we would expect the EAF to be Gaussian for $(\nu, \eta] \notin \mathcal{D}$ with the expected value and variance specified by (4.3) and (4.3). However, additional constraints are needed for this to be true, since this is not a sum over independent identically distributed variables. Theorem 2.1 in [Peligrad, 1996] gives a central limit result for a sum of random variables that may be applied to our case. Fix $(\nu, \eta] \notin \mathcal{D}$, let $\eta \geq 0$ and define

$$Q[n] = (X[n+\eta]X^*[n] - M_{XX^*}[n+\eta, -\eta]) e^{-j2\pi\nu(n+\eta)} \quad (4.5)$$

for $n = 0, \dots, N - 1 - \eta$. We form a triangular array by letting N increase, $N = \eta + 1, \eta + 2, \dots$, to get

$$\mathbf{Q} = \begin{bmatrix} Q[0] & 0 & 0 & \cdots & 0 \\ Q[0] & Q[1] & 0 & \cdots & 0 \\ Q[0] & Q[1] & Q[2] & \cdots & 0 \\ \vdots & \vdots & \vdots & \cdots & \vdots \\ Q[0] & Q[1] & Q[2] & \cdots & Q[N - 1 - \eta] \end{bmatrix}. \quad (4.6)$$

In order for Theorem 2.1 in [Peligrad, 1996]) to apply, we need \mathbf{Q} to be strongly mixing, which is a mathematical upper bound on how much dependency there is in the data. As we consider two data points that are far enough apart in time, the data points must be statistically independent of each other. We also need \mathbf{Q} to satisfy the Lindeberg condition to ensure that none of the variables have distributions with too heavy tails. Also, the Lindeberg condition and the additional condition

$$\sup_N \left\{ \frac{1}{\sigma_A^2(\nu, \eta)} \sum_{n=0}^{N-\eta-1} M_{XX^*}[n + \eta, 0] M_{XX^*}[n, 0] \right\} < \infty \quad (4.7)$$

will make certain that all the variances of the individual variables are small compared to the sum of the variances. If these conditions are fulfilled, Theorem 2.1 in [Peligrad, 1996]) states that

$$\frac{\widehat{A}_{XX^*}(\nu, \eta] - \mu_A(\nu, \eta]}{\sigma_A(\nu, \eta]} \xrightarrow{\mathcal{L}} \mathcal{N}^C(0, 1), \quad (\nu, \eta] \notin \mathcal{D}, \quad \eta \geq 0, \quad (4.8)$$

where $\xrightarrow{\mathcal{L}}$ denotes convergence in law [Ferguson, 1996]. Repeating the calculations for $\eta < 0$ yields similar results. Thus, we need to have a bounded degree of dependency, we need to ensure that the variance does not concentrate to a few of the variables in the sum, and we need the tail behavior of the random variables to be moderate. In this case, the centered and normalized EAF at $(\nu, \eta] \notin \mathcal{D}$ will converge in law to a Gaussian variable with zero mean and unit variance as N increases. This central limit theorem does not provide rates of convergence, and in some degenerate cases the joint distribution of $\widehat{A}_{XX^*}(\nu, \eta]$ over several $(\nu, \eta]$ may not be asymptotically multivariate Gaussian.

The thresholding procedure will be applied to the magnitude squared of the EAF, thus we need to know the distribution of this quantity as well. Assuming that the conditions are fulfilled, such that $\widehat{A}_{XX^*}(\nu, \eta]$ for fixed $(\nu, \eta] \notin \mathcal{D}$ has a Gaussian distribution, and $\left| \widehat{A}_{XX^*}(\nu, \eta] \right|^2$ will be χ^2 -distributed. However, what kind of χ^2 -distribution depends on the so-called *relation* of the EAF. The relation is simply the expectation of the squared complex-valued variable, i.e., $r_A(\nu, \eta] = \mathbb{E} \left\{ \widehat{A}_{XX^*}^2(\nu, \eta] \right\}$, thus it corresponds to the complementary dual-time correlation at $\eta = 0$. The term relation is taken from [Picinbono and Bondon, 1997], where the complementary dual-time correlation of a discrete-time process is termed the relation sequence. We find that for an analytic process $X[n]$ corresponding to a real-

valued strictly underspread process, we have

$$r_A(\nu, \eta] = O\left(\log\left[\frac{N}{T}\right]\right) \quad \text{if } |\eta| > T, \quad (4.9)$$

and $r_A(\nu, \eta] = 0$ for $|\nu| > \Omega$. The order term is again due to the use of the discrete Hilbert transform. The relation will be negligible for $(\nu, \eta] \notin \mathcal{D}$, thus we have

$$\frac{|\widehat{A}_{XX^*}(\nu, \eta] - \mu_A(\nu, \eta)]|^2}{\sigma_A^2(\nu, \eta]} \stackrel{d}{=} \frac{1}{2}\chi_2^2 + O\left(\frac{|\log(N)|^2}{N - |\eta|}\right) + o(1) \quad (4.10)$$

for most of the values of $(\nu, \eta]$ in the ambiguity plane, whereas a relation with unity value would lead to a χ_1^2 distribution [Barber and Nason, 2004]. These distributions have different variances, such that it is important to know the relation of the EAF in order to chose a correct threshold. The order term $O\left(\frac{|\log(N)|^2}{N - |\eta|}\right)$ is due to the relation, while $o(1)$ is due to the convergence to the Gaussian distribution.

4.1.2 Moments for some special cases

While we (asymptotically) retrieve the Gaussian distribution for the EAF, we fail to obtain simple interpretable forms for $\sigma_A^2(\nu, \eta]$. For this reason, it is convenient to derive the first and second order structure directly for some commonly used classes of processes. We consider three simple classes of processes, namely stationary processes, white nonstationary processes and deterministic signals in Gaussian white noise.

Stationary process

The Hermitian ambiguity function of a stationary process $X[n]$ is given by (2.17). The EAF based on one realization will have an expected value

$$\mu_A(\nu, \eta] = D_{N-|\eta|}(\nu)M_{XX^*}[\eta]e^{-j\pi\nu(N+\eta-1)}, \quad (4.11)$$

and a variance

$$\sigma_A^2(\nu, \eta] = (N - |\eta|)(1/2 - |\nu|) \int_{\max(0, -\nu)}^{1/2 - \max(0, \nu)} \frac{S_{XX^*}(f + \nu)S_{XX^*}(f)}{1/2 - |\nu|} df + O(1). \quad (4.12)$$

The term $O(1)$ stems from the use of the limiting behavior of $D_N(\nu)$ in the calculations (this also applies to (4.13), (4.14) and (4.16)). We see that $\mu_A(\nu, \eta]$ is not zero for $\nu \neq 0$, but rather decays with ν as $D_{N-|\eta|}(\nu)$. However, $D_N(\nu)$ will approach a delta function as $N \rightarrow \infty$, such that the EAF is asymptotically unbiased. For convenience, an analytic process corresponding to a real-valued stationary white process is denoted an analytic white process. An analytic white process is thus a process with a power spectral density

that is zero for negative frequencies, and constant for non-negative frequencies. Of course the analytic white process is not actually a white process, the name merely reflects the correlation structure of the corresponding real-valued process. If $X[n]$ is an analytic white process, the integral in (4.12) equals unity and the variance of the EAF decays like $N - |\eta|$ in η and like $1/2 - |\nu|$ in ν . Informally, we say that the greater similarity between $X[n]$ and an analytic white process, the more the variance of the EAF will decay like $(N - |\eta|)(1/2 - |\nu|)$.

Uniformly modulated process

One of the simplest cases of real-valued nonstationary processes is a uniformly modulated white process. Let $X[n]$ be the analytic extension of $\sigma_X[n]\epsilon[n]$, where $\epsilon[n]$ is a Gaussian white process with variance $\sigma_\epsilon^2 = 0.5$ and $\sigma_X^2[n]$ is the time-varying variance with a DTFT $\Sigma_{XX^*}(\nu)$. The EAF has an expected value

$$\mu_A(\nu, \eta) = \Sigma_{XX^*}(\nu) e^{j\pi(1/2 - |\nu|)\eta} (1/2 - |\nu|) \text{sinc}[\eta(1/2 - |\nu|)] + O(1), \quad (4.13)$$

where $\Sigma(0) = O(N)$ and $\text{sinc}(f) = \sin(\pi f)/(\pi f)$. The variance of the EAF is given by

$$\sigma_A^2(\nu, \eta) = (N - |\eta|)(1/2 - |\nu|) \int_{-1/2+|\nu|}^{1/2-|\nu|} \frac{|\Sigma(f)|^2}{N - |\eta|} e^{j2\pi f\eta} df + O(1). \quad (4.14)$$

The EAF is biased as an estimator for the Hermitian ambiguity function, even if the maximum of the $\text{sinc}(\cdot)$ function will ensure that the EAF is largest at $\eta = 0$. Note that the bias increases as ν increases. The relation for the uniformly modulated case and the stationary case was calculated in [Hindberg et al., 2008], where it was shown that the relation decreases in magnitude as ν and η increase.

Deterministic signal in white noise

We consider the signal $X[n] = g[n] + \epsilon[n]$ where $g[n]$ is an analytic deterministic sequence and $\epsilon[n]$ is an analytic white process with variance σ_ϵ^2 . For deterministic signals, the expectation operator will have no effect, and the EAF is a deterministic quantity. However, the EAF of a deterministic signal may still suffer from the fact that we are only considering a finite length segment of a possibly infinite length signal, such that the EAF of a deterministic signal may not equal the theoretical Hermitian ambiguity function of the signal. We denote $\widehat{A}_{gg^*}(\nu, \eta)$ the EAF of $g[n]$, and find the expected value of the EAF of $X[n]$ as

$$\mu_A(\nu, \eta) = \widehat{A}_{gg^*}(\nu, \eta) + \sigma_\epsilon^2 e^{-j\pi\nu(N+\eta-1)} D_{N-|\eta|}(\pi\nu) e^{j\pi\eta/2} \text{sinc}(\pi\eta/2). \quad (4.15)$$

Likewise, we find the variance of the EAF as

$$\sigma_A^2(\nu, \eta) = \sigma_\epsilon^2 (\mathcal{G}(\nu, \eta) + \mathcal{G}(-\nu, -\eta)) + \sigma_\epsilon^4 (N - |\eta|)(1/2 - |\nu|) + O(1) \quad (4.16)$$

where

$$\mathcal{G}(\nu, \eta) = \int_{\max(-\nu, 0)}^{1/2 - \max(0, \nu)} \left| \sum_{t=0}^{N-1-|\eta|} g[t - |\eta|I(\eta < 0)]e^{-j2\pi ft} \right|^2 df. \quad (4.17)$$

Here,

$$I(\zeta) = \begin{cases} 1 & \text{if } \zeta \in C \\ 0 & \text{if } \zeta \notin C \end{cases} \quad (4.18)$$

for some element ζ and some set C , is the indicator function. If the support of $\widehat{A}_{gg^*}(\nu, \eta)$ is limited, the moments of the EAF will be dominated by the behavior caused by the Gaussian white noise outside the support of the Hermitian ambiguity function of $g[n]$. Thus, the variance will behave approximately like the variance for Gaussian white noise and the relation will be negligible outside the support of $\widehat{A}_{gg^*}(\nu, \eta)$.

4.2 Thresholding Procedure

We estimate the Hermitian ambiguity function of an underspread zero-mean random process based on the EAF. Since the process is underspread, $|\mu_A(\nu, \eta)| \ll \sigma_A(\nu, \eta)$ for most (ν, η) , and so thresholding is an admissible estimation procedure. If the variance $\sigma_A^2(\nu, \eta)$ is known, we would, based on the distributional results in Section 4.1.1, threshold the EAF as

$$\widehat{A}_{XX^*}^{(T)}(\nu, \eta) = \begin{cases} \widehat{A}_{XX^*}(\nu, \eta) & \text{if } \left| \widehat{A}_{XX^*}(\nu, \eta) \right|^2 > \lambda^2 \sigma_A^2(\nu, \eta) \\ 0 & \text{if } \left| \widehat{A}_{XX^*}(\nu, \eta) \right|^2 \leq \lambda^2 \sigma_A^2(\nu, \eta), \end{cases} \quad (4.19)$$

where λ^2 is some given threshold. This is strictly speaking a correct treatment only for processes satisfying the constraints presented in Section 4.1.1, but we expect that the distributional result is valid under less constrained scenarios. The conditions are sufficient, but by no means necessary, for the distributional result to hold. If we divide the magnitude squared of the EAF by $\sigma_A^2(\nu, \eta)$ for each point (ν, η) , we retrieve a set of *correlated* positive random variables. For any such collection, we may note from [Olhede, 2007], that a threshold $\lambda_K^2 = 2 \log(K[\log(K)])$ may be used. In our case, $K = 2N$ where N is the number of observations, as we threshold the EAF frequency by frequency, across the total collection of all time lags. The risk of this non-linear estimator for sums of unequally weighted χ_1^2 's was calculated in [Olhede, 2007][p. 1529].

4.2.1 Estimating the variance

In general $\sigma_A^2(\nu, \eta)$ is *not* known, and previous results have shown that $\sigma_A^2(\nu, \eta)$ takes different forms depending on the spreading of the process. The variance of the EAF is often smooth in ν and η , and may exhibit a decay in (ν, η) that resembles that of the variance of the EAF of an analytic white process. We choose to estimate the variance as if $X[n]$ is an

analytic white process, and thus only need to find the scale σ_ϵ^4 of the data. To determine σ_ϵ^4 from the EAF, we use a median absolute deviation procedure, which has been used for estimating the scale of correlated data before [Johnstone and Silverman, 1997]. The median absolute deviation is a robust estimator, with a breakdown point of 50 %. We note that this procedure requires a $\frac{1}{2}\chi_2^2$ distribution, thus we need the relation of the EAF to be zero. An estimator of σ_ϵ^4 over any region $\mathcal{M}_k \subset [-1/2, 1/2] \times [-(N-1), (N-1)]$ is defined as

$$\widehat{\sigma}_\epsilon^4(\mathcal{M}_k) = \frac{1}{\ln(2)} \operatorname{median} \left\{ \frac{|\widehat{A}_{XX^*}(\nu, \eta)|^2}{\sqrt{(N-|\eta|)(1/2-|\nu|)}} \right\}_{(\nu, \eta) \in \mathcal{M}_k}. \quad (4.20)$$

A suitable threshold procedure simply corresponds to using

$$\widehat{\sigma}_A^2(\nu, \eta) = \widehat{\sigma}_\epsilon^4(\mathcal{M}_k)(N-|\eta|)(1/2-|\nu|) \quad (\nu, \eta) \in \mathcal{M}_k. \quad (4.21)$$

as an estimate of $\sigma_A^2(\nu, \eta)$ in (4.19), and employing the thresholding. Note that the threshold decreases with increasing η and ν , taking into account the sampling properties of the EAF.

In (4.20), the ambiguity plane has been segmented into $k = 1, \dots, K$ regions \mathcal{M}_k . We have seen that the variance of the EAF for non-white processes normalized by $(N-|\eta|)(1/2-|\nu|)$ will be approximately constant in some regions of the ambiguity plane. Ideally, we would estimate σ_ϵ^4 separately in these areas, but of course, we do not generally know how to segment the ambiguity plane. Instead, we estimate the variance of the EAF by segmenting the ambiguity plane into suitable user-tuned regions \mathcal{M}_k and apply (4.20) to each region. If $K = 1$, i.e., σ_ϵ^4 is estimated by the same value in the entire ambiguity plane we denote the result after thresholding as the thresholded EAF, $\widehat{A}_{XX^*}^{(T)}(\nu, \eta)$. Likewise, if $K > 1$ we denote the results of the thresholding as the locally thresholded EAF, $\widehat{A}_{XX^*}^{(LT)}(\nu, \eta)$. Note that for processes that are not strictly underspread, our thresholding procedure will identify regions where the mean of the EAF is sufficiently distinct in magnitude from the variance of the EAF. This in essence corresponds to comparing the magnitude of the Hermitian ambiguity function at a point with the magnitude at other points.

Equation (4.20) is not appropriate unless $(N-|\eta|)(1/2-|\nu|) = O(N)$, which is a problem at the very rim of the ambiguity plane. In this area, (4.12) and (4.14) are not good approximations of the variance. Asymptotically these rim coefficients are of no importance, but for a finite number of samples two approaches can be made. We can either treat the coefficients as if (4.12) and (4.14) were appropriate, or we can set the coefficients for which $(N-|\eta|) < n_0$ or $(1/2-|\nu|) \times 2N < n_0$ equal to zero for some suitable $n_0 = O(1)$. These coefficients will have little effect on (4.20), as this is a robust estimator.

4.2.2 Spread

We have proposed an estimate of the Hermitian ambiguity function in the entire ambiguity plane that facilitates a simple estimator for the spread of the process. The total spread

of the Hermitian ambiguity function of $X[n]$ over a region \mathcal{S} in the ambiguity domain is given by

$$\xi_X(\mathcal{S}) = \frac{\int \sum_{\mathcal{S}} I(|A_{XX^*}(\nu, \eta)| \neq 0) d\nu}{\int \sum_{\mathcal{S}} d\nu}, \quad (4.22)$$

and $0 \leq \xi_X(\mathcal{S}) \leq 1$. A process $X[n]$ is compressible in the ambiguity domain if $\xi_X(\mathcal{S}) \ll 1$. If $\widehat{A}_{XX^*}(\nu, \eta]$ is an estimator of the Hermitian ambiguity function, then we obtain an estimated spread $\widehat{\xi}_X(\mathcal{S})$ by replacing $A_{XX^*}(\nu, \eta]$ with $\widehat{A}_{XX^*}(\nu, \eta]$ in (4.22). Extended underspread processes will be approximated by the thresholded EAF to the region of their essential support, i.e., where their magnitude is non-negligible in comparison to the rest of the ambiguity plane. If any other estimator was employed, be it simply the EAF or the FT of an estimator of any of the three other second-order moments, we would in general get a function that is nonzero for the entire ambiguity plane. Thus, we would have to do some manner of thresholding anyway to estimate the spread.

4.3 Numerical Examples

We consider some simple examples to examine the thresholding procedure. In order to approximate the mean square error of the estimator, we need a value to compare the estimate with. The true Hermitian ambiguity function does not exhibit any finite sample issues with spreading in local frequency and time lag due to finite sample effects. We can never observe such values in a finite sample, because the maximum concentration of energy will behave like the number of sample points, and thus will be finite for a finite sample length. We compare the estimator with a function for which we insist on the ideal support of the true Hermitian ambiguity function, but that only takes finite sample length realizable values, i.e., we compare the estimators to $\mu_A(\nu, \eta]I((\nu, \eta] \in \mathcal{D})$. If the process under consideration is an analytic process obtained from a real-valued process, \mathcal{D} is the support of the Hermitian ambiguity function of the real-valued process.

For the locally thresholded EAF, we divide the ambiguity plane in three squared annuli, where \mathcal{M}_1 is the region where $|\eta| \leq N/3$ and $|\nu| \leq 1/6$. The outer region \mathcal{M}_3 is given by $|\eta| > 2N/3$ and/or $|\nu| > 1/3$, and the remaining points in the plane form the middle region \mathcal{M}_2 , this is illustrated in Figure 4.1 for $N = 256$. The segmentation is chosen simply because we know that the Hermitian ambiguity function has its maximum value at the origin, and we expect it to decay with ν and η . For single-component processes, this decay is reasonable to assume. We estimate the mean square error of the estimator by Monte Carlo simulation, averaged over 5000 realizations of the given processes. The total mean square error of the estimator is the sum over all points of the estimated mean square error. Throughout this section, $\epsilon[n]$ denotes a real-valued Gaussian white noise process with unit variance $\sigma_\epsilon^2 = 1$ and the sample length is $N = 256$, unless otherwise specified. We have chosen to treat the rim of the EAF as the rest of the function, but it would be easy to equivalently set the rim coefficients to zero and not use these coefficients when forming

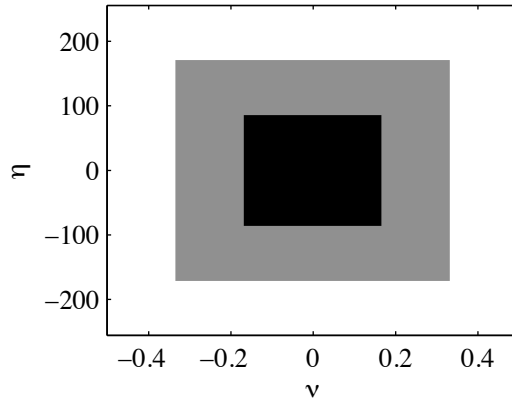


Figure 4.1: Partitioning of the ambiguity plane for estimating the variance in the local thresholding scheme.

the estimator $\hat{\sigma}_\epsilon^4$. Simulation studies verify that using such methods has little impact on the mean square error of the estimator, but significantly improves the estimated spread.

4.3.1 Moving average process

We consider the analytic process $X[n]$ corresponding to a real-valued stationary moving average process $Y[n] = \sum_{i=0}^L \theta_i \epsilon[n-i]$, where

$$\boldsymbol{\theta} = \begin{bmatrix} 1 \\ 0.33 \\ 0.266 \\ 0.2 \\ 0.133 \\ 0.066 \end{bmatrix}. \quad (4.23)$$

Both thresholding procedures give quantities that are zero for most values of $(\nu, \eta]$ outside $\nu \neq 0$, which corresponds to a substantial improvement compared to the EAF. We show the results of the estimated total mean square error and the estimated spread in Table 4.1. The total mean square error of the thresholded estimate is actually reduced by more than a factor of 100 compared to the EAF, which is a substantial reduction. The locally thresholded EAF has a lower mean square error than the thresholded EAF in this case, which is expected since our chosen partition of the ambiguity plane matches the behavior of the process under consideration. The estimated spread is larger than the true spread due to the analytic signal spreading energy in η and the points at the rims that have not been successfully thresholded, but still reflects the fact that $X[n]$ is underspread. Using the discrete analytic signal and problems with edge effects makes the inflated spread inevitable.

	Moving average	Uniformly modulated	Time-varying moving average
Mean square error EAF	204 (465)	331 (71.9)	510 (138)
Mean square error thresholded EAF	9.79 (5.58)	1.74 (0.516)	3.13 (1.77)
Mean square error locally thresholded EAF	9.51 (4.37)	1.71 (0.468)	2.94 (1.25)
Estimated spread thresholded EAF	11 (14)	5.7 (9.0)	11 (16)
Estimated spread locally thresholded EAF	9 (10)	5.6 (7.9)	9 (13)

Table 4.1: Estimated total mean square error (standard deviation) in 10^5 , and estimated spread (standard deviation) in 10^{-4} .

The mean square errors in Table 4.1 might seem high, but we remember that this is the total sum of the mean square error over 261632 pixels.

4.3.2 Uniformly modulated process

Next, we consider the analytic extension of a real-valued non-stationary, uniformly modulated process $Y[n] = \sigma_1[n]\epsilon[n]$ with $\sigma_1[n] = \sin(2\pi f_0 n)$ and $f_0 = 0.0908$. In this case, the Hermitian ambiguity function is only supported on three points, namely the points $(0, 0]$ and $(\pm 2f_0, 0]$. Thresholding has reduced the mean square error with a factor over one hundred compared to the EAF results, and again the locally thresholded EAF has a lower mean square error than the thresholded EAF. The theoretical spread of this process is 1.1466×10^{-5} . Even if the estimated spread is too high, it is still low enough to suggest that $X[n]$ is underspread.

4.3.3 Time-varying moving average

We combine the moving average with the uniformly modulated process, thus defining a time-varying moving average process $Y[n] = \sigma_1[n] \sum_{i=0}^L \theta_i \epsilon[n-i]$, with $f_0 = 0.042$. We consider the analytic process $X[n]$ corresponding to $Y[n]$, and employ the thresholding methods to the EAF. The total mean square error is shown in Table 4.1, and it shows a distinct improvement for the thresholding. The total estimated spread demonstrates that the Hermitian ambiguity function of this process is extremely sparse. Figure 4.2 shows the results for two intersects in the ambiguity plane, the lines $\nu = 0$ and $\eta = 0$. We have kept the points corresponding to the conventional autocorrelation function of the moving average part of the process for $\nu = 0$, except for the point $\eta = \pm 4$ but the support is still reflected. For $\eta = 0$ we have peaks at $\nu = 0$ and $\nu = \pm 2f_0$, as we expect from $\sigma_1[n]$.

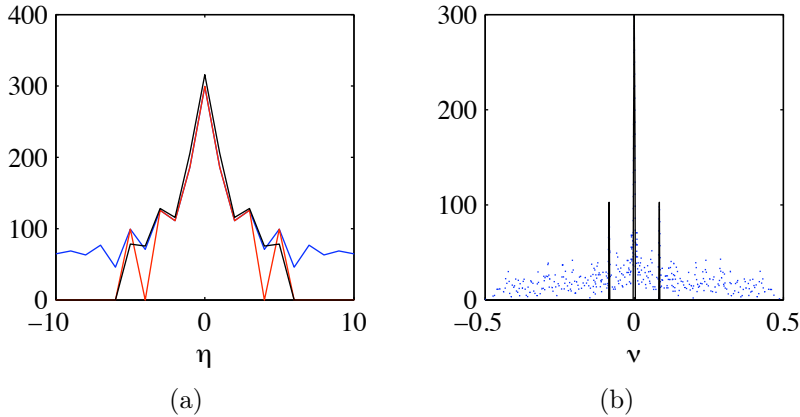


Figure 4.2: For one realization of the time-varying moving average process. (a) $\left| \widehat{A}_{XX^*}^{(LT)}(0, \eta) \right|$ (red), $\left| \widehat{A}_{XX^*}(0, \eta) \right|$ (blue) and $|\mu_A(0, \eta)| I((\nu, \eta) \in \mathcal{D})$ (black). (b) $\left| \widehat{A}_{XX^*}^{(LT)}(\nu, 0) \right|$ (black) and $\left| \widehat{A}_{XX^*}(\nu, 0) \right|$ (blue).

4.3.4 Deterministic chirp in additive Gaussian white noise

We consider the case of the analytic, deterministic linear chirp, $g[n] = \exp[j\pi(2\alpha n + \beta n^2)]$, immersed in an analytic white noise process. The chirp has a starting frequency $\alpha = 0.1$, an end frequency of 0.33 (which gives a chirp rate $\beta = 9.0196 \cdot 10^{-4}$), and the noise has variance 0.6. Figure 4.3 shows the EAF and the locally thresholded EAF for one realization of the process. The Hermitian ambiguity function of a linear chirp should ideally be concentrated on the line intersecting $(0, 0]$ with a gradient of $\partial/\partial\nu A_{gg^*}(\nu, \eta) = \beta^{-1}$, such that theoretically we expect the Hermitian ambiguity function to be nonzero only for one value of ν for each value of η . Because we deal with a finite segment of the chirp, the line will be thicker in the ambiguity domain, but still we expect the EAF to be mostly concentrated around this line. We see that the EAF is substantially corrupted by noise, even if the line caused by the chirp is visible. The thresholding has removed most of the noise and kept almost all (ν, η) on the line. As noted, the line is thicker than what we expect from the theoretical Hermitian ambiguity function, and the thickness is larger for large values of $|\eta|$.

4.4 Discussion

We have proposed an estimator of the Hermitian ambiguity function based on thresholding the EAF obtained from one realization of the process. The estimator has the advantage that it does not increase the support in the ambiguity function, while it has a small variance compared to the EAF. An estimate of the spread in the ambiguity domain is

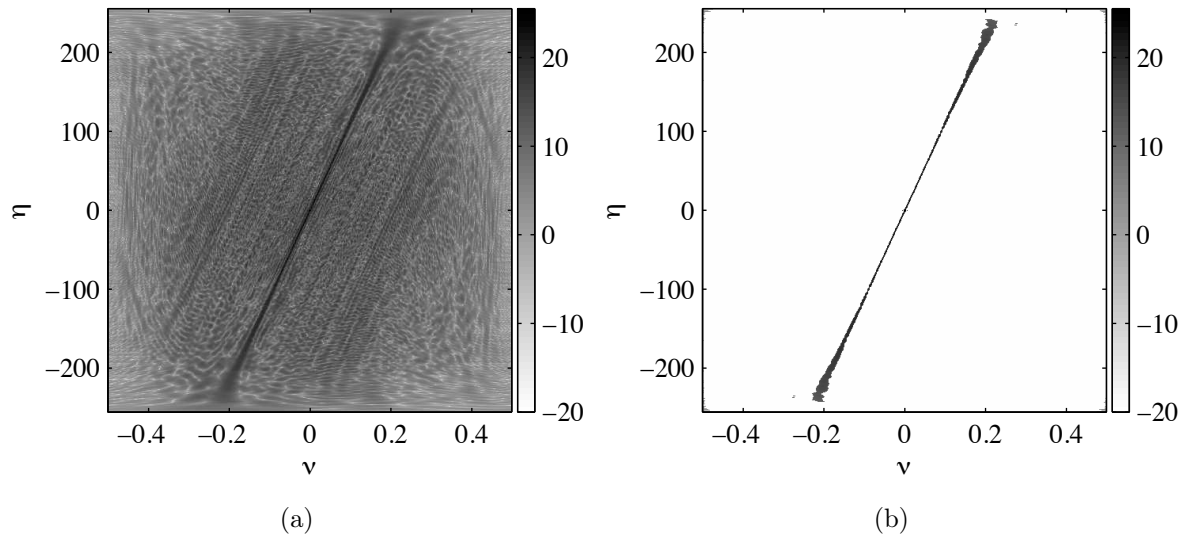


Figure 4.3: (a) $10 \log_{10} \left| \widehat{A}_{XX^*}(\nu, \eta) \right|^2$ and (b) $10 \log_{10} \left| \widehat{A}_{XX^*}^{(LT)}(\nu, \eta) \right|^2$ for one realization of the chirp in additive noise.

readily obtained from this estimator as well, and the numerical examples showed that the estimator has a much lower mean square error than the EAF. However, as is often the case in estimation, we need to know the value of an unknown variance in the estimation procedure. We have chosen to approximate the variance of the EAF of the process under consideration as the variance of the EAF of a stationary white noise process. Thus, we only need to estimate the scale of the data from the EAF itself. This method will work for processes that are close to white noise processes in some manner, and might be considered as somewhat naive for a general process. To improve the estimator, a better method for estimating the variance of the EAF needs to be specified, which is a possibility for further work.

Chapter 5

Generalized Spectral Coherence

We have seen how the second-order moments of complex-valued harmonizable processes can be represented through Hermitian and complementary quantities. However, these quantities are not normalized, such that it is difficult to measure the relative importance of contributions in the moments. In addition, we always need two quantities to completely describe the second-order moments of a complex-valued improper process, one Hermitian and one complementary. We propose measures that describes the second-order behavior of $X(t)$ in an objective and normalized manner, while utilizing both the Hermitian and complementary information in one dimensionless quantity. These measures will be denoted generalized spectral coherences.

By generalized spectral coherences, we understand coherence measures that have been extended from the conventional stationary definition, to a version that accommodates non-stationarities. Stationary processes have no spectral correlations, thus spectral coherences does not make sense for only one stationary process. Rather, coherences are conventionally defined as a univariate measure of spectral correlation between mutually stationary processes. Since nonstationary processes are correlated across frequencies, one can talk about auto spectral coherence, i.e., spectral coherences involving only one process. The generalized coherence will be a bivariate function, either of time and frequency or of two frequency variables. We focus on the time-frequency spectral coherence, but we also present the dual-frequency coherence since it is closely related.

5.1 Time-Frequency Coherence

The frequency content of harmonizable processes may change with time, and we have seen that this may be expressed through the correlation between the process itself and its modulated increment process. We want to define an objective and dimensionless measure of how strong this correlation is, and to that end we will consider estimating the process $X(t)$ from $d\tilde{X}(f) \exp(j2\pi ft)$. The mean square error of any estimate $\hat{X}(t)$ is defined as

$$\epsilon^2 = \text{E} \left\{ \left| X(t) - \hat{X}(t) \right|^2 \right\}. \quad (5.1)$$

A linear estimator of $X(t)$ is constructed by

$$\widehat{X}(t) = \alpha d\widetilde{X}(f) \exp(j2\pi ft) \quad \alpha \in \mathbb{C}. \quad (5.2)$$

If we minimize the mean square error ϵ^2 with respect to α , we obtain the linear minimum mean square error ϵ_L^2 of this estimate as

$$\epsilon_L^2 = \mathbb{E} \{ |X(t)|^2 \} (1 - |\gamma_{X,L}(t, f)|^2), \quad (5.3)$$

where

$$|\gamma_{X,L}(t, f)|^2 = \frac{|P_{XX^*}(t, f)|^2}{M_{XX^*}(t, 0)S_{XX^*}(0, f)} \quad (5.4)$$

is the time-frequency squared correlation coefficient of the estimate.

By Schwartz' inequality we can easily show that $0 \leq |\gamma_{X,L}(t, f)|^2 \leq 1$. The interpretation is that if the squared correlation coefficient has a value close to unity, then $X(t)$ is estimable as a linear function of $d\widetilde{X}(f)e^{j2\pi ft}$. The time-frequency squared correlation coefficient is thus a normalized quantity that measures the correlation between the process itself and its modulated increment process at a fixed time and frequency. This suggests that $|\gamma_{X,L}(t, f)|^2$ may be used as a measure of the time-frequency magnitude squared coherence, and we denote $|\gamma_{X,L}(t, f)|^2$ the time-frequency Linear Magnitude Squared Coherence (or the time-frequency LMSC) of a complex-valued harmonizable process. The time-frequency LMSC is identical to the magnitude squared coherence measure based on Hilbert space inner product considerations proposed in [Hanssen and Scharf, 2003]. Note that $|\gamma_{X,L}(t, f)|^2$ only depends on the Hermitian second-order quantities of the process.

Since the process and the increment process are in general complex-valued, we should not limit ourselves to estimate $X(t)$ as a linear function of $d\widetilde{X}(f)e^{j2\pi ft}$. A widely linear estimator forms an estimate of $X(t)$ as a linear combination of $d\widetilde{X}(f)e^{j2\pi ft}$ and its complex conjugate $d\widetilde{X}^*(f)e^{-j2\pi ft}$ [Picinbono and Chevalier, 1995], i.e.,

$$\widehat{X}(t) = \alpha d\widetilde{X}(f)e^{j2\pi ft} + \beta d\widetilde{X}^*(f)e^{-j2\pi ft} \quad \alpha, \beta \in \mathbb{C}. \quad (5.5)$$

Thus, $\widehat{X}(t)$ is no longer a linear function of $d\widetilde{X}(f)e^{j2\pi ft}$. However, the moment of order k of $\widehat{X}(t)$ is completely defined from the moments of order k of $d\widetilde{X}(f)e^{j2\pi ft}$ and $d\widetilde{X}^*(f)e^{-j2\pi ft}$, which characterizes a form of linearity [Picinbono and Chevalier, 1995]. The mean square error associated with this estimate is given by (5.1). By minimizing the mean square error with respect to α and β , we obtain the so-called widely linear minimum mean square error

$$\epsilon_{wL}^2 = \mathbb{E} \{ |X(t)|^2 \} (1 - |\gamma_{X,wL}(t, f)|^2), \quad (5.6)$$

where

$$|\gamma_{X,wL}(t, f)|^2 = \frac{\gamma_N(t, f)}{\gamma_D(t, f)}, \quad (5.7)$$

with

$$\begin{aligned} \gamma_N(t, f) &= (|P_{XX^*}(t, f)|^2 + |P_{XX}(t, -f)|^2) S_{XX^*}(0, f) \\ &\quad - 2\text{Re}\{e^{j4\pi ft} S_{XX}(2f, -f) P_{XX}^*(t, -f) P_{XX^*}(t, f)\} \end{aligned} \quad (5.8)$$

and

$$\gamma_D(t, f) = M_{XX^*}(t, 0) [|S_{XX^*}(0, f)|^2 - |S_{XX}(2f, -f)|^2]. \quad (5.9)$$

Here, $|\gamma_{X,WL}(t, f)|^2$ is the time-frequency squared correlation coefficient of the widely linear estimate.

The coefficient $|\gamma_{X,WL}(t, f)|^2$ is a normalized quantity that has a value close to unity if $X(t)$ is estimable as a widely linear function of $d\tilde{X}(f)e^{j2\pi ft}$. We propose the quantity $|\gamma_{X,WL}(t, f)|^2$ as an alternative time-frequency magnitude squared coherence of harmonizable processes, which we denote the time-frequency Widely Linear Magnitude Squared Coherence (or time-frequency WLMSC). Note that $|\gamma_{X,WL}(t, f)|^2$ depends on both the HKR-spectrum and the CKR-spectrum, both dual-frequency spectra and the variance of the process. We see that the numerator of $|\gamma_{X,WL}(t, f)|^2$ depends on the magnitude squared of both KR-spectra, which can be seen as an expansion of $|\gamma_{X,L}(t, f)|^2$ to include the complementary functions. But it also contains the real part of a cross term that makes $|\gamma_{X,WL}(t, f)|^2$ depend on the phase of the complex-valued KR-spectra as well. We also recognize the first factor in $\gamma_D(t, f)$ from the denominator of $|\gamma_{X,L}(t, f)|^2$, while the second factor again includes the complementary information.

Time-frequency coherence measures for harmonizable processes based on widely linear estimation were also discussed in [Schreier, 2007; Schreier, 2008a], where a coherence measure was used to determine the fit of approximating the process $X(t)$ at time t with a local ellipse at (t, f) . We estimate the process at time t as a widely linear function of the increment process at frequency f to obtain our coherence measure. In [Schreier, 2007; Schreier, 2008a], the process is estimated as a widely linear function of both the increment process at frequency f and the increment process at frequency $-f$, thus $X(t)$ is estimated from four quantities. This coherence measure may be applied to cases where separating the behavior for positive and negative frequencies are not necessary. However, since complex-valued processes will not have a symmetric frequency content, we would in general not mix positive and negative frequencies. We also note that [Schreier, 2008b] discusses correlation coefficients for complex-valued random variables, a topic closely related to coherence measures for complex-valued random processes.

5.2 Dual-Frequency Coherence

The increment process $d\tilde{X}(f)$ of a harmonizable process $X(t)$ is in general a non-orthogonal random function, i.e., it exhibits correlation across different frequencies. To quantify this correlation, we consider the dual-frequency coherence of the process. Following along the same lines as for the time-frequency coherence, we derive a useful definition of the dual-frequency coherence by estimating the increment process at a single frequency, $d\tilde{X}(f + \nu)$, from the increment process at another frequency, $d\tilde{X}(f)$. By minimizing the mean square error associated with estimating $d\tilde{X}(f + \nu)$ as a linear function of $d\tilde{X}(f)$, we obtain the minimum mean square error

$$\epsilon_L^2 = \text{E} \left\{ |d\tilde{X}(f + \nu)|^2 \right\} (1 - |\rho_{X,L}(\nu, f)|^2), \quad (5.10)$$

where

$$|\rho_{X,L}(\nu, f)|^2 = \frac{|S_{XX^*}(\nu, f)|^2}{S_{XX^*}(0, f) S_{XX^*}(0, f + \nu)}. \quad (5.11)$$

Thus, $|\rho_{X,L}(\nu, f)|^2$ can be used as a measure of the dual-frequency LMSC of the process [Hanssen and Scharf, 2003]. Like the time-frequency LMSC, the dual-frequency LMSC only depends on Hermitian quantities of the process, actually it only depends on the Hermitian dual-frequency spectrum.

If we estimate $d\tilde{X}(f + \nu)$ from $d\tilde{X}(f)$ by a widely linear estimator, and subsequently minimize the mean square error, the minimum mean square error of the estimate is found to be

$$\epsilon_{WL}^2 = \text{E} \left\{ |d\tilde{X}(f + \nu)|^2 \right\} (1 - |\rho_{X,WL}(\nu, f)|^2), \quad (5.12)$$

where

$$|\rho_{X,WL}(\nu, f)|^2 = \frac{\rho_N(\nu, f)}{\rho_D(\nu, f)}, \quad (5.13)$$

with

$$\begin{aligned} \rho_N(\nu, f) &= (|S_{XX^*}(\nu, f)|^2 + |S_{XX}(2f + \nu, -f)|^2) S_{XX^*}(0, f) \\ &\quad - 2\text{Re}\{S_{XX}(2f, -f)S_{XX^*}^*(2f + \nu, -f)S_{XX^*}(\nu, f)\}, \end{aligned} \quad (5.14)$$

and

$$\rho_D(\nu, f) = S_{XX^*}(0, f + \nu) [|S_{XX^*}(0, f)|^2 - |S_{XX}(2f, -f)|^2]. \quad (5.15)$$

This defines the dual-frequency WLMSC $|\rho_{X,WL}(\nu, f)|^2$, which utilizes the complementary dual-frequency spectrum as well as the Hermitian dual-frequency spectrum of the process. The connection between $|\rho_{X,L}(\nu, f)|^2$ and $|\rho_{X,WL}(\nu, f)|^2$ is the same as the connection between $|\gamma_{X,L}(t, f)|^2$ and $|\gamma_{X,WL}(t, f)|^2$, in that the numerator and denominator has been expanded in similar ways to include the complementary information. Note that $|\rho_{X,L}(0, f)|^2 = 1$ and $|\rho_{X,WL}(0, f)|^2 = 1$ for all f , which is just to say that there is full coherence between $d\tilde{X}(f)$ and $d\tilde{X}(f)$. This equals the standard single-frequency magnitude squared auto-coherence for stationary processes.

5.3 Geometry

The orthogonality condition states that the mean square error of the best linear estimate of a variable Z based on a variable Q is orthogonal to Q [Picinbono, 1993]. Likewise, the mean square error of the best widely linear estimate of Z is orthogonal to both Q and Q^* [Picinbono and Chevalier, 1995]. In the widely linear case, the estimate of $X(t)$ can be seen as the projection of $X(t)$ onto the vector space spanned by $d\tilde{X}(f)e^{j2\pi ft}$ and $d\tilde{X}^*(f)e^{-j2\pi ft}$, as illustrated in Figure 5.1(a). The magnitude squared coherence $|\gamma_{X,WL}(t, f)|^2$ is the magnitude squared of the cosine of the angle associated with the Hilbert space inner product

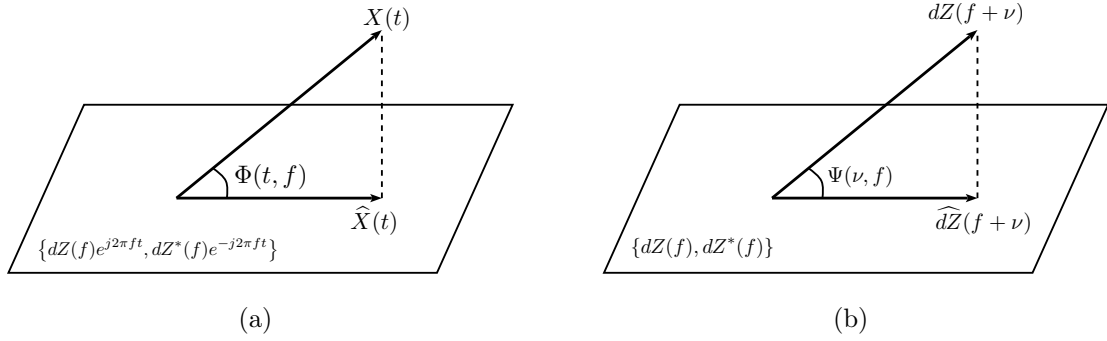


Figure 5.1: (a) The projection of $X(t)$ onto the vector space spanned by $d\tilde{X}(f) \exp(j2\pi ft)$ and $d\tilde{X}^*(f) \exp(-j2\pi ft)$. (b) The projection of $d\tilde{X}(f + \nu)$ onto the vector space spanned by $d\tilde{X}(f)$ and $d\tilde{X}^*(f)$.

between the process and the estimate,

$$|\gamma_{X,WL}(t, f)|^2 = |\cos[\Phi(t, f)]|^2 = \frac{|\langle X(t), \hat{X}(t) \rangle|^2}{\langle X(t), X(t) \rangle \langle \hat{X}(t), \hat{X}(t) \rangle}. \quad (5.16)$$

As the angle $\Phi(t, f)$ approaches zero, $X(t)$ will be contained in the vector space spanned by $d\tilde{X}(f)e^{j2\pi ft}$ and $d\tilde{X}^*(f)e^{-j2\pi ft}$, and a small value of $\Phi(t, f)$ implies a value of $|\gamma_{X,WL}(t, f)|^2$ close to unity.

For the dual-frequency WLMSC, the estimate of $d\tilde{X}(f + \nu)$ is the projection of $d\tilde{X}(f + \nu)$ onto the vector space spanned by $d\tilde{X}(f)$ and $d\tilde{X}^*(f)$, as seen in Figure 5.1(b). Thus, $|\rho_{X,WL}(\nu, f)|^2$ is the magnitude squared of the cosine of the angle associated with the Hilbert space inner product $\langle d\tilde{X}(f + \nu), \widehat{d\tilde{X}(f + \nu)} \rangle$, i.e.,

$$\begin{aligned} |\rho_{X,WL}(\nu, f)|^2 &= |\cos[\Psi(\nu, f)]|^2 \\ &= \frac{|\langle d\tilde{X}(f + \nu), \widehat{d\tilde{X}(f + \nu)} \rangle|^2}{\langle d\tilde{X}(f + \nu), d\tilde{X}(f + \nu) \rangle \langle \widehat{d\tilde{X}(f + \nu)}, \widehat{d\tilde{X}(f + \nu)} \rangle}. \end{aligned} \quad (5.17)$$

As the angle $\Psi(\nu, f)$ approaches zero, $d\tilde{X}(f + \nu)$ will be contained in the vector space spanned by $d\tilde{X}(f)$ and $d\tilde{X}^*(f)$, and $|\rho_{X,WL}(\nu, f)|^2$ will approach unity. The dual-frequency and the time-frequency LMSC will have equivalent interpretations as the magnitude squared of the cosine of the angle associated with Hilbert space inner products. The difference is that for the LMSCs, the estimate $\widehat{d\tilde{X}(f + \nu)}$ can be seen as the projection of $d\tilde{X}(f + \nu)$ onto the vector space spanned by $d\tilde{X}(f)$, and the estimate $\hat{X}(t)$ is the projection of $X(t)$ onto the vector space spanned by $d\tilde{X}(f) \exp(j2\pi ft)$.

5.4 Properties

The magnitude squared coherence measures obtained in (5.7) and (5.13) are valid for all complex-valued harmonizable processes. We will consider three important subclasses of complex-valued processes, namely proper processes, analytic processes, and real-valued processes. We will also briefly sketch how the coherence measures can be extended to cross-coherences.

5.4.1 Proper processes

The complementary quantities of a proper complex-valued process are zero everywhere, which implies that $|\gamma_{X,WL}(t, f)|^2 = |\gamma_{X,L}(t, f)|^2$ and $|\rho_{X,WL}(\nu, f)|^2 = |\rho_{X,L}(\nu, f)|^2$. Thus, for proper processes, widely linear estimation reduces to linear estimation, and the proposed magnitude squared coherences will not add any new information.

5.4.2 Analytic processes

The analytic process $X(t)$ corresponding to the real-valued process $Y(t)$ has the spectral representation in (2.21), with $d\tilde{X}(f) = 2d\tilde{Y}(f)u(f)$. There is no correlation between the increment process at a positive frequency and the increment process at a negative frequency. In [Hindberg and Hanssen, 2007] this was found to lead to $S_{XX}(2f, -f) = 0$ for analytic processes. This is incorrect, $S_{XX}(2f, -f)$ for an analytic process corresponding to a real-valued harmonizable process will in fact never be zero for all non-negative frequencies (it can be zero for some values of f). The expressions for the time-frequency WLMSC and dual-frequency WLMSC will not simplify for analytic, improper processes. However, they will have a limited support in the plane,

$$|\gamma_{X,WL}(t, f)|^2 = \begin{cases} |\gamma_{Y,WL}(t, f)|^2 & \text{for } f \geq 0 \\ 0 & \text{for } f < 0 \end{cases} \quad (5.18)$$

and

$$|\rho_{X,WL}(\nu, f)|^2 = \begin{cases} |\rho_{Y,WL}(\nu, f)|^2 & f \geq 0, f \geq -\nu \\ 0 & \text{elsewhere.} \end{cases} \quad (5.19)$$

Thus the time-frequency WLMSC of an analytic process has the same support as the HKR-spectrum of an analytic process, and likewise the dual-frequency WLMSC has the same support as the Hermitian dual-frequency spectrum.

5.4.3 Real-valued processes

For real-valued processes, the Hermitian and the complementary quantities are identical. The increment process is still complex-valued, however, such that the potential for using widely linear estimation is still there. In general, $|\gamma_{X,WL}(t, f)|^2 \neq |\gamma_{X,L}(t, f)|^2$ and

$|\rho_{X,WL}(\nu, f)|^2 \neq |\rho_{X,L}(\nu, f)|^2$ for real-valued processes. In determining the time-frequency WLMSC of real-valued processes, we estimate a real quantity $X(t)$ from a complex quantity $d\tilde{X}(f) \exp(j2\pi ft)$. For real-valued processes, the numerator of $|\gamma_{X,WL}(t, f)|^2$ reduces to

$$\gamma_N(t, f) = 2 |P_{XX^*}(t, f)|^2 S_{XX^*}(0, f) - 2 \operatorname{Re}\{e^{-j4\pi ft} S_{XX^*}(2f, -f) P_{XX^*}^2(t, f)\}. \quad (5.20)$$

Thus, the time-frequency WLMSC may be useful even for real-valued processes. Also, $|\gamma_{X,WL}(t, f)|^2$ will be singular for $f = 0$ for real-valued processes, since $d\tilde{X}(0)$ is real-valued. We may use the time-frequency LMSC for this line solely, such that $|\gamma_{X,WL}(t, 0)|^2 = |\gamma_{X,L}(t, 0)|^2$.

For the dual-frequency coherence, $|\rho_{X,WL}(\nu, f)|^2$ will be singular at $f = 0$ for real-valued processes. Since $d\tilde{X}(0)$ is real-valued, it does not make any sense to estimate $d\tilde{X}(-\nu)$ as a widely linear function of $d\tilde{X}(0)$. To deal with the singularity at $f = 0$, we carry out the analysis on the analytic process corresponding to the real-valued process. Note that for real-valued processes, the dual-frequency WLMSC has the symmetries

$$|\rho_{X,WL}(\nu, f)|^2 = |\rho_{X,WL}(-\nu, -f)|^2 = |\rho_{X,WL}(\nu + 2f, -f)|^2 = |\rho_{X,WL}(-\nu - 2f, f)|^2. \quad (5.21)$$

Analyzing the analytic process gives us the magnitude squared coherence $|\rho_{X,WL}(\nu, f)|^2$ of the real-valued process in the region $f \geq 0, f \geq \nu$. By the symmetries in (5.21) we can determine $|\rho_{X,WL}(\nu, f)|^2$ in the entire f - ν plane from this.

5.4.4 Generalized Cross-Coherences

We can easily extend the results to cross-coherences, i.e., coherences between a pair of mutually harmonizable random processes. Let $d\tilde{X}(f)$ and $d\tilde{Y}(f)$ be the increment processes of the two mutually harmonizable random processes $X(t)$ and $Y(t)$, respectively. By estimating $Y(t)$ from $d\tilde{X}(f)e^{j2\pi ft}$ as in Section 5.1, we obtain the time-frequency magnitude squared cross-coherences $|\gamma_{XY,L}(t, f)|^2$ and $|\gamma_{XY,WL}(t, f)|^2$. Likewise, we find the dual-frequency magnitude squared cross-coherences $|\rho_{XY,L}(\nu, f)|^2$ and $|\rho_{XY,WL}(\nu, f)|^2$ by estimating $d\tilde{Y}(f - \nu)$ from $d\tilde{X}(f)$ following the lines of Section 5.2. In contrast to the auto-coherence case, the cross-coherences will in general have $|\rho_{XY,L}(0, f)|^2 \neq 1$ and $|\rho_{XY,WL}(0, f)|^2 \neq 1$. Note that $|\rho_{XY,L}(0, f)|^2$ is the conventional single-frequency magnitude squared cross-coherence between two mutually stationary processes.

5.5 Discussion

We have presented alternative measures with which we can represent the second-order statistical information of the process in the time-frequency and the dual-frequency domain. We showed how previously defined spectral coherence measures can be obtained through a linear estimation scheme. These measures only depend on the Hermitian quantities of the

process. Since we generally deal with complex-valued quantities, and since the increment process is generally complex-valued, we proposed to use a widely linear estimation scheme to define alternative spectral coherence measures. These alternative measures simultaneously utilize the Hermitian and complementary quantities of complex-valued processes, as well as providing dimensionless and objective measures of the behavior of the process in the time-frequency and dual-frequency domain. We showed that the WLMSCs reduce to the corresponding LMSCs for proper processes, but for analytic processes, real-valued processes and of course general complex-valued processes, the WLMSC may provide additional insight into the second-order structure of the process.

Chapter 6

Stochastic Differential Equations

An interesting field where the HKR-spectrum of random processes gives additional insight into the problem is the field of stochastic differential equations. Differential equations are very important in mathematical modeling of physical systems, and we solve differential equations in order to learn something about the underlying process that the equation governs. Stochastic differential equations have been extensively studied from a mathematical point of view (see e.g. [Øksendal, 2002; Gardiner, 2004]). To solve a stochastic differential equation directly, we need to know how to integrate a random function. Two main different definitions of stochastic integration exist, namely the Itô integral and the Stratonovich integral [Øksendal, 2002]. The ambiguous nature of stochastic integrals makes stochastic differential equations difficult to handle. For random processes, we consider the moments of the process rather than the process itself, and we have focused on the time-frequency domain in particular. Inspired by [Hanssen, 2009], we will use the HKR-spectrum to analyze stochastic differential equations. We restrict our attention to the Hermitian second-order quantities, without any assumptions of propriety of the process.

6.1 Differential Equation Basics

We first introduce linear ordinary differential equations (ODEs) mathematically, and discuss how to represent the ODE in the time-frequency domain. A general ODE of order M has the form

$$a_M \frac{d^M}{dt^M} X(t) + \cdots + a_1 \frac{d}{dt} X(t) + a_0 X(t) = G(t), \quad (6.1)$$

where $X(t)$ is the process of interest, $G(t)$ is a driving process and $\{a_m\}_{m=0}^M$ is a set of complex-valued coefficients we denote the system coefficients. We express this as the linear system

$$\mathfrak{L}\{X(t)\} = G(t), \quad (6.2)$$

with the linear differential operator defined by

$$\mathfrak{L} = \sum_{m=0}^M a_m \frac{d^m}{dt^m}. \quad (6.3)$$

We will without loss of generality assume that $a_M = 1$. An ODE is stochastic if either the driving force $G(t)$ is a random process or if one or more of the system coefficients are random variables. We assume that $X(t)$ belongs to the class of harmonizable, complex-valued, zero-mean processes, and $G(t)$ either belongs to the same class or is a deterministic signal. The M -order derivative of the harmonizable process $X(t)$ exists in the mean square sense if and only if

$$\iint |f\nu|^M S_{XX^*}(\nu, f) d\nu df < \infty. \quad (6.4)$$

This result was presented for stationary processes in [Yaglom, 1987], the corresponding result for harmonizable processes is obtained similarly. We assume that the derivative of $X(t)$ always exists up to the desired order M .

Since we are dealing with nonstationary random processes, the frequency content of the process may change with time, and since the ODE is originally specified in time, the time-frequency domain seems to be the best domain for analyzing the second-order moments of a stochastic ODE. Time-frequency representation of differential equations has been considered in a recent series of papers, see [Galleani and Cohen, 2002; Galleani and Cohen, 2004a; Galleani and Cohen, 2004b; Yang and Cohen, 2005; Galleani and Cohen, 2006a; Galleani and Cohen, 2006b]. However, these papers express the differential equations through the Wigner-Ville time-frequency spectrum. There are two main reasons why the KR-spectra should be preferred over the Wigner-Ville for ODEs. The standard reason is that the Wigner-Ville spectrum has no physical interpretation, while the HKR-spectrum has an interpretation as a measure of correlation across time and frequency. Specifically for differential equations, we prefer to represent an ODE of order M through the HKR-spectrum, since this results in an ODE of the same order M in the time-frequency domain. If we use the Wigner-Ville representation, the corresponding ODE in time-frequency will be of order $2M$, which will lead to a much more complicated problem.

6.1.1 System interpretation

General system theory states that a linear and time-invariant system can be represented through its impulse response, and the output of the system is given as a convolution between the input and this impulse response. The system has an even simpler representation in the Fourier domain, where the FT of the output is the product of the FT of the input and the FT of the impulse response. Let us then consider the system specified in (6.1) in the Fourier domain, to see if we can simplify the system representation. Since $X(t)$ and $G(t)$ are harmonizable, they have the spectral representation in (2.1) with increment processes $d\tilde{X}(f)$ and $d\tilde{G}(f)$, respectively. If we insert the spectral representation of $X(t)$ and $G(t)$

in the system, we get

$$\int e^{j2\pi ft} [(j2\pi f)^M + \dots + a_1 j2\pi f + a_0] d\tilde{X}(f) = \int e^{j2\pi ft} d\tilde{G}(f). \quad (6.5)$$

Thus

$$D(f)d\tilde{X}(f) = d\tilde{G}(f), \quad (6.6)$$

where we have defined the *characteristic function* $D(f)$ of the ODE as

$$D(f) = \sum_{m=0}^M a_m (j2\pi f)^m = (j2\pi)^M \prod_{i=1}^M (f - p_i). \quad (6.7)$$

If $D(f) \neq 0 \forall f$, i.e., $\text{Im}\{p_i\} \neq 0 \forall i$, we get

$$d\tilde{X}(f) = \frac{1}{D(f)} d\tilde{G}(f), \quad (6.8)$$

which can be expressed in the time domain as

$$X(t) = h(t) \star G(t). \quad (6.9)$$

The impulse response is defined as

$$h(t) = \int \frac{1}{D(f)} e^{j2\pi ft} df. \quad (6.10)$$

Thus, $X(t)$ is the output from a linear time-invariant system with impulse response $h(t)$ and input $G(t)$. The output $X(t)$ of a linear time-invariant system is ensured to be harmonizable if the input $G(t)$ is harmonizable and the condition

$$\iint \left| \frac{S_{GG^*}(\nu, f)}{D(f)D(f+\nu)} \right| d\nu df < \infty. \quad (6.11)$$

is fulfilled [Yaglom, 1987]. In general we need $D(f) \neq 0 \forall f$ to satisfy this condition, unless we design the input signal such that possible singularities become removable. This will place strict system-dependent restrictions on the form of $G(t)$. We will not consider this case, and thus demand that $D(f) \neq 0 \forall f$. Note that if $G(t)$ is deterministic, $d\tilde{G}(f) = G(f)df$, where $G(f)$ is the FT of $G(t)$.

The method of transforming an ODE to the Fourier domain is a standard approach to solving the equation, since solving the ODE in the Fourier domain only consists of dividing by $D(f)$ on both sides of the equation. As long as we can transform back to the time domain, this approach is quite simple. However, for stochastic differential equations we still have problems with stochastic integration. If some of the system coefficients are random variables, we need to solve a stochastic integral to obtain $h(t)$. If $G(t)$ is a random process, the convolution in (6.9) will be a stochastic integral. Even if this system interpretation of the ODE provides additional insight into the problem, we still cannot solve the stochastic ODE from this.

The impulse response

We take a closer look at the impulse response $h(t)$ of the ODE. If we assume that all system coefficients are deterministic, the impulse response is defined in (6.10). This is an ordinary deterministic integral which we can solve using standard residue theory [Cauchy, 1890] (see e.g., [Ablowitz and Fokas, 2003] for a tutorial). We recall that we have assumed that $D(f)$ has no real-valued roots. The residue of a function $z(f)$ at pole $f = p_i$ with multiplicity m_i is defined as [Ablowitz and Fokas, 2003]

$$\text{Res}(z(f), p_i) = \lim_{f \rightarrow p_i} \frac{1}{(m_i - 1)!} \frac{d^{m_i-1}}{df^{m_i-1}} z(f) (f - p_i)^{m_i}. \quad (6.12)$$

Thus, the impulse response is given by

$$h(t) = \frac{1}{(j2\pi)^{M-1}} \sum_{i=1}^{M_d} \text{Res} \left(\frac{e^{j2\pi ft}}{\prod_{i=1}^M (f - p_i)}, p_i \right) \tilde{u}(t, p_i), \quad (6.13)$$

where we have defined

$$\tilde{u}(t, p_i) = \begin{cases} u(t) & \text{Im}\{p_i\} > 0 \\ u(t) - 1 & \text{Im}\{p_i\} < 0, \end{cases} \quad (6.14)$$

and $\{p_i\}_{i=1}^{M_d}$ are all the distinct roots of the characteristic function.

If $M_d = M$, we have

$$h(t) = \frac{1}{(j2\pi)^{M-1}} \sum_{i=1}^M \frac{e^{j2\pi p_i t}}{\prod_{m \neq i} (p_i - p_m)} \tilde{u}(t, p_i), \quad (6.15)$$

which can be written as

$$h(t) = \frac{u(t)}{(j2\pi)^{M-1}} \sum_{i=1}^{M_p} \frac{e^{j2\pi p_i t}}{\prod_{m \neq i} (p_i - p_m)} + \frac{u(t) - 1}{(j2\pi)^{M-1}} \sum_{i=M_p+1}^M \frac{e^{j2\pi p_i t}}{\prod_{m \neq i} (p_i - p_m)}. \quad (6.16)$$

Here, $\{p_i\}_{i=1}^{M_p}$ is the set of poles with positive imaginary values, and $\{p_i\}_{i=M_p+1}^M$ is the set of poles with negative imaginary values. The first term in (6.16) thus determines the impulse response for $t \geq 0$. If $D(f)$ only has roots with positive imaginary values, i.e., $M_p = M$, the system is causal. The concept of causality is important in real-time systems, in many cases it is necessary that there is no output from the system prior to the input starting. In order to design a causal system, $D(f)$ can only have roots with positive imaginary values.

6.1.2 The HKR-spectrum of differential equations

In order to express the ODE in (6.1) in the time-frequency domain, we need to know the HKR-spectrum of the derivatives of a harmonizable process $X(t)$. The cross HKR-spectrum

of $X_i(t) = a_i d^i X(t)/dt^i$ and $X_m(t) = a_m d^m X(t)/dt^m$ is given by

$$R_{X_i X_m^*}(t, f) = a_i a_m^* (-j2\pi f)^m \left(\frac{d}{dt} + j2\pi f \right)^i R_{XX^*}(t, f). \quad (6.17)$$

Thus, it is completely determined as a function of the HKR-spectrum of $X(t)$. By forming the HKR-spectrum from each side of (6.1), we get the time-frequency representation of the ODE, which is a linear ODE in the time-frequency domain,

$$\left[\sum_{i=0}^M a_i (j2\pi f)^i \right]^* \left[\sum_{m=0}^M a_m \left(\frac{d}{dt} + j2\pi f \right)^m \right] R_{XX^*}(t, f) = R_{GG^*}(t, f), \quad (6.18)$$

or

$$\sum_{m=0}^M a_m \left(\frac{d}{dt} + j2\pi f \right)^m R_{XX^*}(t, f) = \frac{R_{GG^*}(t, f)}{D^*(f)}. \quad (6.19)$$

Note that the ODE in time-frequency is of the same order M as the original ODE in time. By considering the ODE in the time-frequency domain, we avoid stochastic integration, and we still obtain information about how the system changes with time. We can solve this ODE in time-frequency with standard methods. However, closed-form expressions of the HKR-spectrum of $X(t)$ are harder to find when the order M increases or the driving force $G(t)$ is complicated. Numerical solutions are possible, but they will be slow since we need to solve a different ODE for each frequency f .

6.1.3 Time-varying coefficients

If the coefficients are allowed to be time-varying, the FT of (6.1) will contain convolutions in frequency between the FT of the time-varying coefficients and $d\tilde{X}(f)$. In this case, we cannot solve for a simple expression for $d\tilde{X}(f)$ and find $X(t)$ from that. We can of course express this kind of a differential equation in the time-frequency domain, but solving for the HKR-spectrum of $X(t)$ will require a deconvolution. However, if the coefficients have a polynomial time dependency, we avoid convolutions because a multiplication with t in time results in a derivation with respect to f in frequency. We find the HKR-spectrum between $X_1(t) = \gamma_1 t^\mu \frac{d^m}{dt^m} X(t)$ and $X_2(t) = \gamma_2 t^\zeta \frac{d^i}{dt^i} X(t)$ to be

$$R_{X_1 X_2^*}(t, f) = \gamma_1^* \gamma_2 t^\mu \left(\frac{\partial}{\partial t} - j2\pi f \right)^m \left(t - \frac{d}{2\pi j df} \right)^\zeta (j2\pi f)^i R_{XX^*}(t, f). \quad (6.20)$$

From this, we can find the corresponding time-frequency representation of a general ODE in time with system coefficients given as polynomials. We see that this results in a partial differential equation (PDE) in time-frequency. The Wigner-Ville time-frequency representation of ODEs with time-varying coefficients of general forms was presented in [Galleani and Cohen, 2004a; Galleani and Cohen, 2006b]. Here, the coefficients are not assumed to have a polynomial form explicitly, however no examples of other forms are provided in these papers. We limit ourselves to solving ODEs with time-invariant coefficients in the remaining.

6.1.4 Homogeneous solution

An ODE will have a solution consisting of a homogeneous solution, which is the solution to the undriven ODE

$$\sum_{m=0}^M a_m \left(\frac{d}{dt} + j2\pi f \right)^m R_{XX^*}(t, f) = 0. \quad (6.21)$$

and a particular solution that involves the driving force. The homogenous solution to the ODE in the time-frequency domain is

$$R_{XX^*}(t, f) = \sum_{i=1}^{M_d} c_i(f) t^{m_i-1} e^{j2\pi(p_i-f)t}, \quad (6.22)$$

where again $\{p_i\}_{i=1}^{M_d}$ are the M_d distinct roots of the characteristic function and m_i is the multiplicity of the root p_i . The coefficients $\{c_i(f)\}_{i=1}^{M_d}$ are determined from the initial conditions of the ODE. We note that if a root of $D(f)$ has a positive imaginary value, this corresponds to the characteristic equation of the ODE having a root with negative real value. Thus, the fact that only roots with positive imaginary values contribute for positive time instants is related to the stability of the system. If we have a root of the characteristic equation with a positive real value, the solution will grow exponentially, leading to an unstable system for $t > 0$. For $t < 0$, the system is unstable if a root of the characteristic equation has a negative real value.

From a system point of view, we are mainly interested in the particular solution to the ODE, since the particular solution relates the output to the input. We also note that if the homogeneous solution is non-zero for one value of t is non-zero for all values of t (except maybe $t = 0$). In real-world scenarios, we are restricted by the concept of time. Usually, both the input signal and output signal will have a start time and an end time. If we require an output with limited time support, the homogeneous solution must be zero everywhere. Finally, we note that finding initial conditions in the time-frequency domain that corresponds to initial conditions given in the time domain is not a trivial task.

6.2 Particular Solutions in the Dual-Frequency Domain

Particular solutions of ODEs can, as already mentioned, be found by transforming the ODE to the Fourier domain. We likewise propose to find a particular solution to our ODE in time-frequency by transforming the time-frequency ODE to the dual-frequency domain. We start by assuming that the coefficients of the ODE are deterministic. The increment processes of $X(t)$ and $G(t)$ are related through (6.8), and if we form the dual-frequency spectrum from both sides of this equation, we get

$$D^*(f)D(f + \nu)S_{XX^*}(\nu, f) = S_{GG^*}(\nu, f). \quad (6.23)$$

Since we have assumed that $D(f) \neq 0$, this can also be written as

$$S_{XX^*}(\nu, f) = \frac{S_{GG^*}(\nu, f)}{D^*(f)D(f + \nu)}. \quad (6.24)$$

We find the HKR-spectrum of $X(t)$ through an inverse FT of $S_{XX^*}(\nu, f)$ with respect to ν ,

$$R_{XX^*}(t, f) = \frac{1}{D^*(f)} \iint \frac{e^{j2\pi\nu(t-\xi)}}{D(f + \nu)} R_{GG^*}(\xi, f) d\nu d\xi, \quad (6.25)$$

which can be expressed as

$$R_{XX^*}(t, f) = R_{HH^*}(t, f) \star_t R_{GG^*}(t, f). \quad (6.26)$$

Here, \star_t denotes convolution with respect to the variable t , and

$$\begin{aligned} R_{HH^*}(t, f) &= \frac{h(t)}{D^*(f)} e^{-j2\pi ft} \\ &= \frac{e^{-j2\pi ft}}{-j(2\pi)^{2M-1} \prod_{i=1}^M (f - p_i^*)} \sum_{i=1}^{M_d} \text{Res} \left(\frac{e^{j2\pi ft}}{\prod_{i=1}^M (f - p_i)}, p_i \right) \tilde{u}(t, p_i) \end{aligned} \quad (6.27)$$

is the HKR-spectrum of the impulse response. Note that since $h(t)$ is a deterministic quantity, $R_{HH^*}(t, f)$ is not a second-order moment, but rather just a deterministic time-frequency representation of $h(t)$.

A particular solution to the ODE in the time-frequency domain is thus given by (6.26), the HKR-spectrum of the output is a convolution between the HKR-spectrum of the input and the HKR-spectrum of the impulse response, which is analogous to the system representation in (6.9). Note that $R_{HH^*}(t, f)$ may also be interpreted as the Green's function [Green, 1828] of the linear system in (6.18). The spectrum $R_{HH^*}(t, f)$ will be peaked in frequency around $f = \text{Re}\{p_i\}$, while the time behavior will be one of decay determined by the values of $\text{Im}\{p_i\}$. Thus, the roots of $D(f)$ directly dictates the behavior of the system in the time-frequency domain. This will be useful when designing systems, where one can specify the roots to get the desired frequencies and decay, and find the corresponding system coefficients.

6.2.1 Random coefficients

We briefly consider the case where one or more of the ODE coefficients are random variables. We still have the relation (6.6) in the frequency domain, but now $D(f)$ is a random quantity. If we assume that $D(f)$ and $X(t)$ are statistically independent, we can potentially solve for an expression of the HKR-spectrum of $h(t)$ using only the first and second order moments of the random coefficients. Indeed, [van Kampen, 2007] states that: ‘‘A stochastic differential equation is a differential equation whose coefficients are random numbers or random functions of the independent variable (or variables). Just as in normal differential

equations, the coefficients are supposed to be given, independently of the solution that has to be found". However, it is unreasonable to assume that the output $X(t)$ is statistically independent of the random function specifying the system itself. Obviously, the output will change if the systems parameters are changed. Otherwise, the system does not affect the output at all, and we would not need to consider the system. If one assumes that the system coefficients are given independent of the solution, we can treat the system as completely deterministic as we have done up to this point. If we have the situation where one or more of the system coefficients are random variables, the ODE may be expressed in the dual-frequency domain as

$$S_{XX^*}(\nu, f) = S_{HH^*}(\nu, f)S_{GG^*}(\nu, f), \quad (6.28)$$

where

$$S_{HH^*}(\nu, f) = \mathbb{E} \left\{ \frac{1}{D^*(f)D(f + \nu)} \right\}. \quad (6.29)$$

This assumes that the input and the system are statistically independent, which is reasonable. If, as before, we define $h(t)$ as the inverse FT of $D^{-1}(f)$, we see that $S_{HH^*}(\nu, f)$ is in fact the dual-frequency spectrum of the random impulse response of the system. We find the HKR-spectrum of the output by a convolution between the HKR-spectrum of the input, and the HKR-spectrum of the random impulse response,

$$R_{HH^*}(t, f) = \mathbb{E} \left\{ h(t) \frac{e^{-j2\pi ft}}{D^*(f)} \right\}. \quad (6.30)$$

Contrary to previous results, $R_{HH^*}(t, f)$ is now the second-order moment of the random impulse response. We cannot find a general closed-form expression of $R_{HH^*}(t, f)$ as we did for deterministic coefficients.

6.3 Differential Equations in Time and Space

Systems such as acoustic or electromagnetic wave fields will not only evolve in time, but also in space. Such a random quantity can be modeled by the random field $X(r, t)$, and the system can be modeled by a PDE in time and space $\mathfrak{L}\{X(r, t)\} = G(r, t)$, with a spatio-temporal differential operator

$$\mathfrak{L}\{\} = \sum_{m=0}^M \sum_{\mu=0}^L a_{m,\mu} \frac{\partial^m}{\partial t^m} \frac{\partial^\mu}{\partial r^\mu}. \quad (6.31)$$

Thus, this is a PDE of order M in t and order L in r . If $X_1(r, t) = \partial^{(\mu+m)} X(r, t) / \partial r^\mu \partial t^m$, and $X_2(r, t) = \partial^{(\zeta+i)} X(r, t) / \partial r^\zeta \partial t^i$, we have the cross HKR time-frequency space-wavenumber spectrum of these given as

$$\begin{aligned} R_{X_1 X_2^*}(r, q, t, f) = & (-j2\pi f)^i (-j2\pi q)^\zeta \\ & \times \left(\frac{\partial}{\partial t} + j2\pi f \right)^m \left(\frac{\partial}{\partial r} + j2\pi q \right)^\mu R_{XX^*}(r, q, t, f). \end{aligned} \quad (6.32)$$

If we form the HKR time-frequency space-wavenumber spectrum of the system, we get the PDE specified by $\mathfrak{L}'\{R_{XX^*}(r, q, t, f)\} = R_{GG^*}(r, q, t, f)$ where

$$\mathfrak{L}'\{\} = \sum_{\substack{m=0 \\ i=0}}^M \sum_{\substack{\mu=0 \\ \zeta=0}}^L a_{m,\mu}^* a_{i,\zeta} (-j2\pi f)^i (-j2\pi q)^\zeta \left(\frac{\partial}{\partial t} + j2\pi f\right)^m \left(\frac{\partial}{\partial r} + j2\pi q\right)^\mu, \quad (6.33)$$

in the time-frequency space-wavenumber domain. We again see that we obtain a PDE of the same orders in this domain, which can be solved by transforming the equation to the dual-frequency dual-wavenumber domain. Following the same procedure as in Section 6.2, we find that

$$D^*(q, f)D(q + \kappa, f + \nu)S_{XX^*}(\kappa, q, \nu, f) = S_{GG^*}(\kappa, q, \nu, f). \quad (6.34)$$

where the characteristic function of the PDE is

$$D(q, f) = \sum_{m=0}^M \sum_{\mu=0}^L a_{m,\mu} (j2\pi f)^m (j2\pi q)^\mu. \quad (6.35)$$

We obtain the HKR time-frequency space-wavenumber spectrum of $X(r, t)$ as

$$R_{XX^*}(r, q, t, f) = R_{GG^*}(r, q, t, f) \star_t \star_r R_{HH^*}(r, q, t, f), \quad (6.36)$$

where we have define the HKR time-frequency space-wavenumber spectrum of the system as

$$R_{HH^*}(r, q, t, f) = \frac{e^{-j2\pi(qr+ft)}}{D^*(q, f)} \iint \frac{e^{j2\pi(\kappa r+\nu t)}}{D(\kappa, \nu)} d\kappa d\nu. \quad (6.37)$$

If $D(\kappa, \nu)$ is separable in κ and ν , we can solve the integral in $R_{HH^*}(r, q, t, f)$ with residue theory, otherwise we can use numerical methods.

The extension from ODEs in time to PDEs in time and spatial coordinates is mathematically straightforward. Instead of a one-dimensional convolution in time, the spectrum of the output is given as a two-dimensional convolution in time and spatial coordinate between the input spectrum and the system spectrum. All the other concepts discussed for ODEs in time, such as random coefficients and homogeneous solutions, are readily defined for PDEs in time and spatial coordinate as well. However, as we will see in Section 6.4.4, there are conceptual differences between dealing with processes that change with time and fields that change with spatial coordinates.

6.4 Examples

We consider some specific systems of differential equations, both analytically and numerically, to further investigate the time-frequency representation of differential equations.

6.4.1 Langevin equation for Brownian motion

First, we look at a simple example that allows for closed-form solutions of the ODE in the time-frequency domain. We define a classical Langevin equation for Brownian motion

$$m \frac{d}{dt} X(t) + \beta X(t) = G(t), \quad (6.38)$$

which was also considered in [Galleani and Cohen, 2006b]. Here, $X(t)$ is the speed of the Brownian particle, m is its mass, and β is the friction coefficient. The driving force $G(t)$ is chosen to be Gaussian white noise with zero mean and variance σ_G^2 . First, we see that the first order ODE has the characteristic function

$$D(f) = mj2\pi f + \beta = mj2\pi \left(f - \frac{j\beta}{2\pi m} \right), \quad (6.39)$$

which has one root with positive imaginary value. Thus, the system is causal. We find the dual-frequency spectrum of $X(t)$ as

$$S_{XX^*}(\nu, f) = \frac{\sigma_G^2}{D^*(f)D(f+\nu)} \delta(\nu), \quad (6.40)$$

which gives us

$$R_{XX^*}(t, f) = \frac{\sigma_G^2}{|D(f)|^2} = S_{XX^*}(f). \quad (6.41)$$

The output is independent of t , implying that $X(t)$ is a stationary process. This is a general result for ODEs driven by stationary random processes, the output will always be a stationary process with a power spectral density equal to $S_{XX^*}(f) = S_{GG^*}(f) |D(f)|^{-2}$. It is implicitly assumed that the driving force has run for an infinite time and that the homogeneous solution is removed in this case.

We would like to see what happens right after the driving force is turned on at $t = 0$. The HKR-spectrum of the impulse response is

$$R_{HH^*}(t, f) = \frac{e^{-j2\pi ft} e^{-\beta t/m}}{m(\beta - j2\pi m f)} u(t). \quad (6.42)$$

We assume that the driving force is turned on at $t = 0$, $G_C(t) = G(t)u(t)$, which has a HKR-spectrum $R_{G_C G_C^*}(t, f) = \sigma_G^2 u(t)$. The output has a HKR-spectrum

$$R_{XX^*}(t, f) = S_{XX^*}(f) (1 - e^{-j2\pi ft} e^{-\beta t/m}) u(t). \quad (6.43)$$

Both the system and driving force is turned on at $t = 0$, i.e., the output need to satisfy $R_{XX^*}(t, f) = 0$ for $t < 0$. Thus, the homogeneous solution must be zero everywhere. We see that as $t \rightarrow \infty$, this will converge to the solution obtained with the driving force $G(t)$, and $X(t)$ will converge to a stationary process as time evolves. We note that limiting the driving

force in time is not equivalent to limiting the output process in time, as $X_C(t) = X(t)u(t)$ has a HKR-spectrum

$$R_{X_C X_C^*}(t, f) = S_{X X^*}(f) \left(1 + \frac{2\pi m f + j\beta}{2j\beta} e^{-j2\pi f t} e^{-\beta t/m} \right) u(t). \quad (6.44)$$

These two HKR-spectra have some similarities, but are not identical. Of course, as $t \rightarrow \infty$, these two solutions will converge to the same result. In [Galleani and Cohen, 2006b], this system was considered for the case where the driving force has been going forever, but the homogeneous solution contribute and has not died off yet. Since the initial condition was not specified in [Galleani and Cohen, 2006b], it is difficult to compare the results.

The problem of linear time-invariant systems driven by stochastic stationary forces that are turned on at a given time was also considered in [Lilly and Lettvin, 2004]. Here, the problem with stochastic integration was not addressed, and solutions of $X(t)$ was expressed through integrals of deterministic functions and what corresponded to the increment process of the stationary process. For this example, using the approach outlined in [Lilly and Lettvin, 2004] to obtain an expression for $X(t)$ and from this creating the HKR-spectrum of the process, we obtain the same result given in (6.43). The solution in [Lilly and Lettvin, 2004] is more general since it allows real-valued roots of the characteristic function, but as noted, we are then no longer ensured to be within the harmonizable class.

6.4.2 System with random coefficients

We briefly discussed ODEs with random coefficients earlier, but analytic solutions are difficult to obtain for this case. By numerical simulations we can see if our intuitive understanding of such a system corresponds with how the system actually works. Let

$$\frac{d^2}{dt^2} X(t) + a_1 \frac{d}{dt} X(t) + a_0 X(t) = G(t), \quad (6.45)$$

where a_1 is real-valued and deterministic and a_0 is a real-valued random variable with a shifted exponential probability distribution

$$p_{a_0}(a) = \lambda e^{-\lambda(a - a_1^2/4)} u(a - a_1^2/4). \quad (6.46)$$

Here, $\lambda = (m - a_1^2/4)^{-1}$, such that $E\{a_0\} = m$ and $\text{Var}\{a_0\} = \lambda^{-2} + m^2$. The roots of the characteristic function of this system is given by $p_{1,2} = (2\pi)^{-1} \left(j a_1/2 \pm \sqrt{a_0 - a_1^2/4} \right)$. We know that the values of the roots will specify the behavior of the system. The fact that $a_0 \geq a_1^2/4$ ensures that the value of a_1 alone determine imaginary value of both roots, which controls the damping of the system. The real part of the roots have equal magnitude and opposite signs, and the magnitude is determined by both coefficients a_0 and a_1 . The system is stable for the same values of t and experiences the same decay for all possible realizations of a_0 , only the frequency for which the system representation peaks changes with a_0 . We denote this frequency as the system frequency $f_{sys} = (2\pi)^{-1} \sqrt{a_0 - a_1^2/4}$. In

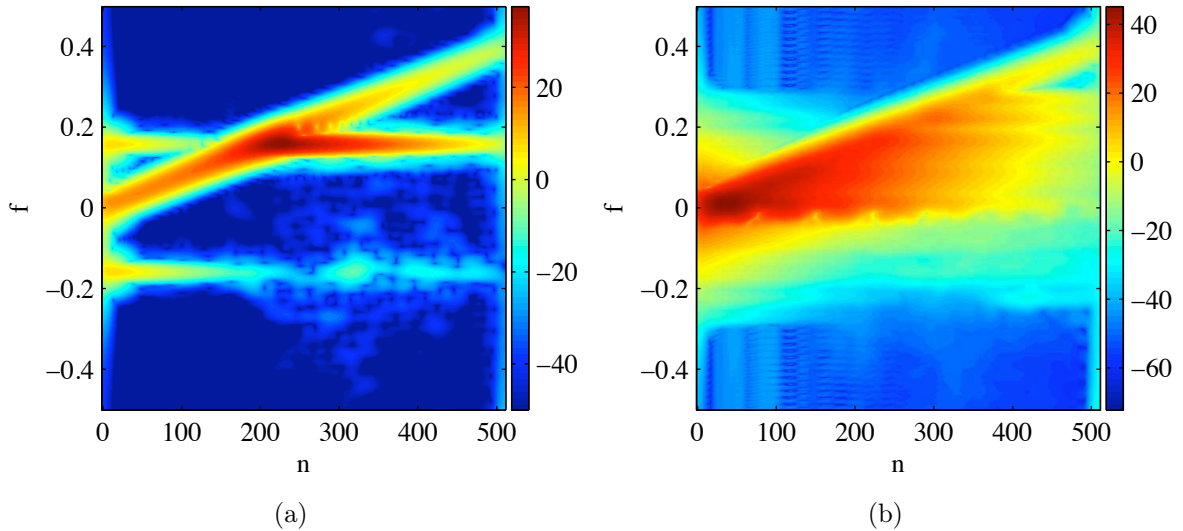


Figure 6.1: $10 \log_{10} \left| \widehat{R}_{XX^*}[n, f] \right|$ for the output of a system with random coefficients, (a) for one realization and (b) averaged over $K = 100$ realizations.

a discrete time simulation, the value of a_0 should have an upper limit specified to avoid aliasing in f_{sys} . For the values chosen in our numerical example, the probability of a_0 being too large and causing aliasing in the system is of order 10^{-8} , which we will ignore.

We perform a numerical simulation of the system by sampling at $t = n = 0, 1, \dots, 511$, and we let the system be driven by a complex-valued chirp $g[n] = \exp[j\pi(2\alpha n + \beta n^2)]$ with starting frequency $\alpha = 0$ and ending at frequency 0.4, which gives a chirp rate $\beta = 7.8 \times 10^{-4}$. We obtain a realization $x[n]$ of $X[n]$ by drawing a value for a_0 from its distribution and apply the Runge-Kutta method of order 4 (see e.g., [Moler, 2004]) to numerically solve the ODE specified by a_0 and a_1 with the driving force $g[n]$. The initial values used were that both $x[n]$ and its derivative are zero at $n = -1$, thus ensuring that the homogeneous solution is removed. We generate $K = 100$ realizations of the system and we estimate the HKR-spectrum of $X(t)$ based on each realization of the sampled process $X[n]$. The HKR-spectrum is estimated with $N_F = 60$, $N_T = 30$, and all windows are zero order DPSSs with $NW_T = 6$ and $NW_F = NW_B = 3$.

Figure 6.1(a) show the HKR-spectrum for one realization $a_0 = 0.9843$, which gives us $f_{sys} = \pm 0.1579$. We see that the output is a combination of the HKR-spectrum of the chirp and the HKR-spectrum of the system until the instantaneous frequency of the chirp coincides with f_{sys} . When the chirp frequency crosses this frequency, the system imposes its frequency on the chirp, and the output is dominated by a pure tone at the positive system frequency from this time on. However, we still see residuals of the chirp after this time. The HKR-spectrum averaged over all K realizations, shown in Figure 6.1(b), illustrates that as we get different values of a_0 , the instantaneous frequency of the chirp

will cross the systems frequency at different time instants, and the output will converge to different tones as n increases. The averaged spectrum is dominated by the behavior around low frequencies, which we would expect from the distribution of a_0 which favors low values of a_0 . If not for the damping, the output would, after some time has passed, behave like a pure tone with a random frequency. The numerical results thus confirm our intuitive understanding of the system.

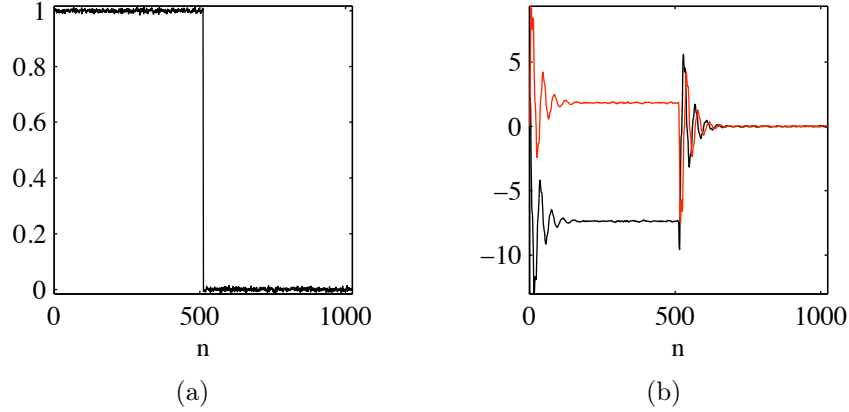


Figure 6.2: (a) A realization of the pulse. (b) The corresponding output from the second-order ODE driven by the realization, where the real part is the black line and the imaginary part is the red line.

6.4.3 Pulse response

In the real-world, one is often interested in a systems response to a pulse of finite duration. This allows us to see how the system responds to a sudden input, how it converges to a stable state and how the output dies out when the driving force is turned on. We consider a second-order ODE in time driven by a rectangular pulse of duration T , $G(t) = u(t)u(T-t)$, where T is chosen large enough for the system to reach its steady state before the pulse is turned off. The impulse response of the system is given by

$$R_{HH^*}(t, f) = \frac{e^{-j2\pi ft} [e^{j2\pi p_2 t} - e^{j2\pi p_1 t}]}{j2\pi(p_2 - p_1)D^*(f)} u(t), \quad (6.47)$$

where we assume that the characteristic function has two distinct roots, $p_1 \neq p_2$, with positive imaginary values. The HKR-spectrum of the driving force is

$$R_{GG^*}(t, f) = \frac{(e^{j2\pi fT} - 1)}{j2\pi f} e^{-j2\pi ft} u(t)u(T-t). \quad (6.48)$$

From (6.26) we have

$$R_{XX^*}(t, f) = \frac{T \operatorname{sinc}(\pi fT) e^{j\pi fT}}{\pi^3 p_1 p_2 D^*(f)} e^{-j2\pi ft} \times \begin{cases} L(t) - 1 & t \leq T \\ L(t) - L(t-T) & t > T \end{cases} \quad (6.49)$$

where

$$L(t) = \frac{p_2 e^{j2\pi p_1 t} - p_1 e^{j2\pi p_2 t}}{p_1 - p_2}. \quad (6.50)$$

We see that $L(0) = -1$, and $L(t)$ approaches zero as t increases. Also, when $t \gg T$, we have $L(t) \approx L(t - T)$, thus the output dies off as t increases.

We show a numerical example where $T = 512$, $N = 2T$ and the system is specified by a characteristic function with roots $p_1 = 0.0264 + j0.005$ and $p_2 = 0.1240 + j0.007$. We add a Gaussian zero-mean white noise process with $\sigma_\epsilon^2 = 2.5 \times 10^{-5}$ to the driving force, and we show a sampled realization $g[n]$ of the driving force in Figure 6.2(a). The noise term will result in an extra term $\sigma_\epsilon^2 |D(f)|^{-2}$ added to the HKR-spectrum of the output in (6.49). Similar to the random system case, we numerically solve the differential equation driven by the realization $g[n]$ to obtain the realization $x[n]$ of the output process shown in Figure 6.2(b). The HKR-spectrum is estimated from this realization, with $N_F = 100$ samples, $N_T = 20$ samples, $v_F[n]$ is a Hanning window, and $v_T[n]$ and $v_B[n]$ are zero order DPSSs with $NW_T = 6$ and $NW_B = 4$.

The numerical results are shown in Fig 6.3, we see that they are consistent with the theoretical results. Both the pulse and system starts at $t = 0$, and the system response

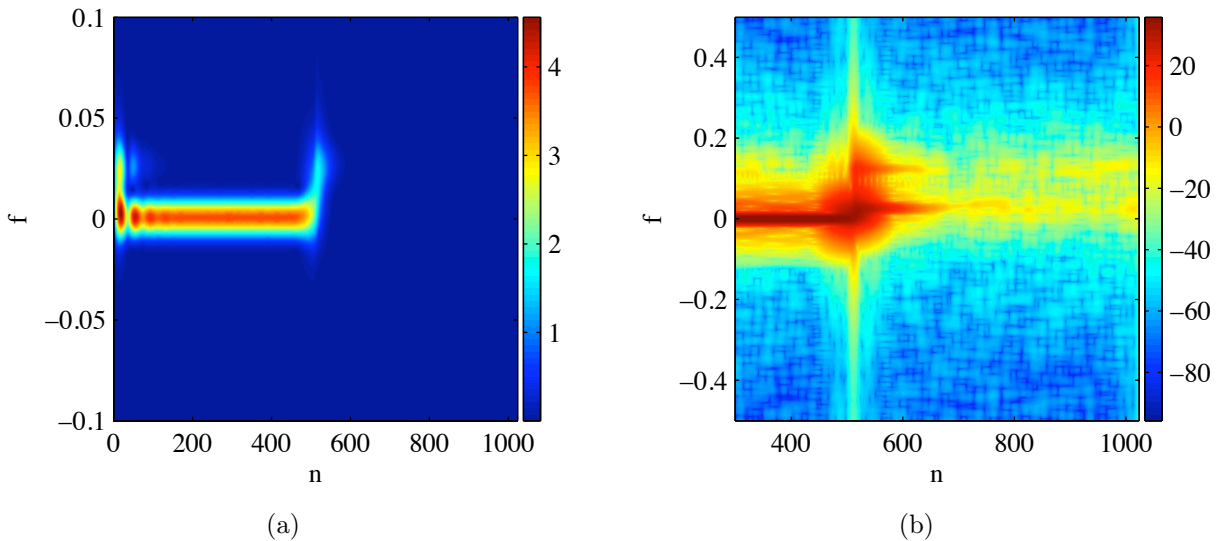


Figure 6.3: For the pulse response. (a) $10^3 \times \left| \widehat{R}_{XX^*}[n, f] \right|$ for $-0.1 \leq f \leq 0.1$. (b) $10 \log_{10} \left| \widehat{R}_{XX^*}[n, f] \right|$ for $n = 300, \dots, 1024$.

dies off quickly. The output is dominated by the pulse until it is turned off. At this time, the system response starts up again, and then decreases with increasing values of n . On a linear scale, we only see the system response influence as a bending of the straight line cause by the pulse at the beginning and end of the interval. On a logarithmic scale,

as shown in Figure 6.3(c), we see that as the pulse is shut off, we get contributions for frequencies $f = 0.0264$ and $f = 0.1240$, which corresponds to p_1 and p_2 , respectively. The contribution at $f = 0.0264$ is largest, this is due to the fact that $\text{Im}\{p_1\} < \text{Im}\{p_2\}$.

6.4.4 Spatial differential equations

Differential equations of random fields is a very interesting topic. We consider a system that is a second order ODE in the one-dimensional spatial variable r ,

$$\frac{d^2}{dr^2}X(r) + 4\pi^2\gamma^2X(r) = G(r). \quad (6.51)$$

This can be thought of as the electromagnetic wave equation of an electric field $X(r)$ that has a separate time and spatial behavior, and the time dependency is purely harmonic. Here, $X(r)$ and $G(r)$ are harmonizable random fields. The coefficient $\gamma^2 \in \mathbb{C}$ in (6.51) has a positive real-part and a positive imaginary part, and is in the case of an electromagnetic wave equation determined by the magnetic permeability, the permittivity and the electrical conductivity of the medium.

We first find the characteristic function of the ODE

$$D(q) = -4\pi^2(q^2 - \gamma^2) = -4\pi^2(q - \gamma)(q + \gamma), \quad (6.52)$$

which gives the spatial impulse response

$$h(r) = \frac{\exp(j2\pi\gamma|r|)}{4\pi j\gamma}. \quad (6.53)$$

Put together, the HKR space-wavenumber spectrum of the system is

$$R_{HH^*}(r, q) = \frac{\exp(j2\pi\gamma|r|)\exp(-j2\pi qr)}{-j16\pi^3\gamma(q - \gamma^*)(q + \gamma^*)}. \quad (6.54)$$

We show $|R_{HH^*}(r, q)|$ for $r = -50, \dots, 50$, $-1/2 \leq q \leq 1/2$, and $\gamma = 0.12 + 0.05j$ in Figure 6.4. The system specified with these values will be investigated numerically later. From Figure 6.4 and (6.54), we see that $R_{HH^*}(r, q)$ will decrease exponentially as we move away from the origin $r = 0$. As a function of q , $R_{HH^*}(r, q)$ will have its maxima at $q = \pm\text{Re}\{\gamma\}$.

The HKR space-wavenumber spectrum of $X(r)$ is given by

$$R_{XX^*}(r, q) = R_{GG^*}(r, q) \star_r R_{HH^*}(r, q). \quad (6.55)$$

If we require the solution to decrease as we move away from $r = 0$, or at least not increase exponentially, we need to remove the homogeneous solution for all values of r . Thus, the boundary conditions of the system will be specified such that $c_1(q) = c_2(q) = 0$, and then (6.55) gives the complete solution of the system.

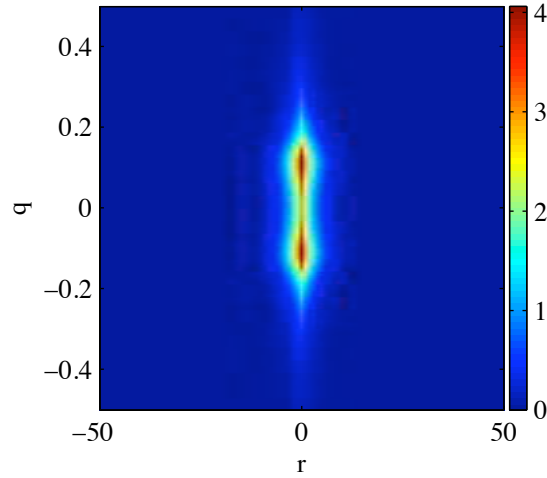


Figure 6.4: The absolute value of the HKR space-wavenumber spectrum of the spatial ODE in (6.51) with $\gamma = 0.12 + 0.05j$.

Homogeneous driving force

Homogeneous random fields have second-order moments that does not depend on the specific location of two spatial coordinates in the field, but only the spatial difference between the coordinates. This will greatly simplify our calculations. We consider the case where the driving force is a homogeneous random field with a spatial correlation that decays exponentially as we consider spatial coordinates farther apart, independent of r , $M_{XX^*}(r, \rho) = \exp(-\alpha\rho)$, where $\alpha \in \mathbb{R}$ and $\alpha > 0$. The driving force has a spatio-wavenumber spectrum

$$R_{GG^*}(r, q) = S_{GG^*}(q) = \frac{\alpha}{2\pi^2 \left(q^2 + \frac{\alpha^2}{4\pi^2} \right)}, \quad (6.56)$$

and the spatio-wavenumber spectrum of $X(r)$ thus is given by

$$R_{XX^*}(r, q) = \frac{S_{GG^*}(q)}{|D(q)|^2}. \quad (6.57)$$

This is a general result for homogeneous driving forces, and we note that the solution does not depend on the spatial variable r . Thus, if the driving force is a homogeneous random field, the output is also a homogeneous random field. The output will be mainly concentrated on the lines $q = 0$ and $q = \pm \text{Re}\{\gamma\}$. We note that this result is similar to the result obtained for ODEs in time driven by a stationary process in Section 6.4.1.

Spatially white driving force

Next, we assume that the driving force is an inhomogeneous random field, i.e., that the probability density of the field is different for different spatial coordinates r . Thus, the

spatio-wavenumber spectrum will depend on the spatial variable r . To simplify our calculations, we assume that any two different points in the field are uncorrelated, i.e., that the field is spatially white. The variance of the process should decrease as we move away from the source $r = 0$. To enable us to find a closed-form expression of the HKR space-wavenumber spectrum of the output, we assume that the variance decays exponentially, $E\{|X(r)|^2\} = \exp(-2\pi b|r|)$, where $b \in \mathbb{R}$ and $b > 0$. The spatio-wavenumber spectrum of the driving force is

$$R_{GG^*}(r, q) = \exp(-2\pi b|r|), \quad (6.58)$$

and it follows that

$$R_{XX^*}(r, q) = \frac{1}{16\pi^4\gamma(q^2 - \gamma^2)^*} \left[\frac{jb e^{j2\pi(\gamma|r|-qr)}}{b^2 + [\gamma - \text{sgn}(r)q]^2} - \frac{\gamma e^{-2\pi b|r|}}{\gamma^2 + [b - j\text{sgn}(r)q]^2} \right], \quad (6.59)$$

where

$$\text{sgn}(r) = \begin{cases} 1 & \text{if } r \geq 0 \\ -1 & \text{if } r < 0. \end{cases} \quad (6.60)$$

The first term will decay like $R_{HH^*}(r, q)$ in r , and will be centered around $q = \text{sgn}(r)\text{Re}\{\gamma\}$, since b is real-valued. The second term will decay like the driving force. In q , this term will be peaked around values related to both b and γ in a non-trivial manner. Specifically, the absolute value of the second term will have a peak at the value of q equal to the real-valued root of the polynomial $q^3 + (b^2 - \text{Re}\{\gamma^2\})q - b\text{Im}\{\gamma^2\}$.

Spatial versus time

Even if the basic definitions for random fields and random processes are very similar, these two types of random functions need to be handled quite differently. For a random process, it is quite natural, in fact for real-world processes necessary, that the process starts at a given time and then evolves with time. Obviously it only evolves in one time “direction”. However, for a random field that originates from a single point, e.g., an audio signal from a speaker, it would be unnatural to assume that the field only propagates in one direction in space. A speaker would typically emit sound in all directions, but with different intensity in different directions. ODEs in time are easier to handle since the time development starts at one time and grows in only one direction. For an ODEs in spatial coordinates, the field will propagate in all directions, and we need to separate near-field behavior (close to the source) from the far-field (far away from the source). As we want to suggest more complicated random fields as driving forces, a seemingly good choice could be a field similar to autoregressive time processes. The field originates from the source point $r = 0$, and spreads in both positive and negative direction (assuming a one-dimensional problem). For an autoregressive field, the field at the spatial coordinate r_0 will be a linear combination of the field in the, say, L spatial coordinates that are closer to the source point than r_0 . However, since spatial coordinates on the negative r -axis and on the positive r -axis share the source point, one will have correlations between negative and positive coordinates. Already for this simple example, the spatial correlation function will be quite complicated.

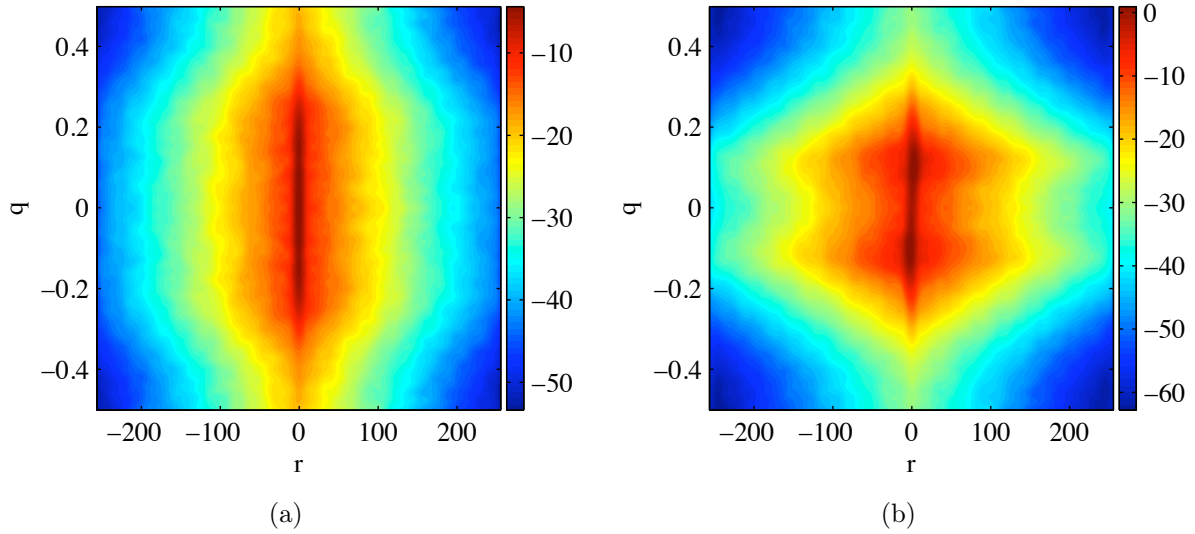


Figure 6.5: The estimates (a) $10 \log_{10} \left| \widehat{R}_{GG^*}[r, q] \right|$ and (b) $10 \log_{10} \left| \widehat{R}_{XX^*}[r, q] \right|$ averaged over $K = 200$ realizations for the spatial ODE driven by a non-white inhomogeneous driving force.

This is only a small example of the problems one encounters when working with spatial problems as opposed to temporal problems.

Numerical example with inhomogeneous driving force

We have seen how we can simplify the calculations and find closed-form expressions of the spatio-wavenumber spectrum of $X(r)$ by assuming that the driving force is either homogeneous or spatially white. Since even finding the spatio-wavenumber spectrum of an inhomogeneous and colored $G(r)$ can be complicated, we will consider this case with numerical methods. Thus, all quantities are now functions of the discrete spatial coordinate r . The driving force is given as an autoregressive random field with additive noise of time-varying variance,

$$G[r] = \begin{cases} 1 & r = 0 \\ \sum_{m=1}^{\min(|r|, 3)} \theta_m G[r - \text{sgn}(r)m] + \epsilon[r] & r \neq 0. \end{cases} \quad (6.61)$$

We let $r = -N/2, \dots, N/2 - 1$, $N = 512$, $\boldsymbol{\theta} = [0.5 \ -0.3 \ 0.1]^T$, $\gamma = 0.12 + 0.05j$ and $\sigma_\epsilon^2[r] = 0.05 \exp(-0.03|r|)$. For the HKR space-wavenumber spectrum estimator, we choose $N_F = 50$, $N_T = 20$, $v_F[m]$ is a Hanning window, and $v_T[\mu]$ and $v_B[m]$ are zero order DPSSs with $NW_T = 6$ and $NW_B = 3$. The HKR space-wavenumber spectrum of the impulse response is shown in Figure 6.5(a), while Figure 6.5 shows the estimated HKR

space-wavenumber spectra of $G[r]$ and $X[r]$. In spatial coordinates, $|R_{HH^*}[r, q]|$ decays quickly as $|r|$ increases, and it is concentrated around the wavenumbers $q = \pm 0.12$, which relates to our choice of γ . We see that the HKR space-wavenumber spectrum of the driving force also decays as $|r|$ increases. The spectrum has contributions concentrated mostly at $|q| \leq 0.2$. For the output $X[r]$, the estimated HKR space-wavenumber spectrum shows how the system $h[r]$ has altered the input $G[r]$. The spectrum still has contributions concentrated mostly at $|q| \leq 0.2$, but now with maxima at $q = \pm 0.12$ due to the impulse response. Also note that the spectrum is more spread out in r for these two wavenumbers.

6.5 Remarks

We have presented how the HKR-spectrum and the time-frequency domain can be used for the analysis of stochastic differential equations. We presented both theoretical results, and numerical examples for several of the systems that were considered theoretically. We considered the simple but interesting examples of systems with a nonstationary driving force consisting of a stationary process with limited time support, and an ODE where one coefficient was a random variable. The pulse response and spatial differential equations examples were inspired by the field of petroleum exploration where pulses of electromagnetic fields are used to analyze the earth below the surface [Nekut and Spies, 1989], where the electromagnetic fields are governed by differential equations. The theory presented here for stochastic differential equations involving harmonizable random fields may be used to improve methods of petroleum exploration. Since differential equations are used to model many real-world systems, the theory will have many other potential applications as well.

Chapter 7

Summary

We have considered harmonizable random processes, and more specifically time-frequency representation of second-order moments of this class of processes. The concept of a harmonizable process and its second-order moments was presented in Chapter 2, both in continuous and discrete time. We saw that the second-order moments of a real-valued process are completely determined by the Hermitian dual-time correlation, the Hermitian dual-frequency spectrum, the Hermitian Kirkwood-Rihaczek time-frequency spectrum and the Hermitian ambiguity function. A complex-valued process has four corresponding complementary quantities as well, and we need both one Hermitian and one complementary quantity to completely describe the second-order moments of the process. We briefly reviewed existing methods for estimating the dual-time correlations and the dual-frequency spectra. In order to simulate from complex-valued improper processes, we considered an existing method aimed at simulating from stationary improper processes, and we proposed an extension of this method that allows us to simulate from nonstationary improper processes. The theory of harmonizable random fields was also introduced.

In Chapter 3, we proposed estimators of the Kirkwood-Rihaczek time-frequency spectra based on the Hilbert space inner product formulation of the spectra. The estimators was shown to be theoretically equivalent to a known estimator, but our implementation is less computational intensive. We discussed how to chose the parameters of the estimator to obtain good resolution, to reduce cross-terms and to ensure the correct normalization in the estimate. The estimators were shown to have an expected value that was a smoothed version of the true spectrum. We implemented the estimators and tried them out on simulated improper data and on real-world real-valued data sets. All the numerical examples showed that our estimators work well.

The estimation of the Hermitian ambiguity function was considered in Chapter 4. The concept of underspread processes was introduced, and we examined the distributional properties of the empirical ambiguity function. Based on these distribution results, we proposed a method of thresholding the empirical ambiguity function, and we proposed to use the results of this thresholding as an estimate of the Hermitian ambiguity function. Numerical examples showed that the thresholding reduced the mean square error of the estimator. At the same time thresholding did not increase the support in the ambiguity domain, which

is what determines if a process is underspread or not.

In Chapter 5 we proposed objective and dimensionless measures of a process' behavior in the time-frequency and dual-frequency domain, these measures were denote spectral coherences. We obtained results consistent with the standard spectral coherences of non-stationary processes through a linear estimation scheme. Extended spectral coherence measures was proposed based on a widely linear estimation scheme, and these spectral coherence measures were shown to utilize the information contained in both the Hermitian and complementary quantities in one quantity.

Finally, we considered stochastic differential equations in Chapter 6. The Hermitian Kirkwood-Rihaczek time-frequency spectrum was used in order to analyze the system determined by the stochastic differential equation. By considering the second-order moments in the time-frequency domain rather than the equation itself, we avoided the problems related to stochastic integration. We discussed how to handle differential equations where the driving force was random, and differential equations driven by a deterministic force where at least one of the system coefficients were random. We transformed the stochastic differential equation to an ordinary differential equation in the time-frequency domain, and solved this equation by the Fourier transform technique. The time-frequency spectrum of the output was found to be a convolution in time between the time-frequency spectrum of the system and the time-frequency spectrum of the driving force. We also considered partial differential equations of harmonizable random fields, which yielded a similar solution where the time-frequency space-wavenumber spectrum of the output was found as the two-dimensional convolution in time and spatial coordinate of the time-frequency space-wavenumber spectrum of the system and the time-frequency space-wavenumber spectrum of the driving force. Analytical and numerical examples were provided that further illuminated this theory.

Bibliography

- M. J. Ablowitz and A. S. Fokas. *Complex Variables: Introduction and Applications*. Cambridge Univ. Press, Cambridge, UK, second edition, 2003.
- F. Auger and P. Flandrin. *Improving the readability of time-frequency and time-scale representations by the reassignment method*. *IEEE Trans. Signal Proc.*, **43**: 1068–1089, May 1995.
- S. Aviyente and W. J. Williams. *Multitaper marginal time-frequency distributions*. *Signal Processing*, **86**: 279–295, 2006.
- S. Barber and G. P. Nason. *Real nonparametric regression using complex wavelets*. *J. Roy. Stat. Soc. B*, **66**: 927–939, 2004.
- M. Bayram and R. G. Baraniuk. *Multiple window time-varying spectrum estimation*. In *Nonlinear and Nonstationary Signal Processing*, edited by W. Fitzgerald, R. Smith, A. Walden and P. Young, pp. 292–316. Cambridge Univ. Press, Cambridge, U.K., 2000.
- P. Borgnat and P. Flandrin. *Time-frequency localization from sparsity constraints*. In *Proc. ICASSP*, pp. 3785–3788. Las Vegas, NV, March 31-April 4 2008.
- A. L. Cauchy. *Oeuvres complètes*. Gauthier-Villars, Paris, France, 1890.
- T. A. C. M. Claasen and W. F. G. Mecklenbräuker. *The Wigner distribution - a tool for time-frequency signal analysis - Part III: Relations with other time-frequency signal transformations*. *Philips J. Res.*, **35**: 372–389, 1980.
- L. Cohen. *Generalized phase-space distribution functions*. *J. Math. Phys.*, **7**: 781–786, May 1966.
- L. Cohen. *Time-Frequency Analysis*. Englewood Cliffs, NJ: Prentice Hall, 1995.
- H. Cramér. *On the theory of stationary random processes*. *Ann. Math.*, **41**: 215–230, January 1940.
- I. Daubechies. *Time-frequency localization operators: A geometric phase space approach*. *IEEE Trans. Inf. Theory*, **34**: 605–612, 1988.
- T. S. Ferguson. *A Course in Large Sample Theory*. Chapman & Hall, London, UK, 1996.

- P. Flandrin. *Time-Frequency/Time-Scale Analysis*. Academic Press, San Diego, CA, 1999.
- P. Flandrin, F. Auger and E. Chassande-Mottin. *Time-frequency reassignment: From principles to algorithms*. In *Applications in Time-Frequency Signal Processing*, edited by A. Papandreou-Suppappola, chapter 5, pp. 179–203. CRC Press LLC, 2003.
- L. Galleani and L. Cohen. *The Wigner distribution for classical systems*. *Physics Letters A*, **302**: 149–155, September 2002.
- L. Galleani and L. Cohen. *Direct time-frequency characterization of linear systems governed by differential equations*. *IEEE Signal Proc. Lett.*, **11**: 721–724, September 2004a.
- L. Galleani and L. Cohen. *Time-frequency Wigner distribution approach to differential equations*. In *Nonlinear Signal and Image Processing: Theory, Methods, and Applications*, edited by K. E. Barner and A. Gonzalo, pp. 127–156. CRC Press, Boca Raton, FL, 2004b.
- L. Galleani and L. Cohen. *The generalized Wiener process for colored noise*. *IEEE Signal Proc. Lett.*, **13**: 608–611, October 2006a.
- L. Galleani and L. Cohen. *Nonstationary stochastic differential equations*. In *Advances in Nonlinear Signal and Image Processing*, edited by S. Marshall and G. L. Sicuranza, volume 6, pp. 1–14. Hindawi Publishing Corporation, New York, NY, 2006b.
- C. W. Gardiner. *Handbook of Stochastic Methods for Physics, Chemistry and the Natural Sciences*. Springer-Verlag, New York, NY, third edition, 2004.
- G. Green. *An essay on the application of mathematical analysis to the theories of electricity and magnetism*. Available at <http://quod.lib.umich.edu/cgi/t/text/textidx?c=umhistmath;idno=AAN8197.0001.001>, 1828.
- A. Hanssen. *Wavefields*. In *Handbook on Array Processing and Sensor Networks*, edited by S. Haykin and K. J. R. Liu, chapter 2. Wiley-IEEE, 2009.
- A. Hanssen and L. L. Scharf. *A theory of polyspectra for nonstationary stochastic processes*. *IEEE Trans. Signal Proc.*, **51**: 1243–1252, May 2003.
- A. Hanssen, H. Hindberg, T. A. Øigård, Y. Birkelund and O. Hanssen. *Analysis of harmonic and subharmonic effects in a transversal flute made from heracleum lacinatum*. In *Proc. of the 7th Nordic Signal Processing Symposium (NORSIG)*. Reykjavik, Iceland, June 7 - 9 2006a.
- A. Hanssen, S. Holm, Y. Birkelund, H. Hindberg and T. A. Øigård. *The sound of rock 'n' roll: analysis and modeling of valve amplifier distortion for electric guitar*. In *Proc. of the IMA 7th Int. Conf. Mathematics in Signal Processing*. Cirencester, UK, December 18 - 20 2006b.
- R. A. Hedges and B. W. Suter. *Numerical spread: Quantifying local stationarity*. *Digital Signal Processing*, **12**: 628–643, 2002.

- H. Hindberg. *The Harmonizable Representation of Complex-Valued Nonstationary Random Processes*. Master's thesis, Dept. of Physics and Technology, University of Tromsø, May 2005.
- H. Hindberg and A. Hanssen. *Generalized spectral coherences for complex-valued harmonizable processes*. *IEEE Trans. Signal Proc.*, **55**: 2407–2413, June 2007.
- H. Hindberg and S. C. Olhede. *Estimation of ambiguity functions with limited spread*. Submitted to *IEEE Trans. Signal Proc.*, 2009.
- H. Hindberg, Y. Birkelund, T. A. Øigård and A. Hanssen. *Kernel-based estimators for the Kirkwood-Rihaczek time-frequency spectrum*. In *Proc. of the 14th EUSIPCO*. Florence, Italy, September 4 - 8 2006.
- H. Hindberg, A. Hanssen and S. C. Olhede. *Thresholding the ambiguity function*. In *Proc. ICASSP*, pp. 3773–3776. Las Vegas, NV, March 31-April 4 2008.
- F. Hlawatsch. *Time-Frequency Analysis and Synthesis of Linear Signal Spaces: Time-frequency Filters, Signal Detection and Estimation, and Range-Doppler Estimation*. Kluwer Academic Publishers, Boston, MA, 1998.
- F. Hlawatsch and G. F. Boudreaux-Bartels. *Linear and quadratic time-frequency signal representations*. *IEEE Signal Processing Magazine*, **9**: 21–67, April 1992.
- L. Isserlis. *On a formula for the product-moment coefficient of any order of a normal frequency distribution in any number of variables*. *Biometrika*, **12**: 134–139, 1918.
- M. Jachan, G. Matz and F. Hlawatsch. *Time-frequency ARMA models and parameter estimators for underspread nonstationary random processes*. *IEEE Trans. Signal Proc.*, **55**: 4366–4381, 2007.
- J. Jeong and W. J. Williams. *Kernel design for reduced interference distributions*. *IEEE Trans. Signal Proc.*, **40**: 402–412, 1992.
- I. M. Johnstone and B. W. Silverman. *Wavelet threshold estimators for data with correlated noise*. *J. Roy. Stat. Soc. B*, **59**: 319–351, 1997.
- J. G. Kirkwood. *Quantum statistics of almost classical assemblies*. *Physical Review*, **44**: 31–37, July 1933.
- W. Kozek. *Matched Weyl-Heisenberg Expansions of Nonstationary Environments*. Ph.D. thesis, Vienna Univ. Technology, Vienna, Austria, 1997.
- Y. Larsen. *Spectral Properties of Harmonizable Random Processes and Fields*. Ph.D. thesis, Department of Physics, Univ. of Tromsø, Norway, December 2003.
- K. Lii and M. Rosenblatt. *Spectral analysis for harmonizable processes*. *Ann. of Statistics*, **30**: 258–297, 2002.
- J. M. Lilly and J.-C. Gascard. *Wavelet ridge diagnosis of time-varying elliptical signals with application to an oceanic eddy*. *Nonlin. Proc. Geophys.*, **13**: 467–483, 2006.
- J. M. Lilly and E. E. Lettvin. *The “switch-on” problem for linear time-invariant operators*. *Signal Processing*, **84**: 763–784, 2004.

- J. M. Lilly and J. Park. *Multiwavelet spectral and polarization analysis*. *Geophys. J. Int.*, **122**: 1001–1021, 1995.
- M. Loève. *Sur le fonctions aléatoire de second ordre*. *Rev. Sci.*, **83**: 297–303, 1945.
- M. Loève. *Sur le fonctions aléatoire de second ordre*. *Rev. Sci.*, **84**: 195–206, 1946.
- M. Loève. *Probability Theory*. New York, NY: Springer-Verlag, fourth edition, 1978.
- R. M. Loynes. *On the concept of the spectrum for non-stationary processes*. *J. Roy. Stat. Soc. B*, **30**: 1–30, 1968.
- S. L. Marple. *Computing the discrete-time ‘analytic’ signal via FFT*. *IEEE Trans. Signal Proc.*, **47**: 2600–2603, September 1999.
- W. Martin and P. Flandrin. *Wigner-Ville spectral analysis of nonstationary processes*. *IEEE Trans. Acoustics, Speech, Signal Proc.*, **33**: 1461–1470, December 1985.
- G. Matz and F. Hlawatsch. *Nonstationary spectral analysis based on time-frequency operator symbols and underspread approximations*. *IEEE Trans. Inform. Theory*, **52**: 1067–1086, 2006.
- C. B. Moler. *Numerical Computing with Matlab*. SIAM, Philadelphia, PA, 2004.
- F. D. Neeser and J. L. Massey. *Proper complex random processes with applications to information theory*. *IEEE Trans. Inform. Theory*, **39**: 1293–1302, July 1993.
- A. G. Nektu and B. R. Spies. *Petroleum exploration using controlled-source electromagnetic methods*. *Proc. IEEE*, **77**: 338–362, February 1989.
- B. Øksendal. *Stochastic Differential Equations: An Introduction with Applications*. Springer-Verlag, Berlin, Germany, fifth edition, 2002.
- S. C. Olhede. *Hyperanalytic denoising*. *IEEE Trans. Image Proc.*, **16**: 1522–1537, June 2007.
- S. C. Olhede and A. T. Walden. *Noise reduction in directional signals using multiple Morse Wavelets illustrated on quadrature Doppler ultrasound*. *IEEE Trans. Biomedical Eng.*, **50**: 51–57, January 2003.
- M. Peligrad. *On the asymptotic normality of sequences of weak dependent random variables*. *J. Theo. Prob.*, **9**: 703–715, 1996.
- B. Picinbono. *Random Signals and Systems*. Prentice-Hall, Englewood Cliffs, NJ, 1993.
- B. Picinbono and P. Bondon. *Second-order statistics of complex signals*. *IEEE Trans. Signal Proc.*, **45**: 411–420, February 1997.
- B. Picinbono and P. Chevalier. *Widely linear estimation with complex data*. *IEEE Trans. Signal Proc.*, **43**: 2030–2033, August 1995.
- M. B. Priestley. *Non-Linear and Non-Stationary Time Series Analysis*. London, U.K.: Academic, 1988.

- J. G. Proakis and M. Salehi. *Communication Systems Engineering*. Upper Saddle River, NJ: Prentice-Hall, second edition, 2002.
- M. M. Rao. *Harmonizable, Cramér, and Karhunen classes of processes*. In *Handbook of Statistics*, edited by E. J. Hannan, P. R. Krishnaiah and M. M. Rao, volume 5, pp. 279–310. Elsevier Science Publishers, Amsterdam, 1985.
- A. W. Rihaczek. *Signal energy distribution in time and frequency*. *IEEE Trans. Inform. Theory*, **14**: 369–374, May 1968.
- A. W. Rihaczek. *Principles of High Resolution Radar*. McGraw Hill, New York, NY, 1969.
- C. P. Robert and G. Casella. *Monte Carlo Statistical Methods*. Springer-Verlag, New York, NY, second edition, 2004.
- P. Rubin-Delanchy and A. T. Walden. *Simulation of improper complex-valued sequences*. *IEEE Trans. Signal Proc.*, **55**: 5517–5521, November 2007.
- J. Sandberg and M. Hansson-Sandsten. *A comparison between different ambiguity domain definitions in stochastic time-frequency analysis*. *IEEE Trans. Signal Proc.*, **57**: 868–877, March 2009.
- A. M. Sayeed and D. L. Jones. *Optimal kernels for non-stationary spectral estimation*. *IEEE Trans. Signal Proc.*, **43**: 478–491, February 1995.
- L. L. Scharf and B. Friedlander. *Toeplitz and Hankel kernels for estimating time-varying spectra of discrete-time random processes*. *IEEE Trans. Signal Proc.*, **49**: 179–189, January 2001.
- L. L. Scharf, P. J. Schreier and A. Hanssen. *The Hilbert space geometry of the Rihaczek distribution for stochastic analytic signals*. *IEEE Signal Proc. Lett.*, **12**: 297–300, April 2005.
- P. J. Schreier. *A new interpretation of bilinear time-frequency distributions*. In *Proc. ICASSP*. Honolulu, HI, April 15-20 2007.
- P. J. Schreier. *Polarization ellipse analysis of nonstationary random signals*. *IEEE Trans. Signal Proc.*, **56**: 4330–4339, September 2008a.
- P. J. Schreier. *A unifying discussion of correlation analysis for complex random vectors*. *IEEE Trans. Signal Proc.*, **56**: 1327–1336, April 2008b.
- P. J. Schreier and L. L. Scharf. *Second-order analysis of improper complex random vectors and processes*. *IEEE Trans. Signal Processing*, **51**: 714–725, March 2003a.
- P. J. Schreier and L. L. Scharf. *Stochastic time-frequency analysis using the analytic signal: Why the complementary distribution matters*. *IEEE Trans. Signal Proc.*, **51**: 3071–3079, December 2003b.
- C. E. Shannon. *Communications in the presence of noise*. *Proc. IRE*, **37**: 10–21, January 1949.

- M. I. Skolnik. *Introduction to Radar Systems*. McGraw Hill, Boston, MA, third edition, 2001.
- D. Slepian. *Prolate spheroidal wave functions, Fourier analysis and uncertainty V: the discrete case*. *Bell Syst. Tech. J.*, **57**: 1371–1429, 1978.
- D. J. Thomson. *Spectrum estimation and harmonic analysis*. *Proc. IEEE*, **70**: 1055–1096, September 1982.
- D. J. Thomson. *Multitaper analysis of nonstationary and nonlinear time series data*. In *Nonlinear and nonstationary signal processing*, edited by W. Fitzgerald, R. Smith, A. Walden and P. Young, pp. 317–394. Cambridge University Press, Cambridge, UK, 2000.
- N. G. van Kampen. *Stochastic Processes in Physics and Chemistry*, p. 396. Elsevier Science, Amsterdam, The Netherlands, third edition, 2007.
- J. Ville. *Théorie et applications de la notion de signal analytique*. *Cables et Trans.*, **2**: 61–74, 1948.
- P. Wahlberg and M. Hansson. *Kernels and multiple windows for estimation of the Wigner-Ville spectrum of Gaussian locally stationary processes*. *IEEE Trans. Signal Proc.*, **55**: 73–84, January 2007.
- E. P. Wigner. *On the quantum correction for thermodynamic equilibrium*. *Phys. Rev.*, **40**: 749–759, 1932.
- E. P. Wigner. *Quantum-mechanical distribution functions revisited*. In *Perspectives in Quantum Theory*, edited by W. Yourgrau and A. van der Merwe. Dover, New York, NY, 1971.
- J. Xiao and P. Flandrin. *Multitaper time-frequency reassignment for nonstationary spectrum estimation and chirp enhancement*. *IEEE Trans. Signal Proc.*, **55**: 2851–2860, June 2007.
- A. M. Yaglom. *Correlation Theory of Stationary and Related Random Functions*. Springer-Verlag, New York, NY, 1987.
- Y. Yang and L. Cohen. *Time-frequency Wigner evolution of the quantum Langevin equation*. *J. Modern Optics*, **52**: 2223–2232, November 2005.